Excitatory effects of dentate gyrus mossy cells and their ability to influence granule cell firing: an optogenetic study in adult mouse hippocampal slices.

Abbreviated title: Excitatory effects of mossy cells on granule cells

Hannah L. Bernstein[1,2], Yi-Ling Lu[1,2], Justin J. Botterill[1,2], Áine M. Duffy[1,2], John J. LaFrancois[1,2], and Helen E. Scharfman[1,2]

[1]Departments of Child & Adolescent Psychiatry, Neuroscience & Physiology, and Psychiatry, and the Neuroscience Institute
New York University Langone Health
550 First Ave.
New York, NY 10016

[2]Center for Dementia Research
The Nathan Kline Institute for Psychiatric Research
New York State Office of Mental Health
140 Old Orangeburg Road, Bldg. 35
Orangeburg, NY 10962

Submitting and Corresponding author: Helen E. Scharfman
Address for correspondence:
Center for Dementia Research
The Nathan Kline Institute for Psychiatric Research
140 Old Orangeburg Road, Bldg. 35
Orangeburg, NY 10962
Office phone: (845) 398-5427
Fax: (845) 398-5422
E-mail: hscharfman@nki.rfmh.org
Alternate: helensch@optonline.net

Number of pages:105
Number of figures, tables, multimedia, and 3D models (separately)
Figures: 13; Tables: 3; Multimedia and 3D models: 0
Number of words for abstract, introduction, and discussion (separately)
Abstract: 238 Introduction: 662 Discussion: 1843

Key Words: Hilus, hilar, CA3, field EPSP, NMDA, late EPSP, inner molecular layer, perforant path

Conflict of interest:
The authors have no competing financial interests.

Acknowledgements:
We thank Karl Deisseroth and Charu Ramakrishnan for their help in this study. This project was supported by NIH F30 MH-110165 (HLB), NIH R01 MH-109305 (HES), the Savoy Foundation (JJB) and NSERC (JJB), and the New York State Office of Mental Health (HES).

ABSTRACT

Glutamatergic dentate gyrus (DG) mossy cells (MCs) innervate the primary cell type, granule cells (GCs), and GABAergic neurons which inhibit GCs. Prior studies suggest that the net effect of MCs is mainly to inhibit GCs, leading one to question why direct excitation of GCs is often missed. We hypothesized that MCs do have excitatory effects, but each GC is only excited weakly, at least under most experimental conditions. To address this hypothesis, MC axons were stimulated optogenetically in slices. A brief optogenetic stimulus to MC axons in the inner molecular layer (IML) led to a short-latency field EPSP (fEPSP) in the IML, suggesting there was a direct excitatory effect on GCs. Population spikes were negligible however, consistent with weak excitation. FEPSPs reflected AMPA/NMDA receptor-mediated EPSPs in GCs. EPSPs reached threshold after GC depolarization or facilitating NMDA receptors. $GABA_A$ and $GABA_B$ receptor-mediated IPSPs often followed EPSPs. At the network level, an

optogenetic stimulus led to a brief, small facilitation of the PP-evoked population spike followed by a longer, greater inhibition. These data are consistent with rapid and selective GC firing by MCs (MC → GC) and disynaptic inhibition (MC → GABAergic neuron → GC). Notably, optogenetic excitation was evoked for both dorsal and ventral MCs, ipsilateral and contralateral MC axons, and two Cre lines. Together the results suggest a way to reconcile past studies and provide new insight into the balance of excitation and inhibition of GCs by MCs.

SIGNIFICANCE STATEMENT

Mossy cells (MCs) of the dentate gyrus (DG) are glutamatergic and innervate granule cells (GCs). The net effect of MCs has been debated because MCs also innervate GABAergic neurons which inhibit GCs. The results shown here suggest that MCs excite numerous GCs, but excitation is weak at GC resting potentials, and requires specific conditions to trigger GC APs. The results are consistent with a GC network that is designed for selective activation.

INTRODUCTION

The DG has been suggested to play an important role in many cognitive and behavioral functions and contributes to diverse pathological conditions (Buckmaster and Schwartzkroin, 1994; Sloviter, 1994; Ratzliff et al., 2002; Scharfman, 2016). Despite its important roles, there are many questions about DG, and one is the role of mossy cells (MCs). MCs are a major cell type of the hilus of the DG, are glutamatergic, and project primarily to the proximal third of the molecular layer (the inner molecular layer; IML; (Amaral et al., 2007; Scharfman and Myers, 2012).The IML axon terminals are primarily in parts of the DG that are far from the MC cell bodies of origin, and mostly contact GC dendrites (Ribak et al., 1985; Buckmaster et al., 1996; Scharfman and Myers, 2012). However, MC also innervate inhibitory neurons with dendrites in the IML (Sloviter, 1994; Buckmaster et al., 1996), and MCs have hilar collaterals, especially near their somata, that can innervate inhibitory neurons also (Scharfman, 1995b; Buckmaster et al., 1996; Larimer and Strowbridge, 2008). The inhibitory neurons of the DG innervate GCs, leading to the ability of MCs to indirectly inhibit GCs.

The purpose of this study was to activate MCs with more selectivity than the past to gain more insight into the excitatory effects of MCs on GCs, especially the influence of MCs on GC discharge of action potentials (APs). We focused on standard experimental conditions because past results that seem conflicting often used conditions where there was hyperexcitability (Sloviter, 1994; Santhakumar et al., 2000; Ratzliff et al., 2002; Jinde et al., 2012). We used both extra- and single cell recordings of GCs because of the possibility that the recording method influences the results, either permitting more MC-mediated excitation to be observed, or more MC-mediated inhibition.

Understanding MC effects throughout the septotemporal axis is also important because MCs have been suggested to inhibit GCs near the MC soma but primarily excite GCs when the MC → GC synapses are distal to the MC soma (Scharfman and Myers, 2012). This hypothesis is primarily based on anatomical data about the MC axon (Scharfman and Schwartzkroin, 1988; Buckmaster et al., 1996; Wenzel et al., 1997) and to our knowledge the physiological effects of the different parts of the projection have not yet been addressed. A variable that is also important to consider is whether dorsal

and ventral MCs differ because there are different characteristics of dorsal and ventral MCs in their ability to generate bursts of action potentials (APs) after pharmacological manipulations (Jinno et al., 2003), differences in dorsal and ventral MCs in calretinin expression (Blasco-Ibanez and Freund, 1997; Fujise et al., 1998), and differences in the dorsal and ventral DG (Moser and Moser, 1998; Kheirbek et al., 2013; Kesner, 2018).

To address these issues, two mouse lines with Cre recombinase (Cre) in MCs were used and a virus encoding channelrhodopsin (ChR2) and enhanced yellow fluorescent protein (eYFP) was injected stereotactically into the DG. The results suggest that optogenetic activation of MC axons in the IML leads to weak excitation of GCs that, remarkably, can be detected in all parts of the septotemporal axis. In addition, optogenetic excitation of MC axons is sufficiently common that extracellular recordings show it. We also show that excitation, although weak, can facilitate the response of GCs to the major cortical input, the perforant path (PP), but facilitation requires precise timing to align the MC-mediated and PP-mediated excitatory synaptic potentials. In contrast, IPSPs inhibit the PP response in a manner that requires much less temporal precision. The results are consistent with the idea that MCs support GC inhibition. However, MC excitation of GCs occurs, is common, and can lead to GC firing under selective conditions. This view is consistent with a network where there is selective activation of GCs, optimal for a function of the DG that has received much attention: pattern separation (Leutgeb et al., 2007; Myers and Scharfman, 2009; Yassa and Stark, 2011; Newman and Hasselmo, 2014; Knierim and Neunuebel, 2016).

METHODS

All procedures were approved by the Institutional Animal Care and Use Committee of The Nathan Kline Institute. All chemicals were purchased from Sigma-Aldrich unless otherwise specified.

I. Terminology

For the purposes of this study, the term **upper blade** refers to the blade that is closest to area CA1, and elsewhere is sometimes called superior or suprapyramidal. The **lower blade** refers to the blade furthest from area CA1, and elsewhere may be

called inferior or infrapyramidal. The crest refers to the area between the upper and lower blade, and elsewhere is sometimes called the apex. **Dorsal** DG refers to the part of the DG that is near the dorsal aspect of the forebrain and is closest to the septum. This area may also be called the **septal** DG, referring to the septal pole of the septotemporal axis. **Ventral** DG refers to the part of the DG in the ventral part of the forebrain, and is closest to the lateral or temporal pole of the septotemporal axis. It may also be called the temporal DG. The **transverse** or **lamellar axis** is a cross section through the hippocampus. Because the hippocampus curves, the transverse plane has a slightly different angle at one part of the hippocampus relative to another (Scharfman and Myers, 2012). Use of the terms are discussed further in the Results.

II. Animals and genotyping

Adult mice (male and female) were used. Two mouse lines were used that had Cre recombinase (Cre) expression in MCs. One mouse line expressed Cre in cells that have the dopamine receptor type 2 (Drd2), which, in the DG, are primarily localized to MCs (Gangarossa et al., 2012; Puighermanal et al., 2015). It has been reported that some GABAergic neurons express Cre in the mice (Puighermanal et al., 2015; Azevedo et al., 2019), so another mouse line with Cre in cells that have the calcitonin receptor-like receptor (Crlr; Jinde et al., 2012) was also used. Notably, the Drd2-Cre mice are not perfect because of the chance GABAergic neurons express Cre, and the Crlr-Cre mice appear to express Cre in ventral CA3 pyramidal cells after a ventral viral injection (see below). Therefore, the confirmation of similar effects in both mouse lines was important, and is described in the Results. The Drd2-Cre mice and Crlr-Cre mice were graciously provided by Drs. E. Valjent and Dr. K. Nakamura respectively. Hemizygous Drd2-Cre males were bred to C57BL/6NCrl females (#027, Charles River Laboratories). Hemizygous Crlr-Cre males were bred in-house to C57BL/6J female mice (#000664, Jackson Laboratories). Hemizygous Drd2-Cre or Crlr-Cre offspring were used for experiments. In a subset of experiments, hemizygous proopiomelanocortin (POMC)-Cre mice (kindly provided by Dr. Rene Hen) were bred with a channelrhodopsin (ChR2) reporter line (Ai32(RCL-ChR2(H134R)/EYFP); #012569, Jackson Laboratories) to produce mice with ChR2 in GCs.

Mice were bred in-house. Breeders were provided a nestlet (2”x2”; W.F. Fisher) and fed Purina 5008 chow (W.F. Fisher). After weaning offspring at 25-30 days of age, mice were housed with others of the same sex (2-4/cage) and fed Purina 5001 chow (W.F. Fisher). At all times, mice were provided food and water *ad libitum*. They were housed in standard mouse cages with a 12 hr light:dark cycle and relative humidity between 64-78%. Mice were housed overnight in the laboratory (2-4/cage) prior to use because non-acclimatized animals exhibit poor DG and CA3 synaptic responses in hippocampal slices. Tail samples were frozen and genotyped later (Mouse Genotyping Core, New York University Medical Center).

III. Viral expression of channelrhodopsin (ChR2)

A. Viruses

The viruses used for optogenetics were adeno-associated virus (AAV) serotype 2-Ef1a-DIO-hChR2(H134R)-eYFP or AAV5-Ef1a-DIO-hChR2(H134R)-eYFP to express humanized ChR2 tagged with eYFP in Cre-expressing cells. Titers for all injected viruses were ~10^{12} vector genomes (vg) per ml. Aliquots of 5 µl of each virus were stored at -80°C until the day of use. Viruses were obtained from the Karl Deisseroth laboratory or the University of North Carolina Vector Core.

B. Surgical injection of viruses

Animals (6-8 weeks old) were anesthetized with 4% inhaled isoflurane in an induction chamber (#V711801; SurgiVet), then transferred to a rodent stereotaxic apparatus (#502063, World Precision Instruments; WPI). Body temperature was maintained at 37°C with a homeothermic heating pad (#507220F, Harvard Apparatus) for the duration of surgery. Isoflurane (1-2%; Aerrane, Piramal Enterprises) mixed with oxygen was delivered through a nose cone (WPI). Buprenex® (buprenorphine; 0.1 mg/kg, subcutaneous; Reckitt-Benkiser Pharmaceuticals) was administered shortly after the onset of anesthesia to reduce discomfort. The skin of the head was shaved, sterilized with Betadine (Purdue Products) and 70% ethanol (Pharmaco-Aaper), and then an incision was made. A hand drill (#177001, Dremel Instruments) was used to create a craniotomy above the injection site. Using a nanoliter-precision automated

syringe pump (#UMP3, WPI) with a syringe (#Nanofil, WPI) and 33-gauge needle (#INanofil-10F, WPI), 150 nl of virus was injected into hippocampus at 100 nl/min. For extracellular and sharp intracellular recordings there was one site, either the left dorsal or left ventral hippocampus (Table 1). For most whole-cell recording, more than one injection site was used (Table 1; see Results). The needle was left at the injection depth for 5 minutes to allow diffusion of the virus before being slowly retracted. The incision was closed with Vetbond (3M Inc.). Animals were transferred to a clean cage and observed until they recovered from anesthesia. They were housed alone until use.

IV. Evaluation of expression

A. Perfusion-fixation

Animals were deeply anesthetized with isoflurane (by inhalation in a closed glass jar) followed by urethane (2.5 g/kg, intraperitoneal or i.p.). The abdominal cavity was opened and the animal was transcardially perfused with ~10 ml 0.9% NaCl in distilled (d)H_2O followed by 20 ml 4% paraformaldehyde in 0.1 M phosphate buffer (PB; pH 7.4), using a 25 gauge butterfly needle attached to a peristaltic pump (#Minipuls 2, Rainin). Brains were removed and postfixed overnight at 4°C and then cut into 50 µm coronal sections using a vibratome (#TPI1000, Ted Pella, or VT1000P, Leica). Sections were collected into cryoprotectant (25% glycerol, 30% ethylene glycol, 45% 0.1M phosphate buffer) and stored at 4°C.

B. Immunohistochemistry

Immunofluorescence was conducted as previously described (Duffy et al., 2013). Free-floating sections were washed in 0.1 M PB (3 times, 5 min each) and transferred to blocking serum (10% normal donkey serum for parvalbumin (PV); 10% normal goat serum for GluR2/3 and neuropeptide Y (NPY), and 0.25% Triton-X 100, diluted in 0.1 M PB) for 1 hour. Sections were then transferred directly to primary antibody solution (0.25% Triton X-100 diluted in 0.1 M PB), incubated with primary antibody (mouse monoclonal to PV (1:500; #MAB1572, Millipore), rabbit polyclonal to GluR2/3 (1:100; #AB1506, Millipore) or NPY (1:1000; #T-4070, Peninsula), and gently agitated on a rotator overnight at 4°C. The next day, sections were washed in PB (3 times, 5 min

each) and then incubated with secondary antibody (AlexaFluor 546 Donkey anti-mouse for PV, goat anti-rabbit for GluR2/3 or NPY, both 1:400, Thermo Fisher Scientific Inc.) in secondary antibody solution (1% normal donkey serum for PV or 1% normal goat serum for GluR2/3 or NPY, and 0.25% Triton-X 100, diluted in 0.1 M PB). After washing in PB (3 times, 5 min each), sections were mounted and allowed to dry at room temperature overnight. Slides were coverslipped using ProLong Gold antifade solution (Thermo Fisher) and stored at 4°C.

Stained sections were imaged on a laser scanning confocal microscope (#LSM 510; Zeiss Inc.). Double fluorescent labeling was quantified using LSM ImageBrowser software (Zeiss). Double labeling was determined by acquiring z-stack images at 1.5-2.0 µm intervals of a cell and locating the brightest optical section of the cell for each color channel. A cell was considered double labeled if the brightest optical sections of a cell were at the same depth. Cells that appeared to be double labeled but were actually overlying one another could be discriminated with this method and an example is shown in the Results.

V. Physiology

A. Field recordings and sharp intracellular recordings

1) Slice preparation

Mice were rapidly anesthetized with isoflurane by inhalation. While deeply anesthetized, mice were decapitated, the brain rapidly dissected and placed in a 4-8°C artificial cerebrospinal fluid (ACSF) with sucrose instead of NaCl (in mM: 252 sucrose, 3.5 KCl, 2.0 $MgSO_4$-7H_2O, 2.4 $CaCl_2$, 1.25 NaH_2PO_4, 26 $NaHCO_3$, 10 D-glucose, pH 7.4). After 1-3 min, the brain was blocked to cut it transversely or horizontally. For transverse sections, slices were cut at an approximately 15° angle to the coronal plane so most of the dorsal hippocampus would be cut along the transverse or lamellar axis. The extreme septal pole was excluded from use because the upper DG blade is abbreviated. For horizontal sections, the dorsal surface of the brain was trimmed so it would lie flat and horizontal sections were cut from the ventral hippocampus until the sections were outside the transverse axis. The extreme pole was not used because it is

outside the transverse axis. We acknowledge that the use of the term transverse is approximate.

For all sectioning, the brain was glued to a metal plate using cyanoacrylate. The metal plate was placed in a holding container filled with chilled sucrose-based ACSF and cut (400 µm thick) using a vibratome (#Microm HM 650V, Richard-Alan Instruments). Sections containing hippocampus and adjacent regions were trimmed and then placed in room temperature sucrose-based ACSF in a beaker with carbogen (5% CO_2/95% O_2) for 1-5 min. Slices were transferred to an interface-style recording chamber (made in-house; Scharfman 2001). Using this chamber, all slices could be maintained under similar conditions immediately after the dissection until the end of the experiment when they were removed and fixed by immersion in 4% paraformaldehyde in 0.1M Tris buffer.

Slices were placed on a nylon mesh, ACSF entered from below, and ACSF was wicked over the mesh and to a distant exit port with Kimwipes®. This arrangement kept slices submerged up to their upper surfaces. Warmed (32°C) humidified air was vented over the surfaces. Slices were in the chamber for 30 min with sucrose-based ACSF at 1-2 ml/min (#Minpuls 2, Gilson) and then NaCl-based ACSF (125 mM NaCl instead of sucrose) was used. Recordings began at least 30 min after the switch from sucrose-based ACSF to NaCl-based ACSF and terminated up to 6 hrs later.

The interface chamber does not allow visualization of DG neurons to judge their health so slices were initially screened for viability using field potential recordings of the response to an electrical stimulus to the PP. For PP stimulation, a stimulating electrode was placed on the slice surface at the point along the hippocampal fissure just below the subiculum where the PP is a white fiber bundle as it enters the DG. Field recordings were made in the GC layer (GCL) at the border with the hilus, either near the crest, or near the center of the upper blade, approximately 250 µm from the stimulating electrode. To assess viability, the population spike was not used because the GCs do not generate many APs normally, so the population spike is normally small. The amplitude of the positivity, upon which the population spike is superimposed, was used instead, since past studies found that when the positivity is >3 mV and the population spike is small (<2 mV) many GCs can be recorded intracellularly with characteristics

consistent with healthy cells (Scharfman, 1991; Scharfman, 1994b; Scharfman et al., 2000; Scharfman et al., 2002).

2) Stimulating and recording electrodes

Monopolar electrodes used for stimulation were made from 35 µm-diameter Teflon-coated stainless-steel wire (A-M Systems Inc.) and triggered in pClamp (Molecular Devices) using 50 µA amplitude, 10-100 µsec duration square pulses, generated from a stimulus isolation unit (#Isoflex, AMPI Instruments).

Electrodes used for extracellular recording were 1-5 MΩ and filled with NaCl-based ACSF. Intracellular “sharp" electrodes were 60-90 MΩ and filled with filtered (0.2 µm polypropylene filters, Nalgene) 1 M potassium acetate in dH_2O. Electrodes were pulled from capillary-filled 1.2 mm o.d., 0.85 mm i.d. borosilicate glass (WPI) using a horizontal puller (#P-87, Sutter Instruments). Signals were digitized at 10 kHz for field and 30 kHz for intracellular recordings (#Axoclamp2B and Digidata 1440A, Molecular Devices). For intracellular recordings, the bridge was balanced whenever current was passed. Cells were not accepted unless their resting potentials were at least -60 mV, action potentials were >90 mV, and their input resistance at -60 mV was >70 MΩ.

B. Whole-cell recording

1) Slice preparation

Mice were prepared as described above, but the sucrose ACSF contained (in mM): 90 sucrose, 80 NaCl, 2.5 KCl, 1.25 NaH_2PO_4, 25 $NaHCO_3$, 10 D-glucose, 4.5 $MgSO_4$-$7H_20$, and 0.5 $CaCl_2$. Only horizontal slices were cut and they were 350 µm thick instead of 400 µm. After slice preparation, slices were placed in a holding chamber (made in-house) in oxygenated (95% O_2, 5% CO_2) sucrose-based ACSF. The holding chamber was placed in a water bath (Poly Pro Water Bath, Revolutionary Science), and the temperature was increased incrementally to 35ºC over 15-20 min and maintained at 35°C thereafter. After slices had been in the holding chamber for 45 min, slices were kept in sucrose-based ACSF and were at room temperature until use.

2) Whole-cell recording

Slices were placed in a recording chamber (Model #RC-27LD, Warner Instruments), held with a nylon mesh (Item #SS-4-500H, Warner) and warmed to 32°C with an in-line heater (Item #SH-27B, Warner) at 6-7 ml/min, controlled by a peristaltic pump (#Masterflex C/L, Cole-Parmer). Slices were visualized with an infrared differential interference microscope (#BX51WI, Olympus). Slices were perfused with NaCl-ACSF containing the same constituents as described above except 1) 130 mM NaCl was used instead of 126 mM for extracellular and sharp recordings, and 2) 2.5 mM KCl was used instead of 3.5 mM. The different concentrations were based on past experience to optimize viability of slices in the different chambers.

Recording electrodes were pulled from borosilicate glass (1.5 mm outer diameter and 0.86 mm inner diameter, Sutter Instruments) using a micropipette puller (#P-97, Sutter) with tip resistance between 5-10 MΩ. Internal solution was filtered (#0.02 µm, Whatman Anotop 10 syringe filter; Fisher) before use and contained (in mM): 130 potassium gluconate, 4 KCl, 2 NaCl, 10 4-(2-hydroxyethyl)-1-piperazine ethanesulfonic acid (HEPES), 0.2 ethylene glycol-bis(β-aminoethyl ether)-N,N,N′,N′-tetraacetic acid (EGTA), 4 adenosine triphosphate magnesium salt, 0.3 guanosine triphosphate tris salt, 14 di-tris phosphocreatine, 0.2-0.5% biocytin, and was adjusted to pH 7.25 using 1M potassium hydroxide. Final osmolarity was 280-290 mOsm without biocytin. Aliquots were frozen (-20°C) until use and used within 6 months.

C. Analysis

1) Morphology

Hippocampal slices were removed from the recording chamber, placed into a beaker of 0.9% saline and then fixed in 4% paraformaldehyde in 0.1M phosphate buffer (PB; pH 7.4). Slices were stored at 4°C until processing. GCs were visualized with brightfield or fluorescent microscopy.

a. Brightfield

Slices were incubated in 1% Triton-X 100 diluted in 0.1M Tris buffer (TB, pH 7.6) for an hour, then transferred to 0.1% H_2O_2 diluted in TB for 30 min. After washing in 0.25% Triton X-100 in TB (3 x 10 min), slices were incubated in ABC solution (Vector

Laboratories) diluted in TB overnight at 4°C as described elsewhere (Scharfman et al., 2002). Slices were washed (3 x 10 min) and then transferred to 0.05% 3,3'diaminobenzidine (DAB, Sigma-Aldrich) with 1 mM $NiCl_2$ in TB for 30 min followed by incubation in 0.05% DAB and 0.0075% H_2O_2 in TB. After the reaction, slices were washed (3 x 10 min, TB) and dehydrated in a graded series of ethanol solutions (1 x 5 min each: 25%, 50%, 75%, 80%, 90%, 95%, all in dH_2O) followed by two incubations for 5 min (each) in 100% ethanol and then slides were transferred to Xylene (2 x 5 min). Slices were coverslipped in Permount (Electron Microscopy Sciences). Images were taken using an upright microscope (#BX61, Olympus) and camera (#Retiga R2000, Teledyne QImaging) with ImagePro Plus software (v. 7; Media Cybernetics).

b. Fluorescence

For the fluorescent peroxidase substrate AmplifluRed (Sigma-Aldrich), slices were rinsed in TB (3 x 10 min) and transferred to 2 µM AmplifluRed and 0.003% H_2O_2 in TB. The reaction was terminated by a 10 min TB rinse followed by counterstaining in using 2 µM Hoechst 33342 (Thermo Fisher) in TB for 10 min. Slices were washed in TB and exposed to a graded series of glycerol solutions (15 min each: 25%, 40%, 55%, 70%, 85%, 90% in dH_2O). Slices were coverslipped in a TB solution containing 0.5% N-propyl gallate and 90% glycerol in 20 mM Tris (pH 8.0). The method is from the Nikon Imaging Center (Harvard Medical School) website (https://nic.med.harvard.edu/ resources/media/). The edges of coverslips were sealed by nail polish.

For Strepavidin-Cy3 (Jackson ImmunoResearch Inc.), slices were treated with 1% Triton X-100 in TB and then transferred to the 0.1% H_2O_2 step described above. Instead of ABC solution, slices were incubated with Strepavidin-Cy3 (1:2000 in 0.25% Triton X-100 in TB) overnight at 4°C. Slices were then treated with the same procedure as described above for AmplifluRed. Images were acquired using a confocal microscope (#LSM 880, Zeiss).

2) Electrophysiology

Recordings were analyzed offline using Clampfit (v. 10.7 or 11.1; Molecular Devices). **Resting membrane potential** (RMP) was defined as the difference between

the MP during recording (without current injection) and the extracellular potential after the recording. $\mathbf{R_{in}}$ (input resistance) was calculated from the slope of the voltage-current (V-I) relation based on steady state measurements of responses to current commands (5 pA steps, -45 pA to +45 pA) from RMP. **Time constant** (τ) was defined as the point when the MP reached 0.63% of the response at steady state. It was determined from the exponential fitted to the onset of the response to a hyperpolarizing 5-10 pA step at RMP using Clampfit. **Action potential** (AP) amplitude was defined at RMP, using the AP elicited by a 500-1500 msec depolarizing current step that was approximately at threshold for AP generation. AP amplitude was measured from 1) RMP to the AP peak and 2) from the point during the depolarizing step that the rapid rising phase began. **Threshold** MP was defined in two ways because the use of this term varies in the literature. One definition of threshold MP was where an AP was triggered if cells were depolarized with the least amount of tonic DC current to produce APs. Second, threshold MP was measured from the response to the minimal depolarizing current command (500-1500 msec duration) from RMP when an AP was evoked in approximately 50% of trials. This second use of the term threshold MP was where the onset of the rapid rise of the AP began. A three-point tangent slope vector was used in Clampfit to find the MP where the rapid rise of the AP began (slope $\geq$ 10 V/s). **Half-width** was defined as the time between AP onset (the time an AP initiated its rapid rising phase) to the time the AP reached half its amplitude. AP rising **slope and decay** slope were defined as the maximum slope of the rising and decay phases.

VI. Optogenetics

A 200 µm-diameter fiber optic cable (#M86L01l, Thorlabs) was modified by removing the ferrule and rubber coating from the tip, stripping approximately 2 cm of covering (cladding), and polishing the bare fiber tip with fine emery cloth. The fiber tip was approximately 150 µm thick and threaded through a glass Pasteur pipette with the tip extruding approximately 2 cm. The Pasteur pipette was held by a micromanipulator (#NMN-21, Narashige) so that it was approximately 3 cm from the slice surface (for extracellular and sharp recordings). The glass holder was slanted 15-20° from vertical. For whole-cell recording, the light fiber was positioned 55° from vertical (or 35° from

horizontal). Blue light was generated by attaching the fiber to a 473 nm DPSS laser (#LRS-0473, Laserglow), after power was adjusted to 10 mW with a power meter (#PM100D, Thorlabs). Light pulses (typically <2 msec duration) were triggered 1/min or in pairs 10-200 msec apart (1 pair, every 1-2 min), or trains of 3-5 pulses at 5, 25 or 100 Hz (also 1 train/1-2 min).

VII. Pharmacology

The AMPA receptor antagonist cyanquixaline (6-cyano-7-nitroquinoxaline-2,3-dione; CNQX disodium salt; Tocris Biosciences) or 6,7-Dinitroquinoxaline-2,3(1H,4H)-dione (DNQX disodium salt; Tocris) was dissolved in 0.9% NaCl to make a 10 mM stock solution, stored at -20°C and defrosted on the day of the experiment. Stock solutions of the NMDA receptor antagonist DL-2-amino-5-phosphonovaleric acid (DL-APV), $GABA_A$ receptor antagonists bicuculline methiodide and the $GABA_B$ receptor antagonist CGP52432 (all from Sigma) as well as the $GABA_A$ receptor antagonist gabazine (Tocris) were prepared in a similar manner.

VIII. Statistics

Results are expressed as means ± standard error of the mean (SEM). Power analysis was used to determine if sample size was adequate, for alpha = 0.05 and 80% power (Statmate2; Graphpad). Statistics were conducted using Prism (v. 8, GraphPad). Comparisons of two groups were made using Student's t-test (unpaired, two-tailed) and one- or two-way Analysis of variance (ANOVA) or repeated measures ANOVA (RMANOVA) for more than two groups. For ANOVAs, Tukey-Kramer post-hoc tests were conducted to assess statistical differences between groups. Interactions are not reported for ANOVAs if they did not reach significance. Planned comparisons were made to compare predefined experimental variables as explained in the Experimental design section below.

Nonparametric tests were conducted when data were not normally distributed or there was heteroscedasticity of variance by Brown-Forsythe and/or Bartlett's tests that could not be corrected by log transformation of the data. For two groups, Mann-Whitney U test was used and the Kruskal-Wallis test for more than two groups.

IX. Experimental design

Animals were injected with virus in the DG of one hemisphere (Fig. 1A). Slices were prepared afterwards from either the ipsilateral or contralateral hemisphere. Recordings were made of GCs extra- or intracellularly. Intracellular electrodes used sharp or patch electrodes. Biocytin was used in some whole-cell recordings to confirm GCs were chosen. An optic fiber was aimed at a sublayer of the DG, usually the IML, and brief light pulses were used to activate ChR2-expressing MC axons in the IML. Planned comparisons were made of 1) recording sites that were either ipsilateral or contralateral to the site of viral injection, 2) effects of MCs that were found in the dorsal vs. ventral DG, 3) effects of MCs that were recorded from the upper blade or another site in the GCL, 4) effects in Drd2-Cre vs. Crlr-Cre mice, and 5) the two sexes.

In some experiments, electrical stimulation of the IML was compared to optogenetic stimulation of the IML, or the PP was stimulated electrically to determine the effect of the MC input on the PP input to GCs. For PP stimulation, the optogenetic stimulus was timed at various delays before or after a PP stimulus. In this way, the effect of the MC input on the PP input was assessed. Pharmacology was used to determine what glutamatergic and GABA receptors mediated GC responses to optogenetic stimulation.

There were several types of controls and these are described in detail in the Results. For example, specificity of the Cre mice was checked. Also, control recordings were made to ensure the degree of light (power, duration) did not influence GCs extracellularly and intracellularly when there was no ChR2 expression. This was checked in Cre- mice and mice that were Cre+ but lacked expression. In the latter, post hoc examination of the brain sections showed there was no expression due to a technical problem (e.g., the needle track missed the DG). In addition, mice with ChR2 in GCs instead of MCs were tested to confirm results were different. Finally, although not strictly defined as controls, a section of the Results is dedicated to experiments that simply address whether the results we obtained could withstand additional tests. This part of the Results is about whether optogenetic stimulation evoked weak excitatory effects in GCs.

RESULTS

I. Specificity of Drd2-Cre mice and Crlr-Cre

A. Drd2-Cre mice

It was important to verify specificity of the Drd2-Cre hemizygous mice (referred to as Drd2-Cre, below) to MCs because a previous description of these mice indicated Cre expression of a small group of hippocampal interneurons (Puighermanal et al., 2015). This was particularly important because some laboratories have used the mice and not discussed interneuron expression. Interneuron expression may depend on the amount of virus that is injected because a recent paper reporting expression in both MCs and interneurons used 500 nl injection (Azevedo et al., 2019) whereas the volume we used, 150 nl, showed little (see below).

To evaluate expression following viral injection, 5 Drd2-Cre mice were injected with AAV2-EF1a-DIO-eYFP (Fig. 1A-B) and euthanized 10-18 days later to examine eYFP expression. As shown in Fig. 1C1, the hilus was labeled extensively at the injection site in the DG. Sections in or near the injection site showed strong eYFP-labeling of neuronal somata in the hilus, with few somata outside the DG, consistent with a Cre line specific for MCs. Sections that were distal to the injection site showed prominent labeling of fibers in the IML (Fig. 1C2-5). The weak IML labeling near the injection site and strong IML labeling distal to the injection site is consistent with the MC axon projection in the distal IML primarily (Buckmaster and Amaral, 2001). In additional experiments, where the viral construct was ChR2-eYFP instead of eYFP alone, expression was similar to Fig. 1 (data not shown).

To address specificity for MCs further, eYFP-expressing cells were double-labeled using an antibody to the 2/3 subunit of the ionotropic glutamate receptor (GluR2/3; Leranth et al., 1996). Mice were either injected in dorsal (n=3) or ventral DG (n=2). An example from a mouse injected dorsally is shown in Fig. 2. For quantification, sections were selected from the injection site and areas next to it (5-7 sections/mouse, 300 µm apart). In the mice injected in dorsal hippocampus, 538/545 (98.6%) of hilar eYFP-expressing cells also expressed GluR2/3 (Fig. 2A-B). For the mice injected

ventrally, 661/695 (94.8%) cells were double-labelled. For these determinations, the hilus was defined as zone 4 of Amaral (Amaral, 1978).

In contrast to double-labeling of eYFP and GluR2/3, no eYFP-expressing cells were labeled using an antibody to PV (Fig. 2C) which stains a major subclass of DG GABAergic neurons called basket cells (also called perisomatic targeting cells; (Sloviter, 1994; Freund and Buzsaki, 1996; Houser, 2007; Hosp et al., 2014). It was extremely rare to find eYFP-expressing cells double-labeled using an antibody to NPY, which is a marker of a major subset of hilar GABAergic cells called HIPP cells (GABAergic neurons with a ***Hi***lar cell body and projection to the terminal zone of the ***P***erforant ***P***ath; (Bering et al., 1997; Freund and Gulyas, 1997; Scharfman et al., 2002; Scharfman and Gray, 2006; Sperk et al., 2007); Fig. 2D). Double-labeling occurred in 4/337 (1.2%) of hilar cells that also expressed eYFP (for dorsal injections) and 9/328 (2.7%) for ventral injections. These data suggest that there was up to 3% of cells that showed expression and were not MCs in Drd2-Cre mice.

B. Crlr-Cre mice

For Crlr-Cre mice, expression of eYFP was similar to Drd2-Cre mice when virus was injected in dorsal hippocampus (Fig. 3A). However, ventral injections led to labeling of a subset of CA3 PCs in CA3b and c (Fig. 3B). The labeling of some CA3 PCs was noted in a prior report (Jinde et al., 2012) but it was not clear whether this varied across the septotemporal axis and if it was sufficient to have physiological effects. We saw the CA3 labeling ventrally after ventral injections only (Fig. 3B). To determine if there was sufficient expression in CA3 to produce a potentially confounding effect, tests were made in slices. As shown in Figure 3B, brief optogenetic pulses (<2 msec) were focused at the CA3 cell layer near the recording site in the CA3 cell layer. Robust field potentials were recorded that were consistent with activation of many CA3 PCs (n=3 slices, 2 mice).

The ChR2-evoked field potentials that were recorded in the PCL had morphology that was not exactly like prior recordings of CA3 population spikes (evoked by electrical stimulation of afferents to CA3, e.g. Scharfman et al., 2003). There was an unusual slow negative deflection before what appeared to be a population spike, but the population

spike was long in duration, making it unusual. Therefore, we checked another mouse line with ChR2 in another cell layer, the GCL to ask if the unusual features of what we recorded in CA3 were due to the use of ChR2 rather than afferent input to activate a population spike. In this mouse line, Cre is expressed in cells with the proopiomelanocortin (POMC) promoter (POMC-Cre mice). This mouse line was crossed to a ChR2 reporter line (see Methods). Progeny had robust ChR2-GFP expression in GCs with a high degree of specificity (Fig. 3) as previously reported (Overstreet et al., 2004). Light directed to the GCL evoked a similar, somewhat unusual population spike (Fig. 3C) as the one evoked in the CA3 PCL using ChR2 (Fig. 3B), when the optogenetic stimulus was weak. These data suggest that optogenetic stimulation evoked PC activation in ventral PCs of Crlr-Cre mice, probably by weak, direct excitation of the ChR2 in PCs. The weak activation and direct excitation contributed to differences from past recordings of population spikes evoked by afferent stimulation. Therefore, subsequent viral injections in Crlr-Cre mice were only made in dorsal DG.

II. Optogenetic responses: evidence that excitation is widespread but weak

A. General information

There were 26 animals injected with virus encoding ChR2 that were used for extracellular and sharp electrode recordings. They were 80.3 ± 7.6 days old when they were used for slice preparation, and the average time between viral injection and slice experiments was 23.9 ± 2.4 days. The majority of the 26 animals were Drd2-Cre (n=18) and the others were Crlr-Cre (n=8). Of the 26 mice, 19 received dorsal injections and the 7 others had ventral injections (Table 1). All Crlr-Cre mice had dorsal injections, for reasons mentioned in the preceding section.

Preliminary experiments tested whether any subfield of the hippocampal slice showed a response to light using extracellular recording and Drd2-Cre mice (1-6 slices /mouse, 6 mice). The objective was to determine whether responses could be detected, and where, so that subsequent experiments could focus on responsive areas. For CA1, sites for optogenetic stimulation were stratum pyramidale, stratum radiatum or stratum lacunosum-moleculare. Recording sites were 100-250 µm away from the tip of the optic fiber and in the same layer. Light pulses were tested that were up to 20 msec long and

10 mW intensity. In CA3, light was focused on stratum oriens, stratum pyramidale, stratum lucidum and stratum radiatum, with recording sites up to 250 µm away and in the same layer. There were no detectable effects of light in area CA1 or CA3. We then turned to the DG in the same slices and recorded in the hilus with the same light pulse durations/intensity, but the optic fiber was directed to different parts of the DG or CA3c. For every site, the optic fiber was directed to a specific sublayer, with a recording 100-250 µm away in the same layer (or the GC layer). Even long pulses (20 msec) failed to exhibit responses in most locations. The one combination of optic fiber position and recording site that was successful used light directed at the IML with a recording position that was in the IML or adjacent to it. With these optogenetic stimulus and recording positions, a brief stimulus could elicit what appeared to be a field excitatory postsynaptic potential (fEPSP) in the IML (Fig. 4). In the GCL and MML there was a similar but smaller response (Fig. 4).

B. Optogenetic stimulation of the IML evokes a fEPSP

The ability to elicit an extracellularly-recorded response to light in the IML suggested numerous GCs responded to the light pulse. The characteristics of the response supported the idea that it reflected EPSPs in GCs. Thus, responses were graded like an EPSP, i.e. increasing the duration of the light pulse led to a graded increase in slope and amplitude (Fig. 4A1-4). The fEPSP had a rapid onset, usually beginning at the end of the light pulse or shortly thereafter (Fig. 4A2). To determine the mean latency to onset, responses were chosen that were between 50 and 100% of the maximum response. The mean latency to onset, measured from the end of the light pulse, was 0.69 ± 0.11 msec (n=42 slices, 16 mice). The mean latency to onset, from the start of the pulse, was less than 3 msec because the light pulses were less than 2 msec long. These latencies suggest that the fEPSP reflects a monosynaptic pathway (MC → GC). Characteristics of latency, slope and amplitude of fEPSPs are shown in Table 2.

Consistent with the idea that fEPSPs were excitatory, and glutamate is the neurotransmitter of MCs (Soriano and Frotscher, 1994; Scharfman, 1995b), the AMPA receptor antagonist CNQX (10 µM) decreased the fEPSP (to 23.7±8.1% of control after

30 min, n=3 slices, 1 slice/mouse), but the $GABA_A$ receptor antagonist bicuculline methiodide did not (BMI; 10 µM; 100.4 ± 0.7% of control at 30 min, n=4 slices, 1 slice/mouse; described further below).

C. FEPSPs are specific for MC axons in the IML

Other characteristics of fEPSPs were identified by changing the position of the optic fiber (Fig. 4B1-2). In 18 slices from 12 mice, minor movements of the optic fiber were made either towards the MML or in the other direction, towards the GCL. In each case the fEPSP decreased greatly even by minor movement of the optic fiber (Fig. 4B2). In contrast, movements of the optic fiber within the IML, either further (up to 300 µm) or closer to the recording pipette, had little effect on the fEPSP amplitude (<5% change in amplitude, n=12 slices in 6 mice; data not shown). The similarity of responses when the light fiber was moved along the IML instead of adjacent layers is consistent with the en passant synapses of MCs in the IML (Buckmaster et al., 1992; Buckmaster and Schwartzkroin, 1994; Buckmaster et al., 1996; Wenzel et al., 1997). Specificity of fEPSPs to the IML was also evident from recordings of a fiber volley before the EPSP with recording sites in the IML (10/34 fEPSPs; Fig. 4C). When a fiber volley was recorded in the IML, the fiber volley was absent when the recording site was moved to the GCL or MML.

To confirm the responses to light were due to activation of MC axons, fEPSPs were tested for sensitivity to WIN 55,212 mesylate (WIN), a cannabinoid receptor type 1 (CB1) agonist which is highly expressed on MC terminals in the IML (Chiu and Castillo, 2008). Exposure to 5 µM (n=2 slices in 2 different mice) or 10 µM (n=1 slice in a 3rd mouse) WIN for 30 min reduced the slope and amplitude of the light-evoked fEPSP to 44.0 ± 4.9% of control in 30 min (Fig. 4D). The fact that the fEPSP was not completely blocked may be due to the weak affinity of WIN for CB1 receptors on glutamatergic terminals relative to non-glutamatergic terminals (Hajos and Freund, 2002).

Specificity of optogenetically-triggered fEPSPs to the IML was also supported by current source density analysis (Fig. 4E1; n=5 slices, 5 mice). Thus, when light was focused on the IML and the recording electrode was systematically moved from the hilus to the hippocampal fissure (along a path oriented perpendicular to the GCL), the

fEPSP increased as the IML was approached and decreased when recordings were further and further away from the IML (Fig. 4E1). In agreement with those data, current source density analysis showed a current sink in the IML (Fig. 4E1; n=3 slices, 1/mouse). In contrast, the response to PP stimulation produced a current sink in the area of the OML or MML, where its synapses are located (Fig. 4E2; n=4 slices, 3 mice).

III. Evidence that optogenetic excitation is common but weak in GCs

At the resting membrane potential (RMP) of GCs, the field potential that appears to be a fEPSP is a negativity that could correspond to an EPSP or a depolarizing IPSP. Therefore, intracellular recordings of GCs were made near the site of extracellular recording with sharp microelectrodes. Sharp microelectrodes allowed intracellular recording in the interface-style recording chamber that was used for extracellular recordings. GCs showed small depolarizations at RMP in 32/34 GCs from 5 slices (5 mice; 1 slice/mouse; Fig. 5A1-2). The two exceptional GCs had no detectable effects of light, suggesting that some GCs either lack input from MC axons that expressed ChR2, or expression of ChR2 was insufficient in the MC axons that innervated these GCs.

The onsets of the light-evoked depolarizations were similar and rapid (<2 msec); Fig. 5A1-2), consistent with the field recordings and a monosynaptic MC → GC pathway. None of these GCs had a suprathreshold response to light at the RMP, which is consistent with the small size of most fEPSPs (the maximum fEPSP recorded in the IML was 1.78 ± 0.39 mV; n=19 slices, 16 mice; Table 2). However, when GCs were depolarized, an AP was elicited at the peak of the depolarization (n=12/12 cells tested; Fig. 5A1-2).

At the depolarized potentials, IPSPs were observed (Fig. 5A2). They truncated the EPSP at 3.8-4.2 msec after the end of the light pulse (Fig. 5A2). Thus, excitation appeared to begin within 2 msec of the end of the optogenetic stimulus and inhibition was evident approximately 2 msec later. This timing is consistent with monosynaptic excitation (i.e., MC → GC) and disynaptic inhibition (MC → GABAergic neuron → GC). However, the latency (to the point during the EPSP when it was truncated sharply by inhibition) was surprisingly rapid for a disynaptic pathway. Therefore it is notable that there is an unusually fast pathway between the primary GABAergic cell in the DG, the

basket cell, and GCs (Norenberg et al., 2010; Hu and Jonas, 2014). Notably, the basket cells has been suggested to mediate the disynaptic inhibitory effects of MCs on GCs (Sloviter, 1991; Sloviter, 1994). However, the results also suggest a possible direct pathway (GABAergic neuron → GC), which is discussed further below.

IV. Controls

A. General information about controls

In 28 slices (7 animals) there was no detectable response to light in the IML or nearby (GCL, MML). The expression of virus was only checked after the recordings were made and the slice was removed and brought to a microscope. In each of these animals the slices had no detectable fluorescence. We assume the reason was the injection needle used to inject virus clogged or the tip of the needle did not reach the hippocampus, because we saw evidence for these possibilities in previous studies.

In addition to these experiments, three mice were used that lacked Cre recombinase and did not have a viral injection. They were recorded with the same conditions (same laser fiber, power, etc.). No response to light could be detected by a recording in the hilus, GCL, IML or MML (n=5 slices), with the light fiber pointed at the IML, <200 µm from the recording sites. Even long pulse durations (up to 50 msec) with increased power (up to 50 mW) were ineffective.

B. Addressing the strength of EPSPs in GCs elicited by optogenetic stimulation

The lack of evidence for a suprathreshold effect of MCs on GCs was surprising given the proximal site of MC input to GC somata. Therefore, we used another approach to confirm the weak effect. We examined the response recorded in stratum lucidum (SL) of CA3 to the same optogenetic stimulus that was used to elicit the fEPSP in the IML (diagrammed in Fig. 5B1a). One would predict that the response would be too small to detect in SL, because few GCs would reach threshold, a requirement for GC axons (mossy fibers) to release sufficient transmitter to produce a fEPSP in SL. A representative example of recordings is shown in Fig. 5B1b. The fEPSP recorded in the IML was small, as described above (Fig. 5B1b, IML). When the recording electrode was moved to the GCL, there only was a small population spike (Fig. 5B1b, GCL). There

was no response recorded in SL (Fig. 5B1b, SL). These data are consistent with the idea that the EPSP elicited by MCs in GCs is indeed a weak EPSP.

The morphology of the fEPSP produced by IML optogenetic stimulation was somewhat surprising, because the population spike occurred late in the fEPSP, after the initial peak. Therefore, we asked if another proximal excitatory synapse, the mossy fiber synapse on CA3 PCs,s behaves in a similar way. This synapse is considered to potentially be very strong, but weak hilar stimulation of GC axons can elicit small fEPSPs in PCs (Skucas et al., 2013; Harte-Hargrove et al., 2015).

Therefore, we compared the MC axon synapse on GC proximal dendrites to the mossy fiber synapse on CA3 PC proximal apical dendrites. We first stimulated the IML optogenetically to obtain a response in the GCL with the typical small, late population spike. Next, we used a weak electrical stimulus to the subgranular zone to activate mossy fibers, and recordings were made in SL and then the PCL of CA3 (Fig. 5B2a-b). The PCL response to weak hilar stimulation was like the GCL response to IML stimulation, qualitatively (Fig. 5B1b, GCL vs. 2b, PCL). In other words, 1) there was a very small population spike-like event, and 2) the population spike-like event occurred later than one would expect of a fEPSP. Therefore, the qualitative characteristics of the MC → GC fEPSP were not consistent with weak activation of a proximal input.

Next, we addressed the possibility that use of ChR2 limited the MC → GC excitation. In other words, the MC → GC pathway was not weak, but using ChR2 made it appear weak because ChR2 interfered with synaptic transmission. For this purpose, we used optogenetic stimulation of GCs (rather than MC axons) to confirm ChR2 could strongly activate a neuron under our recording conditions, and furthermore, such activation would lead to activation of CA3. To do this we used a POMC-Cre mouse line bred with a mouse from a ChR2 reporter line to express ChR2 in GCs and their mossy fibers (see Methods; Fig. 3). Optogenetic stimulation of the GCL was employed to activate GCs above threshold (Fig. 5B3a). In all experiments (8 slices, 4 mice) we found brief light pulses (light pulse duration, <2 msec long) directed at the GCL elicited a very large field potential in a recording from the GCL (Fig. 5B3b, GCL). The morphology of this recording suggested it was a population spike, consistent with activation of GCs.

The IML recording was smaller than the GCL recording (Fig. 5B3b, IML) consistent with the generation of the population spike in the GCL, not the IML.

Moving the recording electrode from the GCL to SL showed the same optogenetic stimulus to the GCL that led to a population spike in the GCL led to a delayed fEPSP in SL of CA3 (Fig. 5B3b). The SL fEPSP began at the peak of the GCL population spike, consistent with direct excitation of GCs followed by excitation of PCs by mossy fiber synapses (Fig. 5B3b). To confirm the mossy fibers were responsible for the fEPSP in SL, we confirmed the fEPSPs had characteristics of mossy fiber synapses in that there was large paired-pulse facilitation (Fig. 5B3b, bottom; Salin et al., 1996). Therefore, expression of ChR2 in GCs did not appear to limit excitation of GCs, and ChR2 expression in mossy fibers did not seem to interfere with synaptic transmission from mossy fibers to CA3 PCs.

We also compared optogenetic stimulation of the IML to electrical stimulation of the IML (Fig. 5C1). Electrical stimulation is not selective for MC axons, so to make electrical stimulation as specific as possible for the IML we used a stimulus electrode that was small in diameter (25 µm diameter) and weak current pulses (10-50 µsec, 50 µA). In this way, current would not be likely to spread to the MML and activate PP axons. To further reduce the likelihood that IML stimulation activated the PP axons, we first tested both the IML and MML as recording sites. We only used slices where an electrical stimulus to the IML evoked a fEPSP that was larger in the IML than the MML (Fig. 5C2). Notably, there always was a small fEPSP one could record in the MML, indicating either some activation of PP axons or volume transmission from the IML. We rejected slices where an IML stimulus elicited a bigger fEPSP in the MML than the IML. This experiment was done in 5 mice using 1 slice/mouse.

The results showed that both electrical and optogenetic stimulation of the IML led to fEPSPs that did not evoke population spikes in the GCL (Fig. 4, 5B-C). In contrast, when the PP was used as an electrical stimulation site in the same slices (Fig. 5C3), population spikes were evoked by the PP stimulus (Fig. 5C3). In this comparison, the stimulus strength for the PP-evoked fEPSP was adjusted so it was similar or smaller in amplitude than the fEPSP evoked by IML stimulation (Fig. 5C2-3). The PP fEPSP

evoked a population spike in the GCL but the IML fEPSP did not (Fig. 5C3), suggesting the PP input was stronger.

Taken together, these data support the idea that the MC input to GCs is a weak input and the weak nature of the input is not due to technical or other limitations of the approach.

V. Short term plasticity

The plasticity of the MC axons in the IML has been a subject of many studies (Hetherington et al., 1994; Kleschevnikov and Routtenberg, 2003; Larimer and Strowbridge, 2008; Hashimotodani et al., 2017). We first examined paired-pulse facilitation and short trains of optogenetic stimuli Optogenetic stimulation was directed to the IML with recordings in the IML to record the fEPSP. For paired pulses, identical stimuli were tested with a range of interstimulus intervals (10-200 msec; Fig. 6A). Stimuli were half-maximal. The second response of the pair was usually similar or smaller than the first (Fig. 6A).

Effects were also tested using electrical stimulation of the IML instead of optogenetic stimulation of the IML (Fig. 6B). Electrical stimulation was made as described for Fig. 5C. That is, slices were only used if the electrical stimulus elicited a fEPSP that was larger in the IML than the MML.

There appeared to be more paired-pulse inhibition using optogenetic stimulation than electrical stimulation, especially using short (10-20 msec) interpulse intervals (Fig. 6A-B). A two-way ANOVA with the type of stimulation and interstimulus interval as factors showed a significant effect of the type of stimulation (optogenetic vs. electrical; $F(1,16)=10.64$; $p=0.005$) and interstimulus interval ($F(9,144)=32.13$; $p<0.0001$) with an interaction ($F(9,144)=4.50$; $p<0.0001$) such that optogenetic stimulation showed significantly more paired-pulse inhibition at short intervals relative to electrical stimulation (Tukey-Kramer post-hoc tests; 10 msec interval, $p=0.037$; 20, $p=0.001$; 30, $p=0.002$; 40, $p=0.003$; 50, $p<0.001$; 60, $p=0.021$). Notably, at the 10 msec interval, the second optogenetic pulse appeared to be ineffective in some cases. This observation is supported by the idea that 10-20 msec interstimulus intervals (50-100 Hz) is above the limit to the frequency ChR2 can be activated effectively (Wang et al., 2007).

Next, we examined short trains of identical stimuli using whole-cell recordings. (A complete description of the optogenetically-evoked EPSPs with whole-cell recording is provided in the next part of the Results.) We used two identical light pulses in patched GCs and tested EPSPs at GC RMP. The results showed similar effects as extracellular recordings. In other words, when the interval was 10 msec there was suppression of the second optogenetically-evoked EPSP and it was very strong inhibition in that the second stimulus elicited no detectable EPSP (Fig. 6C1a, 6D1). This result is consistent with the difficulty using ChR2 at high frequencies mentioned above. When ISI was 40 msec (25 Hz), there was variability from one train to another and facilitation could occur (Fig. 6C1b, 6C2a-b, 6D2). When the interval was 200 msec (5 Hz) there was suppression in some cases (Fig. 6C1c) but facilitation in others (Fig. 6D3). Therefore, some depression and some facilitation occurred for 5 and 25 Hz, suggest that at these frequencies the MC input to GCs has a highly variable effect on the GC.

VI. Whole-cell recordings

A. General information

Whole-cell recordings from GCs were used to confirm findings using sharp electrodes and also address additional questions. For these experiments, viral injection sites were modified to maximize the likelihood that every mouse would show strong expression contralaterally. Because most cases of weak expression had used a ventral injection site, one modification was to change the ventral site slightly and keep the dorsal site the same. Another strategy was to inject virus at >1 site (Table 1).

All mice were injected in the left hemisphere as follows: 3 mice received dorsal injections, 2 were ventral, and 6 had one injection that was modified so that it was slightly more dorsal to the ventral site (Table 1). We refer to the modified site as “mid.” Another 12 mice had 2 injections (either 1 mid and 1 ventral or 1 dorsal and 1 ventral) and the remaining 3 mice had 3 injections (1 dorsal, 1 mid, and 1 ventral). Mice with multiple injections were used primarily for slices from the hemisphere contralateral to the viral injection sites. Crlr-Cre mice were only injected once, in the dorsal DG, for reasons discussed above (Fig. 3).

There were 57 whole-cell recordings of GCs in 31 mice. Most GCs (50/57 or 87.7%) had robust optogenetic responses. “Robust” is defined here as a light response that was elicited responses consistently. These 50 GCs were 98.8 ± 2.9 days old at the time of recording and the average time between viral injection and recording was 35.3 ± 3.1 days. The majority of the 50 GCs were from Drd2-Cre (44 cells) and the others were Crlr-Cre mice (6 cells). The majority of the 50 GCs were from males (34 cells) and the rest of the GCs were from females (16 cells). A maximum of 3 cells were sampled per mouse.

The 7 GCs without robust optogenetic responses had either no response or an inconsistent response that was small depolarization (<0.3 mV). There was no sign from the animals that were used or the intrinsic properties of the cells with weak responses that they were unusual or unhealthy (Table 3). They did not appear to be young adult-born neurons because they did not have characteristics of young adult-born cells, such as a relatively depolarized RMP and relatively high Rin (Overstreet et al., 2004; Schmidt-Hieber et al., 2004; Esposito et al., 2005; Ge et al., 2007; Table 3). There was no evidence that GABAergic neurons in the GCL were sampled, because the patched cells did not exhibit the large, monophasic afterhyperpolarization (AHP), weak spike frequency adaptation or a brief half-width of AP like DG GABAergic neurons; (Scharfman, 1995a; Freund and Buzsaki, 1996; Scharfman et al., 2000). The morphology was also consistent with typical mature GCs (described further below).

B. EPSPs were common

Next, light was directed to the IML and a GC was recorded approximately 200 µm away. Of 50 cells with robust responses to light, all had depolarizations at RMP (Fig. 7A1). To determine if IPSPs were evoked, 41 of the 50 cells were tested both at RMP and depolarized potentials where IPSPs are usually distinguished from EPSPs because they are hyperpolarizing. In 24/41 (54.8%) of cells there were no detectable hyperpolarizations. We refer to these 24 optogenetic responses without hyperpolarizations as EPSPs because the depolarizations were graded, triggered APs at their peak (if GCs were depolarized) and could be blocked by antagonists of glutamate receptors (discussed further below). The remaining 17/41 (45.2%) cells

showed EPSPs followed by hyperpolarizations. These responses are referred to as EPSP-IPSPs because APs were inhibited during the hyperpolarizations, and hyperpolarizations were blocked by GABA receptor antagonists (described further below).

1) Voltage clamp

Voltage clamp was used to address whether the EPSP and IPSP components could be better distinguished than in current clamp and if any other components would become detectable in voltage clamp that were not in current clamp. In voltage clamp, EPSPs corresponded to inward currents (Fig. 7A; n=3) and IPSPs corresponded to outward currents (Fig. 8A, see below). Therefore, recordings in current clamp agreed with the recordings in voltage clamp from the same cell. This was done in 3 cells only because switching from current to voltage clamp in the same cell could destabilized the recording.

2) EPSP characteristics

Characteristics of optogenetic responses were measured in cells that exhibited EPSPs without IPSPs and are shown in Fig. 7B. Characteristics of EPSP-IPSPs are discussed afterwards, in Fig. 8. The EPSPs of both groups are compared at the end in Fig. 9.

a. Duration of optogenetic stimulation

For the purposes of characterization, all cells were stimulated with a light pulse duration that was between 50% and 100% of the maximal response. The reason was that it was that same as extracellular recordings described above. When averaged across all cells, the average light duration for EPSPs was brief (1.50 ± 0.11 msec; range, 0.50-2.50; n=24 cells).

b. Latency, rise time, amplitude and duration

EPSPs were first measured using optogenetic stimuli triggered between -65 and -75 mV because this membrane potential range typically allowed one to discriminate an

EPSP as depolarizing and IPSP as hyperpolarizing. It was also used because more depolarized potentials revealed a late EPSP (discussed further below). Therefore, the characteristics at -65 to -75 mV mainly describe the early EPSP.

The latency from the onset of the light pulse to the onset of the EPSP was 3.13 ± 0.12 msec (range, 2.40-4.10; n=16 cells). Measured from the end of the light pulse to the onset of the EPSP, the latency to onset of the EPSP was 1.62 ± 0.17 (range, 0.40-3.04; n=16 cells; Fig. 7B1). Thus, regardless of the method to measure latency, the latencies are consistent with monosynaptic transmission, i.e., MC axons releasing glutamate on dendrites of GCs.

The rise time of the EPSP, measured from the EPSP onset to the EPSP peak, was 5.83 ± 0.54 msec (range, 2.20-10.45; n=16 cells; Fig. 7B1). The latency to peak, measured from the end of the light pulse to the peak of the EPSP was 6.59 ± 0.57 msec (range, 3.87-12.40; n=16 cells; see Fig. 8B).

The mean peak amplitude of EPSPs was 1.89 ± 0.27 mV (range, 0.39 - 3.60 mV; n=16 cells; Fig. 7B1). Thus, EPSPs were small at -65 to -75 mV. These data are consistent with small fEPSPs and small EPSPs in GCs using sharp electrodes (Figs. 4-5).

The half-duration was measured in two ways. First, half-duration was measured from the EPSP onset to the point on the EPSP decay when the EPSP had declined to half its peak amplitude. Mean half-duration was 45.93 ± 5.70 msec (range, 23.00-99.60; n=16). When half-duration was measured from the end of the light pulse, the mean half-duration was 47.55 ± 5.74 msec (range 24.20-100.50, n=16; Fig. 7B2). The mean half-duration contrasts with the half-duration of EPSP-IPSPs (Fig. 7B3), where the mean half-duration was measured in a similar way, starting from the end of the light pulse and ending at the point on the decay that was half the peak amplitude. In other words, this is a comparison of the entire EPSP response and the entire EPSP-IPSP response. Notably, the half-duration of the EPSP-IPSP response was over 7x longer than the EPSP response (330.74 ± 19.36 msec; range 184.90-376.60, n=10 cells; Fig. 7B3). The differences between mean half-durations were significant (Mann-Whitney U test, $p<0.0001$, U statistic 0, meaning all values of EPSP-IPSPs were greater than all values of EPSPs).

c. Pharmacology

Early EPSPs at -65 to -75 mV appeared to be glutamatergic and mediated by AMPA receptors because they could be blocked by the ionotropic receptor antagonist DNQX (10 µM; n=3; Fig. 7C).

C. Regulation of firing by EPSPs

1) EPSPs are weak

EPSPs appeared to be weakly excitatory because they were small, brief, and did not trigger APs at RMP. APs could be triggered at depolarized potentials however, and the AP was typically triggered during a late EPSP (Fig. 7D1) which developed as cells were depolarized (Fig. 7E). However, some EPSPs rarely triggered APs even if depolarized to a membrane potential near threshold (Fig. 7D2). To obtain a better understanding of these ‘failures’ to initiate APs, we conducted more tests. GCs were depolarized to a membrane potential just below their threshold membrane potential. Optogenetic stimuli were triggered 1/minute for at least 3 trials. In these cells (n=3), 16/27 (59.2%) optogenetic stimuli triggered an AP. The results are consistent with the general finding that EPSPs are weak.

2) Late EPSPs and their role in GC firing

As mentioned above, when APs occurred at depolarized potentials, they were usually triggered during what appeared to be a late EPSP (Fig. 7D1, E). The late EPSP was identified by an increase in the EPSP duration with depolarization (Fig. 7D-E), which was significant when EPSP half-duration was measured at many membrane potentials (one-way ANOVA; $F(5,87)=3.33$; $p=0.005$; Fig. 7F1). This effect was unlikely to be due to an increase in the early EPSP because the initial peak of the EPSP did not increase in amplitude with depolarization (one-way ANOVA, $F(5,87)=0.24$; $p=0.944$; Fig. 7F2).

The late EPSP appeared to be generated by NMDA receptors because it was substantially reduced by the NMDA receptor antagonist DL-APV (50 µM; n=3; Fig. 7G). The effect of APV was observed primarily at depolarized potentials but not at relatively

hyperpolarized potentials (Fig. 7G), consistent with the observation of late EPSPs emerging at depolarized potentials.

These data suggested that NMDA receptors are important to GC firing triggered by EPSPs at depolarized potentials. We hypothesized that the Mg^{2+}-dependent block of the NMDA receptor at hyperpolarized potentials normally limited firing at potentials near RMP. To test this hypothesis, $[Mg^{2+}]_o$ was lowered to 0 mM (nominally) in the ACSF to remove the voltage dependent block of the NMDA receptor (n=3). The results showed that EPSPs could trigger APs even at RMP under these conditions. However, more than one stimulus was necessary (Fig. 7H). Thus, under normal conditions 2-3 pulses of light did not trigger APs at RMP (Fig. 6C) but they did when 0 mM Mg^{2+} was used in the ACSF (Fig. 7H).

During exposure to 0 mM Mg^{2+}-ACSF, the effect of the second and third pulse was facilitatory if the interstimulus interval was 40 msec (Fig. 7H). This appeared to be due to the large size of the late EPSP at the time the second and third stimulus (Fig. 7H). These data support the idea that the MC → GC pathway is normally suppressed by the Mg^{2+}-dependent block of NMDA receptors. The data are also interesting because they suggest that the NMDA receptor may mediate the facilitation that occurred during short 25 Hz trains (Fig. 6C) where the interstimulus interval was 40 msec. The frequency of 25 Hz is in the beta range (approximately 15-30 Hz; Chapman et al., 1998) which is notable because of the suggestions that beta activity is involved in memory (Kay, 2014), and the suggestions that MCs contribute to memory processing in the DG-CA3 (Buckmaster and Schwartzkroin, 1994; Lisman et al., 2005; Henze and Buzsáki, 2007; Myers and Scharfman, 2009; Myers and Scharfman, 2011; Knierim and Neunuebel, 2016; Nakazawa, 2017; Bui et al., 2018).

3) Intrinsic properties and their influence on afferent input to GCs

Figure 7I shows that intrinsic properties of the GC also could facilitate the ability of optogenetic stimuli to trigger APs at depolarized potentials because input resistance increased with depolarization. An increase in GC input resistance with depolarization was reported before using rats and sharp electrodes (Scharfman, 1994a) as well as rat cortical neurons (Thomson and Deuchars, 1997). Here we tested intrinsic properties in

two ways. First, current steps were triggered from RMP, with each step increasing by the same increment (Fig. 7I1). The responses to the current steps did not show increase with the same increment however. The responses to a small step, e.g. 10 pA, showed very little change in membrane potential; the responses to 3x the step (in this example, 30 pA) elicited a response that was >3x the response to the 10 pA step (Fig. 7I1). Next, R_{in} was calculated for 48 GCs at RMP using a current step approximately 5 pA in amplitude. There was a significant correlation between RMP and R_{in}, with greater R_{in} in cells that had more depolarized RMPs (Fig. 7I2). In addition, we found that the slopes of the I-V curves for GCs were non-linear; at depolarized potentials the change in slope reflected an increased R_{in} (not shown). The implication is that the GC will be more affected by an input, such as the MC input, if it is depolarized from RMP, a possibility that has been raised before (Scharfman, 1995b).

D. EPSP-IPSPs

In Figure 8A1, an EPSP followed by an IPSP is shown. In the same cell in voltage clamp, the EPSP and IPSP corresponded to inward currents followed by outward currents (Fig. 8A; n=3).

IPSPs were divided into those which were robust, meaning they occurred after every stimulus (n=12; Fig. 8A) and those that were inconsistent (n=5; Fig. 8B). In all cases, EPSPs preceded the IPSP, with one exception. In the exceptional cell an EPSP occurred before the IPSP initially, and then waned so that the IPSP appeared to be generated without an EPSP.

Robust IPSPs had two peaks in 7/12 cells (e.g., Fig. 8A1). At -65 to -75 mV, the mean latency (from the end of the light pulse) to the early peak of the IPSP was 32.12 ± 3.71 msec (range, 23.93-43.10; n=5; Fig. 8C). The late IPSP peaked at 131.96 ± 4.66 msec (range 119.63-142.90; n=5; Fig. 8C), which was significantly different (Mann-Whitney U test, p=0.008; U statistic 0; Fig. 8C).

The mean amplitude of the early peak was -5.10 ± 1.23 (range 2.20-7.75, n=5) at -65 to -75 mV. The late peak was -5.83 ± 0.98 (range 2.84-7.37, n=5). Amplitudes of both IPSP components were greater at more depolarized potentials; Fig. 8D). A two-way ANOVA showed a significant effect of membrane potential (F(1,20)=33.66;

p<0.001) but amplitudes of early and late IPSPs were not significantly different at any given membrane potential (F(1,20)=0.04; p=0.840; Fig. 8D).

The mean half-duration of the entire EPSP-IPSP response was 330.74 ± 19.36 msec (range 184.90-376.60, n=5) at -65 to -75 mV, as shown in Fig. 7B3. This duration was checked at three membrane potentials like Fig. 8D, and there were no significant differences (RMANOVA, F(2,31)=1.52; p=0.234).

1) IPSPs are inhibitory

Evidence that IPSPs were inhibitory was obtained by depolarizing GCs to the membrane potential where APs occurred spontaneously (Fig. 8E). Spontaneous APs were inhibited when EPSP-IPSPs were triggered. Note that during the brief EPSP before the IPSP it was not evident that an AP was triggered despite the depolarized membrane potential (similar to Fig. 7D2). This observation suggested that the EPSP was suppressed by the IPSP, which is discussed further below.

2) Pharmacology

As shown in Figure 8F1, the AMPA receptor antagonist DNQX (10 µM) could block the IPSP (n=3) but some cells showed DNQX-resistant IPSPs (n=3, Fig. 8F2). In 2 of the 3 cells with resistance to DNQX, the IPSPs were reduced by DNQX but not completely blocked. In 1 of the 3 cells, there was a weak EPSP-IPSP initially (Fig. 8F2). Adding both DNQX and DL-APV (50 µM) did not block the IPSP but gabazine did (Fig. 8F2).

These experiments raise the possibility that IPSPs were generated by the MC → GABAergic neuron → GC pathway but glutamatergic receptors other than AMPA and NMDA receptors mediate the activation of GABAergic neurons. Another explanation is that ChR2 was expressed in GABAergic neurons and they were directly activated, which led to IPSPs in GCs that were resistant to DNQX. Direct activation is consistent with the short latency to onset of the DNQX-resistant IPSPs (measured from the onset of the light pulse, 2.95, 3.94, 4.68 msec; measured from the end of the light pulse, 2.45, 2.44, 3.18 msec). These latencies are consistent with a monosynaptic pathway, i.e., direct activation of GABAergic neurons that lead to an IPSP in GCs. On the other hand,

as noted above, some DG interneurons are unusually rapid in their activation and their ability to inhibit GCs is also remarkably fast (Norenberg et al., 2010; Hu and Jonas, 2014).

It is important to note that both recordings in Fig. 8F were from slices selected near the injection site. Although the evidence for GABAergic neurons expressing virus at the injection site was weak (Fig. 2), even a small amount of ChR2 in interneurons located directly beneath an optic fiber might lead to their activation, since many hilar interneurons have a low threshold for activation by the PP (Scharfman, 1991) and activation by GCs (Scharfman et al., 1990). Hilar interneurons are also sensitive to insult or injury (Johansen et al., 1987; Sloviter, 1989; Matsuyama et al., 1993; Scharfman, 1999; Choi et al., 2007; Frankowski et al., 2019) so they could be sensitive to light emitted from a fiber optic close to their cell bodies. These factors are consistent with the idea that some of IPSPs were due to direct activation.

E. GC morphology

Biocytin was included in the internal solution to determine if they could have been young, adult-born cells, semilunar GCs (Williams et al., 2007), or GABAergic neurons. A randomly-selected subset of GCs were examined either using brightfield (n=9) or fluorescent microscopy (AmplifluRed, n=8; Streptavidin-Cy3, n=3). An example of a filled GC is shown in Fig. 8G and is consistent with mature GCs. Thus, GCs were typically located in the center of the GCL or in the part of the GCL near the IML, where mature GCs are typically located (Radic et al., 2017). The GC somata were similar in shape (oval) and size (8-10 µm, measured along the long axis of the soma) to mature GCs (Amaral et al., 2007; Rahimi and Claiborne, 2007; Pierce et al., 2011). The dendrites extended throughout the ML and there were numerous spines, characteristics of mature GCs (Frotscher et al., 2000; Amaral et al., 2007; Rahimi and Claiborne, 2007). None of the characteristics suggested they were immature, semilunar, or GABAergic. Their intrinsic properties did not either (Table 3).

F. Comparison of EPSPs and EPSP-IPSPs

One question that arises when considering the data about “EPSPs” and “EPSP-IPSPs” is whether these two groups represent different responses to optogenetic stimulation or they are actually one group. In other words, EPSPs are the same but sometimes IPSPs are recruited. To address this question, EPSPs of the “EPSPs” group were compared to EPSPs of the “EPSP-IPSP” group (Fig. 9).

1) Age and viral incubation time

There were no detectable differences in the age of the animals used to elicit EPSPs vs. EPSP-IPSPs (EPSP: 92.2 ± 3.2 days, range 78-108, n=24 cells; EPSP-IPSP: 106.3 ± 6.2 days, range 73-143, n=17; Mann-Whitney U test, p=0.137, U statistic 148). The viral incubation times were not significantly different either (EPSPs: 30.0 ± 2.9 days, range 14-41, n=24 cells; EPSP-IPSPs: 43.1 ± 7.4 days, range 15-95, n=17; Mann-Whitney U test, p=0.434, U statistic 174).

2) Duration of optogenetic stimulus

The light pulse durations for the “EPSP” group were significantly longer than the “EPSP-IPSP” group although only by a fraction of a msec (EPSP: 1.50 ± 0.11 msec; range 0.50-2.50, n=24; EPSP-IPSPs 1.05 ± 0.17 msec, range 0.50-2.00, n=11; Mann-Whitney U test, p=0.012, U statistic 73; Fig. 9A). These data suggest that a short light pulse duration might produce more IPSPs. However, light pulse durations that were initially tested in each cell were extremely brief (0.1-0.5 msec), making this possibility unlikely.

3) Comparison of EPSPs

a. Latencies

The latencies to the onset of EPSPs from the EPSP group and EPSPs of the EPSP-IPSP grop are shown in Fig. 9B1. There were no significant differences (Student’s t-test, t=0.068, df 25, p=0.946).

Regarding differences between latency to peak, both types of EPSPs and the two peaks of the IPSP were significantly different (p<0.0001, Kruskal-Wallis statistic 22.67; Fig. 9B2). Post-hoc Dunn’s tests showed that the EPSPs from the EPSP group

and EPSPs from the EPSP-IPSP group were not significantly different from each other ($p>0.99$; Fig. 9B2).

Regarding the differences of each type of EPSP to each type of IPSP, each EPSP was significantly different from the late IPSP (EPSP of the EPSP group, $p=0.010$; EPSP of the EPSP-IPSP group, $p<0.001$; Fig. 9B2). The EPSP of the EPSP-IPSP group was significantly different from the early IPSP ($p=0.003$) but the EPSP of the EPSP group was not significantly different from the early IPSP, by the $p<0.05$ criterion ($p=0.055$; Fig. 9B2).

b. Amplitude

Other measurements showed similarity of the two types of EPSPs. For example, the amplitudes of EPSPs from the "EPSP" group were not significantly from the EPSPs of "EPSP-IPSP" group at -65 to -75 mV (EPSP of EPSP group: 1.89 ± 0.27 mV, range 0.39-3.60, n=16; EPSPs of EPSP-IPSP group: 1.52 ± 0.28 mV, range 0.46-2.99, n=10; Student's t-test, $t=0.944$, df 24, $p=0.354$). However, when all membrane potentials were tested, a difference in voltage-dependence was revealed. For these comparisons, GCs were tested at membrane potentials ranging from -35 to -95 mV (Fig. 9C). The EPSPs of the "EPSP-IPSP" group were significantly depressed at depolarized potentials (Fig. 9C) but this had not been the case for the "EPSP" group (Fig. 7F1). A two-way RMANOVA with group ("EPSP" or "EPSP-IPSP" group) and membrane potential (10 mV ranges from -35 to -95) as factors showed that there was no effect of group ($F(1,34)=0.32$; $p=0.578$) but a significantly effect of membrane potential ($F(5,100)=14.83$; $p<0.001$). There was a significant interaction of group x membrane potential ($F(5,100)=19.20$; $p<0.001$) such that EPSPs from the "EPSP-IPSP" group declined with depolarization (Post-hoc Sidak's test, the two most hyperpolarized ranges significantly different from all of the other membrane potential ranges, all $p<0.001$; Fig. 9C). These data suggest that the EPSP from the EPSP group and EPSPs of the EPSP-IPSP group were similar, but the latter were truncated by the IPSP, supporting the idea that the IPSP suppressed the EPSP.

c. IPSPs suppress EPSPs

To address the hypothesis that IPSPs suppressed EPSPs of the EPSP-IPSP group further, we examined EPSP-IPSPs before and after exposure to the $GABA_A$ receptor antagonist BMI and $GABA_B$ receptor antagonist CGP52432 (n=4; Fig. 9D). The results showed that EPSPs increased in amplitude and duration after exposure to the $GABA_A$ receptor antagonist BMI and the $GABA_B$ receptor antagonist CGP52432 (Fig. 9D1). The increase in the EPSP was primarily at depolarized potentials where GABA receptor antagonism revealed a late EPSP (Fig. 9D2).

The effects of $GABA_A$ vs. $GABA_B$ receptor antagonists were examined by first adding BMI to the ACSF and then CGP52432 (n=4; Fig. 9E-F). Representative responses are shown in Fig. 9E and plotted in Fig. 9F. Initially the EPSP-IPSP of the GC did not evoke APs even at depolarized membrane potentials (Fig. 9E1). After BMI, the early IPSP was blocked and the early EPSP increased about 2-fold (Fig. 9E1-2, 9F1-2). When the late IPSP was blocked by adding CGP524432, the optogenetic stimulus evoked a late EPSP (Fig. 9E3). The late IPSP appeared to have little effect on the early EPSP (Fig. 9F3).

G. Summary of patch clamp data

Together the data suggest that EPSPs are composed of an early and a late component. The early component is clear, although small, at hyperpolarized potentials and the late component is evident at relatively depolarized potentials. In addition, IPSPs can be triggered. The early IPSP appears to overlap the early and late EPSPs and can influence them. The late IPSP appears to overlap the late EPSP and can inhibit the late EPSP (Fig. 9E-F).

In addition to the evidence that the IPSP suppressed the EPSP, the EPSP appeared to suppress the IPSP, at least in some cases. The evidence for this is from 3 GCs which initially showed an EPSP in response to optogenetic stimulation, and there was no detectable hyperpolarization even if the cell was depolarized. The same optogenetic stimulus evoked an IPSP after exposure to ACSF with 0 mM Mg^{2+}. Two of the 3 cells also were exposed to increased (5 mM) $[K^+]_o$. Therefore the ability to recruit the IPSP may be increased by changes in the circuitry due to increased $[K^+]_o$. and/or facilitating NMDA receptors. The latter is consistent with a previous study showing that

NMDA receptors are present at MC → GABAergic neuron synapses (Hashimotodani et al., 2017).

In summary, early and late EPSPs appear to be superimposed on early and late IPSPs and there is a variable net effect, sometimes with and sometimes without a detectable IPSP.

VII. Network effects of optogenetic stimulation

A. Weak excitation of the GC network

The results of whole-cell recording suggest that MCs have a weak excitatory effect on GCs and an inhibitory effect, but the data do not address the net effect on the DG network. Therefore, we returned to field potential recordings where the average of numerous GCs around the recording electrode are sampled at one time.

One way to address the question is to ask how much optogenetic stimulation excited or inhibited the APs in GCs that are produced by the PP input. Therefore, we tested effects of an optogenetic stimulus before or after an electrical stimulus to activate the PP. The main objective was to determine if the optogenetic prepulse facilitated or inhibited the PP-evoked population spike. Notably, a recent study examined the commissural projection of the DG, a major component of which is MC axons, and reported inhibition of the population spike only (Hsu et al., 2015). We predicted that there could be weak facilitation, reflecting the weak EPSP. However, the prepulse might need to be timed so the MC-mediated EPSP would summate with the PP-mediated EPSP to producing a larger population spike. This timing might not have been tested previously.

Figure 10A shows the recording site in the GCL and the stimulating electrode in the PP. The site of stimulation was on the hippocampal fissure rather than the ML to avoid direct stimulation of DG neurons because they can have dendrites that reach the hippocampal fissure (Scharfman, 1995a). Light was directed to the IML near the GCL recording site.

It is often difficult to elicit a population spike if the PP is stimulated electrically in a slice, consistent with the fact that GCs have RMPs far from their threshold (Staley et al., 1992; Williamson and Patrylo, 2007). To make it possible to elicit population spikes

using electrical stimulation, three approaches were taken. First, slices were stimulated strongly, which led to population spikes in some slices (Fig. 10A-C). Second, 5 mM $[K^+]_o$ was used in the ACSF and weaker stimuli were used. In our experience the increase in $[K^+]_o$ (from 2-3 to 5 mM) increases the population spike evoked by electrical stimulation of the PP but epileptiform activity is not produced (Scharfman, 1994b; Scharfman, 1995a; Scharfman et al., 2000; Fig. 10C). Third, two electrical stimuli to the PP were timed so that they were 40 msec apart, because this is an interval that leads to paired-pulse facilitation of the population spike evoked by electrical stimulation of the PP (Fig. 10D).

Independent of the method used to obtain a large population spike, the primary effect of an optogenetic prepulse, when timed before the PP stimulus, was inhibition of the population spike (Fig. 10B-D). Note that when there was inhibition, there was inhibition of all population spikes, those that were small (1-2 mV) and those that were larger (up to 6 mV; data not shown).

When the the optogenetic stimulus occurred 0-2 msec after the PP stimulus, there was a small facilitation of the population spike in 5/15 (33%) of the slices (mean, 11.34 ± 3.2%; Fig. 10B,D,E). When the prepulse was >2 msec before PP stimulus, inhibition of the population spike occurred in 15/15 (100%) of slices (mean, 69.3 ± 11.3%, 15 slices, 8 mice; Fig. 10B-E). If the prepulse was between 0 and 2 msec before the PP stimulus there was inhibition or facilitation of the population spike (Fig.10B-E).

In a subset of slices numerous delays between the optogenetic stimulus and PP stimulus were tested (Fig. 10E). In these slices, any light pulse before the PP stimulus inhibited the population spike and often there was very strong inhibition. Any light pulse after the PP stimulus facilitated the population spike, and the facilitation was relatively weak. If the light pulse coincided with the PP stimulus, strong inhibition or weak facilitation occurred, a variable result (Fig. 10E).

The weak facilitation is consistent with results described above showing that light pulses generate small monosynaptic EPSPs. Results from intracellular recordings supported this idea, illustrating a rapid time course of light-evoked EPSPs, so there was only a narrow window of time for the light-evoked and PP-evoked EPSPs to summate maximally, i.e. to have their peaks align and therefore boost the PP-evoked EPSP

significantly (Fig. 10F1-3; sharp electrode recordings in 3 GCs). Outside that short temporal window the optogenetically-elicited EPSP had little effect on the PP-evoked EPSP (Fig. 10F2 vs. 10F3). These data suggest a very specific temporal window when MCs can facilitate the PP-evoked GC population spike. Also, facilitation also appears to be weak relative to inhibition.

B. The GABAergic neuron subtype underlying optogenetically-elicited inhibition

Interestingly, the population spike could be greatly inhibited by a prepulse of light, but the underlying positivity, upon which the population spike is superimposed, did not appear to be affected (Fig. 10B-D). These experiments with field recordings were only done in mice with one viral injection and were typically over two slice widths from the stereotaxic coordinates used to inject virus. Therefore, few interneurons were likely to be activated directly by ChR2. Instead the data suggest that MCs activate GABAergic neurons which, in turn, inhibit PP-evoked firing of the GC.

The type of interneuron that MCs innervate was first proposed to be the basket cell (Sloviter, 1991; Sloviter, 1994) and then other studies used the term “perisomatic-targeting” for interneurons that included basket-cells and others, such as axo-axonic cells (Freund and Gulyas, 1997). More recently it has been suggested that MCs activate several interneuron cell types (Hsu et al., 2015) and one is the dendritic-targeting HIPP cell (Deng et al., 2020).

To determine if the inhibition of the PP-evoked population spike was mediated by perisomatic-targeting GABAergic neurons or dendritic-targeting GABAergic neurons, we recorded not only in the GCL but also the ML. This was done by recording in the GCL and then moving the recording electrode to the ML (Fig. 11A). To find the best recording site for the PP-elicited EPSP in the ML corresponding to the GCL recording, we tested several recording sites in the OML and MML that were along a perpendicular to the site used for GCL recording (Fig. 11A). That way the recordings in the ML would correspond best to the dendrites of the GCs that were recorded in the GCL. In addition, by testing many sites in the OML and MML the site where the largest fEPSP was evoked could be used. This is important to do because a small fEPSP might reflect volume conduction and it might seem like there was no effect when there actually was an effect closer to

the site of synaptic input. The position of the light fiber remained at the same location in the IML for both GCL and ML recordings (Fig. 11A).

The recordings in the GCL showed blockade of the population spike (Fig. 11B2, center). The recordings in the ML showed that there was a large decrease in the inflection in the fEPSP, which reflects blockade of the population spike (Fig. 11B-C). There was no detectable effect in the underlying fEPSP at the ML or GCL sites (Fig. 11B-C). Thus, recording sites in the GCL and ML both showed that the population spike was mainly inhibited by optogenetic prepulses but not the fEPSP. The results are consistent with the idea that MCs mainly influence the perisomatic-targeting GABAergic neurons which inhibit AP generation, rather GABAergic neurons that target GC dendrites and inhibit EPSPs.

Additional experiments used the $GABA_A$ receptor antagonist BMI, and it blocked the inhibitory effect of the prepulse on the PP-evoked population spike (10 µM; n=3, Fig. 11F, Light+Stim) without altering the light-evoked fEPSP recorded in the IML, elicited by the same light pulse (Fig. 11F, Light). Note that the second population spike evoked in the presence of BMI (Fig. 11F2, Stim), was inhibited by the light pulse in the presence of BMI (Fig. F2, Light+Stim), probably because the late IPSP is resistant to BMI and was still able to block the second population spike. This result is consistent with a contribution of both $GABA_A$ and $GABA_B$ receptors to optogenetic inhibition.

VII. Effects of the septotemporal axis and other variables

A. Dorsal vs. ventral viral injection sites

1) Extracellular recordings

Comparisons of fEPSPs were made for mice injected either in the dorsal or ventral DG (Fig. 12A1). There was no effect of dorsal vs. ventral injection site on latency to onset of fEPSPs (Mann-Whitney U test; p=0.567; U statistic 102). Note latency data were analyzed with nonparametric statistics because latency was measured from the end of the light pulse to the start of the fEPSP and there were several fEPSPs with no detectable latency. There was no significant effect of the site of viral injection on fEPSP slope (Student's t-test, t=1.07, df 33, p=0.293) or amplitude (Mann-Whitney U test, p=0.991; U statistic 73).

This analysis used each slice as a separate data point and should be considered carefully because there was only one slice sampled in some mice and others had as many as 5 slices. Therefore, the data were also analyzed using each mouse as a single sample. When there was more than one slice/mouse, the data from each slice was averaged to produce a single value for that animal. Like the previous analysis, there was no detectable effect of dorsal vs. ventral injection site on slope (Student's t-test, t=0.792, df=11, p=0.445) or amplitude of fEPSPs (Student's t-test, t=0.664, df=11, p=0.521). Because the result did not appear to depend on the use of a slice or a mouse as a sample, and the variance between slices of the same mouse was as large as the variance between mice, the sample was an individual slice for comparisons described below.

We also asked if the site of viral injection influenced the ability to obtain an optogenetic response. There was no significant difference in mice with dorsal or ventral injection of virus (dorsal: 7 slices without responses/33 total slices or 21.2%; ventral: 7/18 or 38.9%; Fisher's exact test, p=0.203). Together the data suggest that dorsal and ventral injections led to similar fEPSPs. If dorsal injections reflect dorsal MC actions and ventral injections reflect ventral MC actions, the data suggest little difference in fEPSPs produced by dorsal and ventral MCs.

2) Patch clamp recordings

Most data from patched GCs were recorded in mice with dorsal injections or more than one injection. Therefore, the influence of dorsal vs. ventral viral injection was not assessed.

B. Ipsilateral vs. contralateral recording sites

1) Extracellular recordings

The effect of slice location relative to the injection site was determined by comparing slices from three locations. As diagrammed in Fig.12A1, the locations were: 1) slices adjacent or at the injection site (called ipsilateral, 'near'), 2) slices ipsilateral but at least two slice-widths (at least 800 µm) from the injection site (ipsilateral, 'far'), and 3) slices contralateral to the injection site. The definitions for ipsilateral 'near' or 'far' slices

were based on studying ChR2 expression and finding that slices at least 800 µm away from the injection site had few (<5) MC somata expressing ChR2. In contrast, slices at the injection site or adjacent to it showed many MCs expressed ChR2 (Fig. 1C1). Slices were positioned in the recording chamber at the same time after the dissection and remained there for all recordings. This approach optimized comparisons of slices from the same mouse.

Latencies to onset were not significantly different between ipsilateral 'near', ipsilateral 'far', and contralateral (Kruskal-Wallis ANOVA; p=0.224; Kruskal-Wallis statistic 2.99). There also were no significant differences in slope (Kruskal-Wallis ANOVA; p=0.299, Kruskal-Wallis statistic, 2.42) or amplitude (Kruskal-Wallis ANOVA; p=0.302; Kruskal-Wallis statistic 2.40).

2) Whole-cell recordings

EPSPs were mainly recorded from GCs that were contralateral to the injection site (21/24 cells or 87.5% were contralateral). In contrast, EPSP-IPSPs were mostly ipsilateral (0/12 cells were contralateral). Differences were significant (Fisher's Exact Test, p<0.0001; Fig. 12A2).

The EPSP-IPSPs that were compared and were primarily recorded ipsilateral to the viral injection site were the EPSP-IPSPs that were large and consistent from trial to trial (e.g., Fig. 8A). Interestingly, the EPSP-IPSPs that were less robust, meaning they were inconsistent from one stimulus to the next (e.g., Fig. 8B) were mostly recorded contralateral to the injection site (4/5 or 80.0%; Fig. 12A2). The differences between the two types of EPSP-IPSPs were significant (Fisher's exact test, p=0.010; Fig. 12A2).

C. Upper vs. lower blade recording sites

1) Extracellular recordings

Optogenetic stimuli were tested for recording sites in the upper blade, crest and lower blade, which were defined, for the purposes of this study, as shown in Fig. 12B1-2 (Scharfman and Witter, 2007). Statistical comparisons were restricted to the upper blade and crest because optogenetic stimuli were tested in the lower blade in only two slices. There were no significant differences between the upper blade and crest

recording locations in latency to onset (Student's t-test, t=0.483; df=11, p=0.639), slope (t=0180, df 12, p=0.986), amplitude (t=0.549, df 11, p=0.594) or half-duration (t=0.238, df 11, p=0.816).

2) Whole-cell recordings

The same percentage of EPSPs were recorded in the upper blade (10 GCs showed EPSPs in the upper blade/21 total GCs with EPSPs, or 47.6%) and crest (10/21 GCs) with one GC (1/21 or 4.8%) in the lower blade.

A comparison of EPSP characteristics was made for GCs in the upper blade and crest because of the small sample size of GCs in the lower blade. There were no significant differences between upper blade or crest EPSPs in latency to onset, latency to peak, amplitude or half-duration (Student's t-tests, latency to onset: t=0.483, df 11, p=0.659; latency to peak: t=1.20, df 11, p=0.256; amplitude: t=0.549, df 11, p=0.594; half-duration: t=0.278, df 11, p=0.816).

For the robust EPSP-IPSPs, the location of one cell was not noted so the sample size was 11. Six/11 GCs were located in the upper blade, 2/11 in the crest, and 3/11 in the lower blade which were not significantly different (Fisher's Exact test, p=0.170). Comparisons of the number of EPSPs recorded in the upper blade, out of all GCs tested, were not significantly different from EPSP-IPSPs in the upper blade (Fisher's Exact Test, p>0.999). The same was true for the crest and lower blade (p=0.139, p=0.106).

D. Slices cut from the dorsal vs. ventral DG

Of mice with optogenetically-evoked fEPSPs, 11 slices were cut from the septal third of the DG using a plane that was approximately 15° from the coronal plane, so the slices would be in the transverse axis (see Methods). Comparisons were made to slices cut horizontally where the slices in the ventral third were selected that are approximately transverse in their orientation (see Methods; Fig. 12B1-2). Although this comparison could assess differences between septal and temporal DG, it is not ideal because some slices were not exactly in the transverse axis. Therefore, it is conservatively described as a comparison of coronal vs. horizontal angles below and in Fig. 12B.

1) Extracellular recordings

There was an effect of slice orientation on latency to onset of fEPSPs, with responses in coronal slices faster than horizontal slices (Mann-Whitney U test, p=0.004; U statistic 31.5; Fig. 12B3). For coronal slices, the time from the end of the light pulse to the onset of the fEPSP was 0 in all fEPSPs. In horizontal slices, the latency was 0.86 msec ± 0.40 msec (range 0-2.00 msec; Fig. 12B3). There were no detectable differences in fEPSP slope or amplitude (Student's t-tests, slope: t=0.844, df 30, p=0.406; amplitude: t=0.325, df 37, p=0.747; Fig. 12B4).

2) Whole-cell recordings

Slices used for whole-cell recording were only in the horizontal plane so comparisons were not made.

E. Viral incubation time

The time after viral injection that a mouse was examined was analyzed to address whether the optogenetically-evoked fEPSP was greater at an early or later time after the viral injection. The relationships between time after injection and fEPSP slope (R^2=0.004), amplitude (R^2=0.049), or latency (R^2=0.020) did not show significant correlations (Pearson's correlation coefficients, all p values>0.05).

For whole-cell recordings, the time after viral injection was not statistically different for EPSPs (30.0 ± 2.9 days, n=24) vs. EPSP-IPSPs (43.1 ± 7.4 days, n=17; Mann-Whitney U test, p=0.434, U statistic 174). The latency to onset for EPSPs showed no correlation between incubation time and latency (Pearson's correlation coefficient, R^2=0.147; p=0.197). The same was true for latency to peak (R^2=0.062; p=0.350). Incubation time and EPSP amplitude also showed no significant correlation (R^2=0.040; p=0.455), and the same was true for EPSP half-duration (R^2=0.053; p=0.484).

F. Drd2-Cre vs. Crlr-Cre mice

1) Extracellular recordings

When fEPSPs from Drd2-Cre and Crlr-Cre mice were compared, latencies to onset of fEPSPs were not significantly different (Mann-Whitney U test, p=0.929; U statistic 158). There were no significant differences in fEPSP slope (Student's t-test, t=1.13, df 33, p=0.265) or amplitude (Mann-Whitney U test, p=0.702, U statistic 135) in the two mouse lines.

2) Whole-cell recordings

When EPSPs of the EPSP group (i.e., without IPSPs) were compared in Drd2-Creand Crlr-Cre mice, there were no significant differences in amplitude or half-duration (Student's t-tests, amplitude: t=1.33, df 24, p=0.195; half-duration: t=0.799; df 24, p=0.432). For EPSP-IPSPs, all mice were Drd2-Cre.

G. Sex

Whole-cell recording was used to compare sexes. The proportion of GC responses in males that were EPSPs, out of all EPSPs recorded in both sexes, was 14/24 (58.3%). The proportion in females was 10/24 (41.7%), which was not significantly different (Fisher's exact test, p=0.387; Fig. 12C1). For EPSP-IPSPs that were robust, exactly half were from males and half were from females (6/12 for males and 6/12 for females; Fig. 12C1). For weak EPSP-IPSPs, all were from males (5/5 or 100%), which was significantly different from females (0/5 or 0%; Fisher's exact test, p=0.008; Fig. 12C1).

When EPSPs were compared in males and females at -65 to -75 mV, there were no significant differences in latency to onset, latency to peak, or amplitude (Student's t-tests, latency to onset: t=1.02, df 14, p=0.329; latency to peak: t=1.35, df 14, p=0.198; amplitude: t= 0.141, df 14, p=0.890; Fig. 12C2) but there was a significant sex difference in half-duration, with a longer duration in males (Mann-Whitney U test, p=0.042, U statistic 11; Fig. 12C3).

When robust EPSP-IPSPs were compared in the two sexes, there were only 2/6 females with IPSPs that had two peaks (33.3%) whereas in males there were two peaks in 4/6 GCs (66.7%) but this was not a significant difference (Fisher's Exact test, p=0.567). Because few female IPSPs had two clear peaks, the maximum amplitudes of

the IPSPs were compared to males. The membrane potential range was -65 to -75 mV. There were no significant sex differences in amplitude (Student's t-test, t=1.17, df 9, p=0.273) or half-duration (Mann-Whitney U test, p=0.662, U statistic 12).

These data suggest few sex differences and those differences that were significant are complex. One interpretation is that males had more robust responses in general, because they had a longer EPSP half-duration, and a greater sensitivity to GABAergic input, in that weak IPSPs were only found in males. This interpretation would be consistent with electrophysiological observations of females during the estrous cycle. Females had smaller mossy fiber fEPSPs than males for most of the estrous cycle (Harte-Hargrove et al., 2015).

DISCUSSION

I. Summary

This study showed that MCs have weak excitatory effects on GCs using optogenetics to activate the MC axons in the IML. EPSPs were extremely common, so much so that a field potential reflecting the EPSP could be recorded in the IML. Also, EPSPs appeared to be common to all parts of the MC projection. Dorsal and ventral GCs, two different Cre lines and both sexes exhibited these EPSPs.

The excitatory effects are described here as weak because EPSPs were small in amplitude. Also, EPSPs were subthreshold at RMP even with the maximal light stimulus and multiple viral injections, and this finding was independent of the recording method or other variables. The results withstood several tests of controls and potential technical limitations.

Although weak using standard conditions, MC excitation of GCs could be strengthened. Manipulations that strengthened excitation enhanced NMDA receptors or reduced GABAergic inhibition.

Regarding MC inhibition of GCs, conclusions are less straightforward because of the possibility that GABAergic neurons were activated directly. However, many characteristics of ChR2-induced inhibition were consistent with the idea that there is a MC → GABAergic neuron → GC pathway that can be powerful (Sloviter, 1994; Jinde et al., 2012; Bui et al., 2018).

Together the data suggest that there is weak MC excitation of GCs by AMPA and NMDA receptors that overlaps with a MC → GABAergic neuron → GC pathway (Fig. 13). The overlap of the EPSP and IPSP lead to a variable net effect, depending on many factors. Most of the time, inhibition dominates. Under special conditions, excitation is sufficient to cause GC firing.

II. Excitation of GCs by MC axons in the IML

EPSP homogeneity

A remarkable finding was the consistency of fEPSPs and EPSPs across the septotemporal axis. This is surprising because there are differences in dorsal and ventral MC expression of calretinin (Blasco-Ibanez and Freund, 1997; Fujise et al., 1998). In addition, ventral MCs show electrophysiological differences from dorsal MCs when there is hyperexcitability (Jinno et al., 2003). Ventral MCs also express more c-fos than dorsal MCs in response to novelty (Duffy et al., 2013; Bernstein et al., 2019). In contrast, the results suggest dorsal and ventral effects of MCs are similar. These data are consistent with the idea that the hippocampus is composed of repeating units or lamella, each with similar circuitry (Andersen et al., 2000). Regarding the c-fos data, septotemporal differences may occur because the behaving animal reflects not only the lamellar circuitry but also the translamellar and extrinsic inputs that act upon the lamellar circuitry.

Weak MC input and strong PP input to GCs

A long-standing question has been whether there is an interaction of the MC input to GCs with the PP input to GCs. We found that the MC input has a bidirectional effect on the PP input, depending on the timing of the MC input relative to the PP input. Thus, if the MC input is timed before the PP stimulus, the ability of a PP input to evoke APs in GCs is primarily inhibited and the effect can be strong. However, if the MC input is timed during or immediately following stimulation of the PP input, the PP input is facilitated, although this effect appears to be weak. There is a small temporal window for the facilitation to occur, but a much longer window for inhibition to occur, suggesting restricted excitation relative to inhibition. Presumably this tight window for facilitation

keeps the activation of GCs selective, consistent with a GC population that is a filter or gate (Acsady and Kali, 2007; Hsu, 2007; Krook-Magnuson et al., 2015), contributes to pattern separation (Leutgeb et al., 2007; Myers and Scharfman, 2009; Yassa and Stark, 2011; Newman and Hasselmo, 2014; Knierim and Neunuebel, 2016), and fires sparsely (Jung and McNaughton, 1993; Myers and Scharfman, 2009; Diamantaki et al., 2016; Pilz et al., 2016; Danielson et al., 2017; GoodSmith et al., 2017; Senzai and Buzsaki, 2017; Hainmueller and Bartos, 2020).

Insight gained from multiple optogenetic stimuli

The data obtained from paired-pulses suggest limited facilitation occurs at the MC → GC synapse. However, a short train of pulses can facilitate MC-driven GC EPSPs. Our data suggest facilitation can occur during trains at beta frequency (25 Hz trains) and possibly theta frequency (5 Hz trains). These observations predict that the MC-GC synapses contribute to beta-associated information processing (including memory; Kay 2014) and possibly theta-associated spatial exploration, consistent with prior studies and discussion (Soltesz et al., 1993; GoodSmith et al., 2017; Hashimotodani et al., 2017; Senzai and Buzsaki, 2017; Bui et al., 2018; Botterill et al., 2019; Jung et al., 2019).

III. Inhibition of GCs by MC axons in the IML

The results suggest that perisomatic-targeting GABAergic neurons are primarily responsible for the MC → GABAergic neuron → GC pathway, consistent with the hypothesis that the intermediary GABAergic neuron in this pathway is a basket cell (Sloviter, 1991; Sloviter, 1994). On the other hand, recent studies suggest that MCs may activate other interneuron subtypes (Hsu et al., 2015).

It was surprising that optogenetic stimulation evoked IPSPs but not in all GCs. Furthermore, some IPSPs were weak. This was surprising because inhibition of the PP-evoked population spike was consistent in inhibiting a PP-evoked population spike ipsi- and contralateral to the viral injection site. One possible explanation is based on the observation that inhibition of the population spike was <100% in many slices. That result

suggests that some GCs underlying the population spike were less inhibited than others. These GCs could be those that do not have IPSPs when patched.

Another possibility is suggested by the studies of EPSP-IPSPs in patched GCs. There were instances where IPSPs occurred after the EPSP was blocked, or the ionic constituents of the ACSF (K^+, Mg^{2+}) were altered. Therefore, IPSPs may be underestimated, because IPSPs can be masked. Together the results support the idea of a complex balance of MC-mediated excitation and inhibition of GCs.

IV. The net effect of MCs on GCs

This study addressed a paradox, that the MC projection makes numerous MC → GC glutamatergic synapses (Buckmaster et al., 1992; Buckmaster and Schwartzkroin, 1994; Buckmaster et al., 1996) but the net effects of MCs on the GC population often appear to be inhibitory (Sloviter, 1994; Hsu, 2007; Jinde et al., 2012; Bui et al., 2018).

One possible 'clue' to resolve the paradox is in the methods of past studies. Thus, most reports of excitatory effects of MCs on GCs have used recordings of GCs in slices where single cell recording or other methods are available that are difficult in vivo (Jackson and Scharfman, 1996; Chancey et al., 2014; Wright and Jackson, 2014; Hsu et al., 2015; Hashimotodani et al., 2017). On the other hand, MC-mediated inhibition of GCs in vivo is often judged only on inhibition of PP-induced GC population spikes (Sloviter, 1991; Jinde et al., 2012). The results from the present study suggest why methods may matter: in slice recordings of single GCs, EPSPs are widespread but subthreshold. If PP-evoked population spikes are studied in slices, as done here, there is only a weak facilitation of the population spike and that effect is only appreciated if the timing of an optogenetic pulse occurs within a very narrow time window.

Why excitation of GCs by MCs is weak - mechanisms

A natural question is why MC-driven EPSPs in GCs are weak. One possibility is that MCs are neuromodulatory to GCs (Jung et al., 2019). This is consistent with the idea that MCs, GCs, and CA3 PCs form a circuit with MCs helping ensure pattern separation (GoodSmith et al., 2019). It is not consistent with the idea that MCs impart their own functional role (Nakazawa, 2017; GoodSmith et al., 2019) having stronger and

more flexible place fields than GCs (Neunuebel and Knierim, 2012; GoodSmith et al., 2017; Senzai and Buzsaki, 2017).

Another question is why the somatic activity of MCs is high (Scharfman and Schwartzkroin, 1988; Scharfman, 1993; Larimer and Strowbridge, 2008; Danielson et al., 2017) if the effect of the terminals in the IML appear to be weakly excitatory. A possible explanation is that there may be inhibitory regulation of MC terminals by cannabinoid receptor type 1 (CB1 receptors) because CB1 activation leads to depressed glutamate release (Chiu and Castillo, 2008; Fig. 13). This idea is also consistent with the characteristics of the high failure rate of the MC → GC synapse (Scharfman, 1995b).

Why would a circuit have an active cell with depressed transmitter release on GCs? One possibility is to provide a circuit where GC activity can be up-regulated substantially and rapidly, i.e., as soon as the depression on the terminal is lifted (Fig. 13). This could make the MC→GC pathway behave in a way that is like an 'on-off' switch. In other words, MCs could 'switch' rapidly from having little excitatory effect on GCs to having a major excitatory effect. Having a major excitatory effect could be essential to activating GCs, because GC RMP is far from threshold.

When would weak MC excitation of GCs become strong enough to trigger GC firing?

When might conditions arise when MC → GC excitation is sufficiently enhanced to evoke GC firing? During pathological conditions, as suggested by studies of trauma (Santhakumar et al., 2000) and a study of seizures (Botterill et al., 2019). During the onset of hyperexcitability accompanying acute trauma or seizures, GCs may depolarize, NMDA receptors become stronger, and GABAergic inhibition weaker or even excitatory (Lillis et al., 2012; Zhang et al., 2012). At this time, MCs appear to cause the GCs to become 'detonators' (Santhakumar et al., 2000; Botterill et al., 2019).

In some normal conditions there may also be strengthening of MC → GC excitation, although no 'detonation'. One example reduced CB1 endogenous agonism. Another is LTP of the MC → GC synapse (Hashimotodani et al., 2017). Another example involves the noradrenergic brainstem projection. When activated, the noradrenergic input depolarizes GCs (Haas and Rose, 1987; Lacaille and

Schwartzkroin, 1988; Stanton et al., 1989). The result is that GCs are placed in a membrane potential range when a subsequent MC input would produce a greater late EPSP. In addition, enhanced MC → GC excitation may occur when tonic inhibition of GCs wanes at times during the estrous cycle (Maguire et al., 2005). Last, strengthening of the excitatory effects of MCs on GCs may occur during sleep, when hippocampal GABAergic neurons are inhibited preferentially (Freund and Gulyas, 1997). Also, CA3 SPW-Rs occur during sleep (Buzsaki, 1986; Buzsaki, 2015) which is important because SPW-Rs in CA3 in slices leads to activation of MCs by the PC backprojecting axons, and subsequent MC → GC excitation (Scharfman, 1994b; Scharfman, 1995b; Scharfman, 2007). These data are consistent with studies of slices with spontaneous SPW-Rs (Swaminathan et al., 2018). Other phenomena such as dentate spikes and implications for memory, which we did not address specifically, are important and addressed elsewhere (Penttonen et al., 1997; Lisman et al., 2005; Henze and Buzsáki, 2007). For these reasons and others, the effects of MCs on GC activity has received much attention, and is likely to continue to do so.

Table 1. Viral injection sites.

		One injection		Two injections		Three injections	
		Dorsal or Ventral		Dorsal and Ventral or Mid and Ventral		Dorsal, Mid, Ventral	
		Coordinate (mm)	Range (±)	Coordinate (mm)	Range (±)	Coordinate (mm)	Range (±)
Dorsal	A-P	2.0	0.0	2.0	0.1	1.9	0.0
	M-L	1.3	0.0	1.2	0.1	1.2	0.0
	Depth	2.2	0.0	2.0	0.1	2.1	0.0
Mid	A-P	none		3.1	0.2	2.9	0.2
	M-L	none		2.4	0.2	2.4	0.0
	Depth	none		2.6	0.2	2.6	0.2
Ventral	A-P	3.2	0.0	3.4	0.1	3.7	0.0
	M-L	2.8	0.0	2.6	0.1	2.6	0.1
	Depth	2.2	0.0	2.8	0.2	3.3	0.0
Use		Extracellular Intracellular (sharp electrode)		Whole-cell		Whole-cell	

Table 1. Legend.

Stereotaxic coordinates used for injections of virus encoding ChR2. For extracellular and sharp electrode recordings, only one injection site was used, either dorsal or ventral. For whole-cell recording, one or more injection sites were used. For two injections, either dorsal and ventral or mid and ventral, the center column lists the coordinates. For three injections, the right column lists the coordinates. Abbreviations: anterior-posterior, A-P; medio-lateral, M-L. Depth refers to depth below the skull surface. All coordinates are relative to Bregma.

Table 2. Characteristics of fEPSPs.

	Light pulse duration (msec)	Latency from onset of pulse (msec)	Latency from end of pulse (msec)	Slope (V/sec)	Amplitude (mV)	Rise time (msec)	Half-duration (msec)
Mean	2.43	4.62	2.31	0.11	1.78	2.42	10.35
SEM	0.37	0.76	0.38	0.02	0.39	0.29	0.60
n	19	20	20	17	19	14	10
Min	0.40	0.00	0.00	0.01	0.20	1.50	7.90
Max	5	10	5	0.45	7.2	6.6	15.9

Table 2 Legend.

Measurements of fEPSPs are listed using a stimulus that elicited a fEPSP that was close to the peak amplitude. The light pulse duration was the duration of the optogenetic stimulus used to elicit fEPSPs. Latency to onset was the time between the light pulse and the onset of the fEPSP, measured either from the start of the light pulse or the end. The slope of the initial (rising) phase of the fEPSP is measured in volts (V) per second (s). Peak amplitude was measured from the baseline just before the stimulus and was measured to the fEPSP peak. The rise time was the duration of the initial (rising) phase and was measured from the fEPSP onset to peak. The half-duration was the time between the end of the light pulse to the point on the decay of the fEPSP when it reached half its peak amplitude.

Table 3. Intrinsic properties of GCs with and without robust responses to optogenetic stimulation.

	Test	RMP	Rin	T	AP amp from RMP	AP amp from threshold	AP overshoot from 0 mV	AP Rising slope	AP Decay slope	Rate of rise:Rate of decay	Threshold from phase plot
	Units	mV	MΩ	msec	mV	mV	mV	V/s	V/s	ratio	mV
Cells with responses											
	Mean	-81.69	301.88	26.14	114.56	71.58	33.69	232.84	-72.32	3.15	-37.53
	SEM	1.16	16.74	1.70	1.94	1.94	1.71	12.33	2.24	0.10	1.00
	n	47	39	36	43	43	43	43	43	43	43
	Min	-91.11	130.50	12.68	76.47	45.56	4.36	98.90	-94.26	2.27	-48.70
	Max	-55.18	540.40	52.60	134.68	93.75	50.93	395.06	-38.77	4.63	-23.59
Cells without responses											
	Mean	-80.95	267.30	32.24	119.03	79.31	40.14	260.59	-80.22	3.28	-38.44
	SEM	1.85	12.16	5.16	2.67	3.19	2.60	12.86	4.34	0.18	1.55
	n	7	7	7	7	7	7	7	7	7	7
	Min	-86.27	229.90	17.87	107.49	69.55	30.37	206.32	-100.43	2.65	-43.21
	Max	-73.90	325.00	60.80	128.41	93.26	49.13	294.26	-67.16	3.95	-32.00

Table 3 Legend.

Intrinsic properties of GCs that had robust optogenetic responses or inconsistent, weak (<0.3 mV) responses are listed. There were no statistical differences (Student's t-tests, all p values >0.05). Abbreviations: amp, amplitude. Measurements are described in the Methods.

FIGURE LEGENDS

Figure 1. Experimental approach and viral expression in Drd2-Cre mice.

A.

1) A schematic of the rodent brain (side view) illustrates the location of the hippocampus (HC) in gray. Dorsal is up; Rostral is to the left.

2-3) A diagram illustrates the injection of AAV either in dorsal (2) or ventral (3) hippocampus. The axon of a dorsal MC (green arrows) is indicated, reflecting the major projection, which extends ipsi- and contralaterally, terminating distant to the cell body in the IML. Green lines without arrowheads are more modest projections to the hilus ipsilateral to the cell body.

B. A schematic of the dorsal mouse DG and proximal CA3 in the coronal plane shows the layers: outer molecular layer (OML); middle molecular layer (MML); inner molecular layer (IML); granule cell layer (GCL); hilus ; area CA3c pyramidal cell layer (CA3c). ML in part C and elsewhere refers to all three sublayers (OML, MML, IML). Upper and lower refer to the two DG blades.

C.

1) Two weeks after dorsal injection of AAV2-eYFP, there was strong fluorescence in the left dorsal hilus near the injection site (arrows). H = hilus.

2) Schematic of the injection and sections that were selected to show expression.

3) Expression in the contralateral hemisphere at a dorsal location similar to 1. Arrows mark staining of axons in the IML, reflecting the termination of MC axons contralateral to the injected somata.

4) Expression ipsilateral and caudal to the injection site is similar to 3, reflecting IML termination of MC axons (arrow) far from the injected somata.

5) Expression contralateral to the injection site, at an anterior-posterior level similar to 4. Expression is mainly in the IML (arrows). Calibrations, 50 μm.

Figure 2. Specificity of Cre expression in MCs.

A.

1) A schematic illustrates the injection of AAV2-eYFP in the left dorsal DG. Sections were taken for B-D from the area near the injection site.
2) The orientation of the tissue sections in B-D.
3) The area outlined by the box in 2 is expanded and many of the cell types are illustrated schematically. MCs are green. Granule cells are black. GABAergic neurons are orange, and all subtypes are not included. An area similar to the box is shown in B-D.

B.

1) Tissue sections were processed using an antibody to GluR2/3 to label glutamatergic neurons.
   Left: EYFP-expressing cells are denoted by the green arrows.
   Center: GluR2/3 labels glutamatergic cells in the hilus (red arrows). The vast majority are MCs.
   Right: The merged image of eYFP and GluR2/3 immunofluorescence shows that eYFP-expressing hilar cells also expressed GluR2/3 (white arrows). These data suggest that the hilar cells expressing Cre were MCs. Calibration, 50 μm. M, molecular layer; G, granule cell layer; H, hilus.
2) The same sections as B1 are shown at higher gain. Calibration, 20 μm.

C. Different sections were stained with an antibody to parvalbumin (PV), a marker of a major class of DG GABAergic neurons.
Left: eYFP-fluorescent hilar cells (green arrows).
Center: PV-immunoreactive cells (red arrows).
Right: The merged image shows no double-labeling. Calibration, 50 μm.

D.

1) An antibody to neuropeptide Y (NPY) was used to stain a major subset of GABAergic hilar cells.
   Left and Center: Many hilar neurons expressed eYFP (green arrows) or NPY (red arrows).

Right: Yellow cells were rare. One area of the hilus with yellow is expanded in D2 to show that some of the yellow cells did not reflect double-labeling, and how double-labeling can be identified. Calibration, 20 μm.

2) The area outlined by the box in D1 is shown at higher gain to illustrate that yellow reflected 2 overlapping cells but not double-labeling.
   Left: A cell expressing eYFP is noted by the green arrow.
   Center: The red arrow points to a different cell with NPY immunofluorescence.
   Right: The merged image shows that the cells denoted by the arrows overlap and therefore yellow is observed, but they are two different cells. Calibration, 10 μm.

Figure 3. Limitations of Crlr-Cre mice.

A.

1) A schematic shows a dorsal injection of AAV2-eYFP to evaluate specificity for MCs in dorsal hippocampus.
2) After dorsal injection of AAV2-eYFP, coronal sections were made of the dorsal HC. A dorsal coronal section shows hilar fluorescence as well as IML fluorescence (arrows), indicating labeling of MCs. The area surrounded by the box is between the hilus and CA3 and is shown at higher gain in 3.
3) Area CA3 showed no fluorescent cells. Calibrations:100 μm (2), 50 μm (3).
4) A schematic illustrates recording sites in slices that were prepared approximately two weeks after AAV2-ChR2 injection. The optical fiber was either directed towards the IML and recordings were made there, or light was directed at stratum lucidum (SL) in CA3 and recordings were made there.
5) Top: An optogenetic stimulus directed to the IML elicited a fEPSP in the IML.
   Bottom: An optogenetic stimulus directed to SL did not elicit a response. No responses were elicited from the PCL either (not shown). Similar data were elicited from 4 other slices (n=5; 1 slice/mouse).

B.

1) A schematic illustrates ventral injection of AAV2-eYFP. Approximately 3 weeks after ventral injection, horizontal sections were made of the ventral HC.

2) A ventral horizontal section shows hilar fluorescence as well as IML fluorescence. Arrows point to fluorescent areas. The area surrounded by the box is shown at higher gain in 3.
3) Arrows point to fluorescent CA3 neurons. Calibrations, 100 μm (2); 50 μm (3).
4) A schematic illustrates the light fiber direction towards the CA3 cell layer and recording at that location.
5) A robust light response was evoked with a short latency. These data suggest a lack of specificity for MCs in ventral hippocampus of Crlr-Cre mice.

C.

1-2) Experiments were conducted to confirm CA3 PCs were activated in B5 because the response morphology (waveform) was somewhat different from a population spike elicited by afferent stimulation (Scharfman et al., 2003). The mouse was from a line where POMC-Cre mice were crossed to a ChR2 reporter line, and ChR2 was tagged with GFP. A micrograph shows GFP fluorescence in GC dendrites and mossy fibers. The box that is outlined is shown at higher gain in 2). Calibrations, 100 μm (1); 50 μm (2).
3) A schematic of the experimental arrangement for a POMC-Cre x ChR2-GFP mouse. The optogenetic stimulus was directed towards the GCL and recordings were made in the GCL.
4) Activation of GCs with increasing light durations shows increasing responses that appear more and more like a population spike. One of the weaker responses (third from the top) is similar qualitatively to the CA3 response in B5, supporting the idea that recordings in B5 reflect activation of CA3 but the morphology was unusual because activation was not maximal.

Figure 4. Optogenetic stimulation of the IML evokes field EPSPs (fEPSPs) in the IML.

A. Either Drd2-Cre or Crlr-Cre mice were used after a single injection of AAV2-ChR2 in either dorsal (Drd2-Cre, Crlr-Cre) or ventral (Drd2-Cre) DG. Field potentials evoked by light were recorded.

1) The experimental arrangement is shown. Light was directed to the IML at least 100 µm from a recording electrode in the IML.
2) Examples of responses to increasing durations of light pulses (blue bars) showed a similar morphology as a fEPSP, and there was a gradual increase in amplitude, like a fEPSP. In this example, increasing the light pulse did not lead to a greater response after approximately 3 msec, which is also shown in 3 and 4.

3-4) FEPSP slope and amplitude are plotted for a subset of mice tested with the same light pulse durations (n=11 slices, 1 slice/mouse).

B. FEPSPs are specific to the IML.

1) The experimental preparation is shown. The recording site was in one location in the IML while the light fiber was moved from the GCL to the IML and then to the MML.
2) A fEPSP was evoked by the optogenetic stimulus when the optic fiber was directed at the IML. The fEPSP decreased when the light fiber was directed at the GCL or MML. The light pulse duration was the same for all recordings.

C. Example of a fEPSP preceded by a fiber volley (arrow) indicating the optogenetic stimulation activated presynaptic fibers in the IML. The volley was not elicited by light directed at the GCL or MML (not shown). The same trace is shown at two different timescales.

D. A fEPSP evoked by an optogenetic stimulus to the IML is shown before and after exposure to WIN 55,212, an antagonist of MC synapses (Chiu and Castillo, 2008).

E.

1) Left: A diagram shows the layers of the DG where recordings were made in response to light activation of the IML.

   Center: Responses elicited by a fixed light stimulus were recorded in many layers sequentially.

   Right: Current source density (CSD) analysis showed a current sink (red) in the IML, as would be predicted by light stimulation activating MC axons preferentially.
2) CSD analysis of responses to weak electrical stimulation of perforant path (PP) axons in the OML and MML. The site of the stimulating electrode is indicated by a black circle with the ball representing the monopolar stimulating electrode tip on

the slice, overlapping the OML and MML. Stimuli (at the dot) were 50 μA, 50 μsec current pulses triggered at 1/min. The CSD showed a current sink in the OML (red). The recordings in 1 and 2 are from the same slice.

Figure 5. Optogenetic activation of MC axons in the IML leads to weak excitation that is reproduced by electrical stimulation of the IML, and contrasts to strong excitation by the PP input.

A.

1) Intracellullar sharp-electrode recordings from two different GCs show the responses to a 1 msec-long light pulse directed to the IML, ~200 μm from the recorded cell. At RMP (-68 or -71 mV in each cell, respectively), a small depolarization was evoked. After depolarizing the cells (to -53 or -52 mV, respectively), the optogenetic stimulus evoked an AP.
2) In a different GC, the light pulse evoked an IPSP (arrow) after the EPSP at -60 mV. The red line marks the time when the EPSP was truncated by the IPSP. The red line suggests that at -79 mV both EPSP and IPSP were depolarizing.

B. Characteristics of fEPSPs elicited by optogenetic stimulation of IML axons.

1) a. The experimental arrangement is illustrated.
   b. Top: Recordings were made in the IML in response to an optogenetic stimulus.
   Center: Recording in the GCL of the response to the same stimulus. An arrow points to an extremely small population spike after the peak of the fEPSP which is consistent with population spikes, which are largest in a cell layer.
   Bottom: The same optogenetic stimulus evoked no clear response in stratum lucidum (SL) of CA3, suggesting that the optogenetic response was too weak to elicit APs in GCs and subsequently activate GC (mossy fiber) synapses on PCs.
2) a. The electrode locations for testing the responses to electrical stimulation of the mossy fibers. Same slice as B1. Methods for preferential mossy fiber stimulation are elsewhere (Skucas et al., 2013).
   b. Top: The response to weak electrical stimulation that is recorded in the CA3 PCL is a small fEPSP with a very small population spike after the peak, like the

GCL recording in B1b. These data are consistent with the idea that the IML response reflects weak activation of a proximal synapse.

Bottom: The recording in SL in response to a stronger electrical stimulus of the mossy fibers shows a large fEPSP can be elicited and there is large paired-pulse facilitation. The large fEPSP size in SL is consistent with past studies showing that the mossy fiber input can be powerful (Scharfman et al., 1990; Henze et al., 2000). The large paired-pulse facilitation is also consistent with mossy fiber activation of CA3 (Salin et al., 1996). Confirmation of these characteristics is important because they support the interpretation that hilar electrical stimulation primarily activated mossy fiber synapses on PCs.

3) Testing whether ChR2 expression limits the size of responses.

a. Similar sites for recording and stimulation were made as for B1 but the mouse expressed ChR2 in GCs and their mossy fibers (Fig. 3). Light was directed to the GCL rather than the IML.

b. Top (IML): Optogenetic stimulation elicited a large negative potential in the IML

Next line (GCL): Optogenetic stimulation evoked a population spike in the GCL, suggesting that ChR2 can induce large responses so it is unlikely to limit fEPSPs.

Third line (SL): The same optogenetic stimulus to the GCL that elicited a population spike in the GCL led to a delayed fEPSP in SL. The fEPSP in the SL began at a short latency after the peak of the population spike in the GCL, suggesting that ChR2 activation of GCs can lead to activation of mossy fibers and a fEPSP in SL. These data suggest ChR2 was not the reason for the inability to activate CA3 in B1b.

Bottom (SL): The SL response to two identical stimuli. The response is consistent with a mossy fiber-evoked fEPSP because there was large paired-pulse facilitation (Salin et al., 1996).

C. 1) The electrode locations for electrical stimulation of the IML.

2) a. Example of a fEPSP elicited by electrical stimulation of the IML. Sequential recordings in different layers showed the largest responses in the IML, consistent with preferential stimulation of the IML axons. Note there is no population spike, consistent with weak activation of the IML inputs.

b. Another example of fEPSPs elicited by IML electrical stimulation, demonstrating IML axons were preferentially stimulated. The fEPSP that was maximal in the IML was small in the MML and flipped polarity in the OML, consistent with fEPSP generation in the IML.

3) In contrast to IML stimulation, electrical stimulation of the PP elicited a fEPSP that could trigger a population spike in the GCL. Same slice as 1. The PP stimulus strength was adjusted so the fEPSP was not greater in amplitude than the fEPSP generated in the IML by IML stimulation. These data suggest that the PP input is strong relative to the MC input.

Figure 6. Short-term plasticity of optogenetic responses.

A.

1) Recordings were made of the fEPSP in response to optogenetic stimulation of the IML. The example shows superimposed optogenetically-evoked fEPSPs triggered in pairs with increasing interstimulus intervals. Identical stimuli were used. Each pair of stimuli was triggered every min. Interstimulus intervals were 10-200 msec and only some of the responses are shown. FEPSPs showed inhibition at short intervals.
2) Comparisons of paired-pulse responses in 6-7 slices from 7 mice. FEPSPs amplitudes were measured and the ratio of the second to the first was calculated for each pair of stimuli. At short intervals there was paired-pulse inhibition. A two-way RMANOVA was conducted to compare optogenetic stimulation (A) and electrical stimulation of the IML (B). Asterisks indicate significant differences ($p<0.05$) in post-hoc comparisons.

B.

1) Example of fEPSPs evoked by electrical stimulation (at the dots) of the IML using the same interstimulus intervals as A. The IML stimulation site and stimulus strength were selected so that the maximal response was always in the IML, rather than the adjacent MML or GCL (see Fig. 5 and the text for details).
2) There was significantly less inhibition at 10-60 msec intervals when electrical stimuli were used.

C.

1) EPSPs were elicited by optogenetic stimulation of the IML in patched GCs. Description of EPSPs is provided in Figure 7.

   a. Five stimuli at 100 Hz show strong suppression of the 2nd-4th responses. The inset shows the same data at higher gain. The same GC was used for a-c.

   b. Five stimuli at 25 Hz show some suppression and some facilitation during the trains.

   c. Five stimuli at 5 Hz shows suppression during the train primarily. Note responses to 25 and 5 Hz were variable (see C2, D).

2) Two trains (a-b) of 4 optogenetic stimuli were triggered at 25 Hz to illustrate the variability of a single GC in responses to 25 Hz.

D. Comparison of EPSP amplitudes in 4 GCs using different frequencies of 3 optogenetic stimuli at RMP. Each color designates a different GC as shown in the legend (upper right).

1) EPSPs were suppressed during 100 Hz trains.

2) More than 1 train at 25 Hz was tested in the same GC (cell 1, blue, and cell 4, red) to show variability of responses to 25 Hz trains.

3) 5 Hz stimuli were tested and showed variable responses. Two trains were tested for cell 4.

Figure 7. Small EPSPs in patched GCs in response to optogenetic stimulation of the IML.

A. A representative example of an EPSP recorded in a GC in response to optogenetic stimulation of the IML.

1) a. A current clamp recording.

   b. The recording in voltage clamp from the same cell shows an inward current in response to the same optogenetic stimulus. Later in the recording is an example of a spontaneous inward current (black arrow).

2) The EPSP/C is shown at higher gain (a, current clamp, b, voltage clamp). In 1a and 2a, the optogenetic stimulus is denoted by an arrow. In 1b and 2b, the optogenetic stimulus is denoted by a bar. The arrow in 2b points to the artifact at

the end of the light pulse, showing that the EPSC often had such a short latency that it began before the light pulse ended, similar to fEPSPs (Fig. 5).

B. Comparisons of optogenetically-evoked EPSPs. The durations of the light pulses were chosen so that a response was elicited between 50% and 100% of the maximum at RMP (power was fixed at 10 mW). The membrane potential was -65 to -75 mV. The EPSPs had no detectable IPSP even if depolarized.

1-2) The latency to onset, rise time and amplitude (1) and half-durations (2) are shown.

3) The half-durations of responses without IPSPs (EPSPs, no detectable IPSP, even if depolarized from RMP) are compared to the responses with IPSPs (EPSPs followed by IPSPs; referred to as “EPSP-IPSPs”; described more in Fig. 8). Differences were significant (asterisk). EPSPs without IPSPs were measured from the end of the light pulse to the point during the EPSP when the depolarization had decayed to half of its peak amplitude. For EPSPs with IPSPs, the measurement was from the end of the light pulse to the time when the IPSP had decayed to half its peak amplitude. IPSPs significantly lengthened the response.

C. EPSPs could be blocked by the AMPA receptor antagonist DNQX (10 μM). A representative example of an EPSP before (Pre) and after DNQX (Post DNQX) shows the blockade of the EPSP by DNQX.

D. Prolonged EPSPs at depolarized potentials trigger APs, suggesting a voltage-dependent late EPSP.

1) An EPSP was triggered at two membrane potentials. At -72 mV, the EPSP was small and did not trigger an AP (inset). At -61 mV, the EPSP triggered a prolonged depolarization and AP.

2) In a different cell, an EPSP was triggered at a depolarized potential where spontaneous APs occurred intermittently. The optogenetic stimulus did not trigger a prolonged depolarization and there was no AP. One of the APs that occurred spontaneously is at the end of the recording (black arrow).

E. Additional examples of voltage-dependent late EPSPs that can trigger APs.

1) Example of a GC response to an optogenetic stimulus at 3 membrane potentials illustrating the emergence of a late phase of the EPSP as the cell was depolarized. An AP appeared to be triggered from the late phase, rather than the early phase.
2) An example of a response to optogenetic stimulation in a different GC illustrates the gradual emergence of the late EPSP and its prominence at potentials depolarized to -60 mV (arrow).

F. EPSPs are significantly prolonged at depolarized potentials, but the initial peak is not affected significantly.
1) Half-durations of EPSPs are plotted at many membrane potentials. The responses elicited within 10 mV ranges were pooled (e.g., -85 to -95 mV). The middle of each range is plotted on the X axis (e.g., -90 mV corresponds the EPSPs elicited between -85 and -95 mV). A one-way ANOVA showed that there was a significant increase with depolarization.
2) Amplitudes of the initial peaks of EPSPs are shown. A one-way ANOVA showed no significant effects of depolarization. The data in 1 and 2 suggest there is an early EPSP and voltage-dependent late EPSP which prolongs the initial EPSP.

G. Late EPSPs could be blocked by APV.
1) A response to an optogenetic stimulus is shown at two membrane potentials before DL-APV (50 μM; Pre).
2) The same stimuli were triggered after exposure to APV (Post APV). The late phase of the EPSP, detected primarily at the more depolarized membrane potential (-50, Top), was reduced by APV. The early EPSP, the primary phase of the EPSP at hyperpolarized potentials (-65 mV, Bottom), showed little effect of APV. Note that the early EPSP was reduced by APV at -50 mV (Top), suggesting that the late EPSP starts during the early EPSP.

H. Effect of reduced concentrations of $[Mg^{2+}]_o$ in the ACSF on optogenetically-evoked EPSPs. Using ACSF without Mg^{2+}, three optogenetic stimuli were triggered at RMP. Stimuli were 40 msec apart, so that the 2nd and 3rd stimuli were triggered during the late EPSP elicited by the previous stimuli. Note the large size of the EPSPs and the ability of stimuli to elicit APs. The inset shows the responses to presentation of the

three stimuli 1/min, showing the large amplitudes of EPSPs and ability to generate APs were reproducible.

I. Effects of membrane potential on intrinsic properties of GCs.

1) An example of a recording from a GC with responses to progressively increased current steps. The incremental changes in current were the same but the incremental change in voltage response increased as steps approached depolarized potentials.
2) Input resistance measured at RMP for most GCs (n=48) shows a significant correlation of membrane potential and input resistance, with input resistance higher in GCs with more depolarized RMPs.

Figure 8. EPSP-IPSPs in patched GCs in response to optogenetic stimulation of the IML.

A. A representative example of a response evoked by optogenetic stimulation with an EPSP and a hyperpolarization afterwards. The hyperpolarization could inhibit firing and was blocked by GABA receptor antagonism so it is called an IPSP.

1) A current clamp recording of the EPSP-IPSP shows a large IPSP which was consistent from stimulus to stimulus and therefore is called strong or robust elsewhere
2) In the same cell, the recording in voltage clamp, at the same membrane potential as 1, was an inward current (EPSC) followed by an outward current (IPSC).
3) The EPSP-IPSP (1) or EPSP-IPSC (2) is shown at higher gain (a, current clamp; b, voltage clamp).

B. An example of an inconsistent or “weak” IPSP. The same optogenetic stimulus was triggered 1/min. Responses, which did not always elicit an IPSP, are superimposed. Of the 17 GCs with IPSPs, 5 were inconsistent and 12 were larger and very consistent (strong or robust, as in A). Because of the inconsistency of the 5 cells they are not included in the quantification in C.

C. Cells with strong IPSPs were recorded between -65 and -75 mV to determine latencies to peak. Most cells had two distinct peaks (n=7/12) and are shown. The

initial peak is noted as early and the second peak is referred to as late. Differences in the latency to peak of early and late IPSPs were statistically significant.

D. The amplitude of the early and late IPSPs increased with depolarization, consistent with mediation by Cl- and K+ as carriers in $GABA_A$ and $GABA_B$ ligand-gated channels, respectively.

E. IPSPs were inhibitory. Recordings are shown from two different cells (1 and 2) where EPSP-IPSPs were triggered at depolarized membrane potentials where spontaneous APs occurred. At these potentials, the EPSP was small and the IPSP was large. During the IPSP, APs did not occur, which is consistent with IPSPs that inhibit AP firing.

F.

1) IPSPs occurred after EPSPs, suggesting a disynaptic circuit (MC → GABAergic neuron → GC). Consistent with that hypothesis, DNQX could block the IPSP. An example of an EPSP-IPSP before and after 10 μM DNQX is shown, illustrating loss of the IPSP after DNQX treatment.
2) An example of a cell that had an EPSP-IPSP that was not fully blocked by DNQX. In control, the IPSP was weak. After DNQX, the EPSP was blocked and a small IPSP remained. This IPSP was blocked by 1 μM gabazine, suggesting the IPSP was mediated by $GABA_A$ receptors. These data could be due to direct activation of GABAergic neurons by the optogenetic stimulus. Consistent with a monosynaptic pathway, the delay from the end of the light pulse to the onset of the IPSP was brief (3.18 msec).

G. Morphology of recorded GCs. An example of a GC labeled by biocytin is shown. It illustrates typical characteristics of mature GCs such as small, oval cell body, position of the cell body in the GCL, large apical dendritic tree extending to the hippocampal fissure, an axon descending into the hilus (arrowhead in the GCL) with boutons in the hilus (arrowhead in the hilus). Taken together with the intrinsic properties of the cells, which were similar to mature GCs (Table 3), the GCs that were sampled were unlikely to be young adult-born GCs, semilunar GCs, or GABAergic neurons.

Figure 9. Comparison of EPSPs and EPSP-IPSPs in response to optogenetic stimulation of the IML in patched GCs.

A. The mean pulse durations used to evoke responses to optogenetic stimulation are shown. Responses were either EPSPs or EPSP-IPSPs. Differences were statistically significant (asterisk). All EPSP-IPSPs are included, those that were robust and those that were weak.

B.

1) The latencies to onset of the EPSPs and EPSP-IPSPs are plotted. Differences were not significant. All EPSP-IPSPs are included, those that were robust and those that were weak.
2) The latencies to peak of the EPSPs with and without IPSPs are shown. Only EPSP-IPSPs with two peaks are included only. Differences were significant.

C. The amplitudes of the early peak of EPSPs are plotted for membrane potential ranges with a midpoint shown on the X axis. For example, -90 corresponds to responses recorded between -85 to -95 mV. The EPSPs that were included were EPSPs of the EPSP-IPSP responses. Amplitudes decreased significantly with depolarization by one-way ANOVA. Asterisks are $p<0.05$ by post-hoc test. The decrease in amplitude with depolarization did not occur for early EPSPs without IPSPs (see previous Fig. 7F2).

D. The amplitudes and durations of EPSPs increased after blockade of IPSPs.

1) An example of the effects of GABAergic receptor blockade is shown for a GC with an EPSP-IPSP. The responses to a fixed optogenetic stimulus were recorded at a fixed membrane potential before drugs (Pre), after 10 μM bicuculline methiodide (BMI) and 10 μM CGP52432 (b; BMI + CGP), and after adding 50 μM DL-APV (c; BMI + CGP + APV). The stimulus evoked an EPSP with greater amplitude and duration after BMI + CGP. APV reduced the EPSP, primarily the late phase, consistent with an NMDA-sensitive late EPSP at depolarized potentials.
2) Comparisons of superimposed traces before (Pre) and after BMI + CGP (BMI + CGP) at two membrane potentials show a strong effect of GABA receptors to suppress the late EPSP.

E. IPSPs suppress firing, and both early and late IPSPs exert this effect.

1) Recordings are shown from a representative experiment where the response to a fixed optogenetic stimulus was triggered during depolarizing and hyperpolarizing steps of injected current. The inset shows the inhibitory effect of the optogenetic stimulus at a more depolarized potential where spontaneous APs occurred.
2) After BMI was added to the ACSF, the early phase of the IPSP was reduced but the late phase was still prominent and there was no firing elicited by the optogenetic stimulus.
3) After CGP was added to the BMI-containing ACSF, the optogenetic stimulus triggered an EPSP without an IPSP. An AP was triggered at depolarized potentials by the optogenetic stimulus showing a strong inhibitory effect of the late IPSP.

F.

1) Data from E are plotted. Amplitudes were measured at fixed times after the optogenetic stimulus corresponding to the peak of the early EPSP (red). early IPSP (blue), and late IPSP (green).
2) BMI reduced the early IPSP and caused the EPSP to increase in amplitude approximately 2-fold.
3) CGP reduced the late IPSP with little effect on the early EPSP.

Figure 10. Bidirectional regulation of PP-evoked population firing by optogenetic stimulation of the IML.

A. A diagram of the experimental arrangement shows light was directed to the IML near the area where extracellular recordings were made. Electrical stimulation was at the hippocampal fissure beneath the subiculum, on the white fiber bundle of the PP as it divides in the ML. Recordings were made in the GCL to record the population spike, and the OML, where the maximal fEPSP in response to the PP input was recorded. The recording sites were placed perpendicular to the GCL layer so the fEPSP corresponded best to the GCL recording of the population spike.

B.

1) The timeline for optogenetic (Light) and electrically-evoked stimuli (Stim).
2) Optogenetic stimulation inhibited the population spike if it was triggered over 2 msec before the PP stimulus. There was facilitation of the population spike if the

light pulse was triggered closer to the PP stimulus. The ACSF contained 5 mM K^+.

C. 1-2) Data from a different slice shows that optogenetic stimulation could block the population spike completely. Note this example, when compared to B, show a variability in the degree the population spike is inhibited. Also, when stimulation occurs close to the PP stimulus, there can be either inhibition or facilitation.

D. The ACSF contained 3.5 mM $[K^+]_o$. Under these conditions, a single electrical stimulus to the PP did not elicit a large population spike, so a pair of electrical stimuli was triggered because this elicits paired-pulse facilitation when the interval is 40 msec. Note that the second stimulus elicits a population spike.

1) The timeline of optogenetic and PP stimulation is shown.
2) Robust inhibition of the population spike occurred when a light pulse was triggered before the second electrical stimulus, reproducing the effects in B-C with another experimental approach.

E. For 3 slices, the interval between the optogenetic stimulus and the PP stimulus is plotted on the X axis and the percent inhibition or facilitation of the population spike is plotted on the Y axis. The maximum inhibition was greater than the maximum facilitation. Inhibition did not occur if the optogenetic stimulus occurred after PP stimulation. Facilitation only occurred if the optogenetic stimulus occurred at or after the PP stimulus. These data are consistent with rapid, weak monosynaptic excitation and slower, stronger disynaptic inhibition of GCs by the optogenetic stimulus.

F. Optogenetic and PP-evoked EPSPs were compared in the same GC in 3 cells from 3 different mice. The figure shows a representative example with a schematic of the timing of stimulation on the left and recordings on the right.

1) Light and PP stimulation were triggered separately to show the optogenetic and PP-induced EPSPs.
2) The optogenetic stimulus was triggered shortly before PP stimulation. The optogenetically- and PP stimulation-evoked EPSPs were not synchronized sufficiently to align their peaks. Dotted lines mark the EPSP peaks.
3) Light was triggered shortly after PP stimulation and led to synchronization of the optogenetic- and PP stimulation evoked-EPSP peaks. The data suggest a

potential reason why facilitation of the population spike occurred when optogenetic stimuli were triggered after PP stimulation.

Figure 11. Evidence that perisomatic-targeting GABAergic neurons are primarily responsible for optogenetic inhibition of the PP-evoked population spike.

A. Recording and stimulating electrode locations for B-C.

B.

1) The timing of optogenetic (Light) and PP stimuli (Stim) for responses in B2.
2) Responses to stimuli were recorded first in the GCL and then the OML (Top: GCL; Bottom: OML). In the GCL, the optogenetic stimulus blocked the PP-evoked population spike with little effect on the positivity upon which the population spike is superimposed. In the OML, the negativity reflecting the fEPSP was relatively unaffected by optogenetic stimulation. However, the inflection corresponding to the population spike was blocked. Therefore, GC firing appeared to be inhibited without effects on the underlying EPSP, consistent with effects of perisomatic-targeting interneurons.

C.

1) A schematic shows the measurement of interval used for the X axis in C2-3.
2) Amplitudes of the PP-evoked population spike are plotted for a range of intervals between the optogenetic stimulus and the PP stimulus.
3) Amplitudes of the fEPSP recorded in the OML in B2 are plotted. The data in 2 and 3 support the findings in B showing that the population spike evoked by PP stimulation could be inhibited by the optogenetic stimulus with little effect on the fEPSP amplitude.

D. A schematic of the recording arrangement for E-F.

E. A schematic of the experimental timeline. Stimuli were triggered every minute in this order: electrical stimulation of the PP, optogenetic stimulation, both PP and optogenetic stimulation. For the latter, the optogenetic stimulus was triggered with the same delay before the PP stimulus. This sequence was repeated throughout the experiment. There was a control period to confirm responses were stable, and then the slice was exposed to 10 μM BMI.

F. Responses are shown for before (1; Pre) and after BMI was added to the ACSF (2; BMI). In the control period, a PP stimulus (1a, Stim) evoked a large population spike and a prepulse of light inhibited it (1b, Light + Stim). When light was triggered by itself (1c, Light), a small fEPSP occurred. After BMI, the light pulse no longer inhibited the population spike elicited by PP stimulation (Compare 1b, Light + Stim, and 2b, Light + Stim). The fEPSP evoked by the light pulse (2c, Light) appeared to be unaffected by BMI, which is consistent with the idea that optogenetic stimulation evoked a fEPSP mediated by glutamate, not GABA. Note a second population spike occurred after BMI (2a, Stim) and was inhibited by light (2b, Light + Stim). This result is consistent with the inability of BMI to block the late IPSP evoked by optogenetic stimulation.

Figure 12. Experimental variables that influenced optogenetic responses.

A. Recording sites are diagrammed to show their position relative to the site of viral injection (e.g., ipsilateral or contralateral to the injection site).

1) Recording positions for a dorsal (left) and ventral (right) viral injection are illustrated. Recordings from slices were either < 2 slice widths (800 μm) from the viral injection (ipsilateral, “near”), ipsilateral but > 2 slice widths away (ipsilateral, “far”), or contralateral (Contra) to the viral injection site. There were no significant differences in fEPSPs elicited by IML optogenetic stimuli at the different locations (data are in the text).
2) The numbers of EPSPs (green) recorded ipsilateral (Ipsi) or contralateral (Con) to the viral injection, out of all EPSPs, are shown. EPSPs were more common contralateral to the viral injection site. Numbers of EPSP-IPSPs (red) are shown in the same way as EPSPs. EPSP-IPSPs were divided into those that had a strong IPSP or a weak IPSP. In contrast to EPSPs which lacked IPSPs, EPSP-IPSPs with a strong IPSP were recorded primarily ipsilaterally. EPSP-IPSPs with weak IPSPs were more common contralaterally than ipsilaterally. Significant differences by Fisher’s Exact test are indicated by asterisks.

B. Comparisons were made of optogenetic responses in the different parts of the DG blades using either coronal or horizontal orientations.

1-2) The upper blade, lower blade and crest regions are demarcated as in prior studies (Scharfman, 1995b) and are shown for 1) coronal and 2) horizontal slice angles.

3) There was a significantly shorter latency to onset of fEPSPs for coronal slices.

4) There were no significant differences in the slopes or amplitudes of fEPSPs.

C. Comparisons of data from male and female mice.

1) The proportions of males vs. females with EPSPs or EPSP-IPSPs with strong IPSPs were not significantly different. For EPSP-IPSPs with weak IPSPs, 100% were in males and 0% were in females, which was statistically significant.

2) There were no significant differences between sexes in EPSP latency to onset, latency to peak or amplitude. The EPSPs in 2 and 3 were those that lacked IPSPs.

3) EPSP half-duration was greater in males (measured at -65 to -75 mV; asterisk).

Figure 13. The MC → GC and MC → GABAergic neuron → GC pathways.

A. The MC → GC pathway.

1) The results support prior anatomical data showing that the axons of MCs that are in the IML (green) excite many GCs (grey) by a direct projection (Buckmaster et al., 1992; Buckmaster et al., 1996; Wenzel et al., 1997). However, the results presented here suggest the effects on each GC are weak (indicated by dotted lines).

2) a. The MC → GC synapse is shown with presynaptic modulation by CB1 receptors and postsynaptic excitation mediated by AMPA and NMDA receptors. The thin green arrow represents presynaptic inhibition, suggested by prior studies identifying that preynaptic CB1 receptors inhibit this synapse (Chiu and Castillo, 2008). Other potential mechanisms are possible also.

b. Effects that strengthen MC → GC synapses are shown. For example, 5 or 25 Hz trains could lead to facilitation of the MC → GC EPSP. Depolarization of the GC was another condition that allowed the MC → GC EPSP to strengthen. A larger EPSP is indicated by a larger green arrow in 2 compared to 1.

B. The MC → GABAergic neuron → GC pathway.

1) The results presented here support prior studies (Sloviter, 1991; Sloviter, 1994) suggesting that excitation of perisomatic-targeting interneurons, such as the pyramidal basket cell that is illustrated, inhibit GCs after the MC excites the basket cell.
2) The $GABA_A$ and $GABA_B$ receptors that appear to mediate IPSPs are shown.

REFERENCES

Acsady L, Kali S (2007) Models, structure, function: The transformation of cortical signals in the dentate gyrus. Prog Brain Res 163**:** 577-599.

Amaral D (1978) A Golgi study of cell types in the hilar region of the hippocampus in the rat. J Comp Neurol 15**:** 851-914.

Amaral DG, Scharfman HE, Lavenex P (2007) The dentate gyrus: Fundamental neuroanatomical organization (dentate gyrus for dummies). Prog Brain Res 163**:** 3-22.

Andersen P, Soleng AF, Raastad M (2000) The hippocampal lamella hypothesis revisited. Brain Res 886**:** 165-171.

Azevedo EP, Pomeranz L, Cheng J, Schneeberger M, Vaughan R, Stern SA, Tan B, Doerig K, Greengard P, Friedman JM (2019) A role of Drd2 hippocampal neurons in context-dependent food intake. Neuron 102**:** 873-886.

Bering R, Draguhn A, Diemer NH, Johansen FF (1997) Ischemia changes the coexpression of somatostatin and neuropeptide Y in hippocampal interneurons. Exp Brain Res 115**:** 423-429.

Bernstein HL, Lu YL, Botterill JJ, Scharfman HE (2019) Novelty and novel objects increase c-fos immunoreactivity in mossy cells in the mouse dentate gyrus. Neural Plast 2019**:** 1815371.

Blasco-Ibanez JM, Freund TF (1997) Distribution, ultrastructure, and connectivity of calretinin-immunoreactive mossy cells of the mouse dentate gyrus. Hippocampus 7**:** 307-320.

Botterill JJ, Lu YL, LaFrancois JJ, Bernstein HL, Alcantara-Gonzalez D, Jain S, Leary P, Scharfman HE (2019) An excitatory and epileptogenic effect of dentate gyrus mossy cells in a mouse model of epilepsy. Cell Rep 29**:** 2875-2889.

Buckmaster PS, Strowbridge BW, Kunkel DD, Schmiege DL, Schwartzkroin PA (1992) Mossy cell axonal projections to the dentate gyrus molecular layer in the rat hippocampal slice. Hippocampus 2**:** 349-362.

Buckmaster PS, Schwartzkroin PA (1994) Hippocampal mossy cell function: A speculative view. Hippocampus 4**:** 393-402.

Buckmaster PS, Wenzel HJ, Kunkel DD, Schwartzkroin PA (1996) Axon arbors and synaptic connections of hippocampal mossy cells in the rat in vivo. J Comp Neurol 366**:** 271-292.

Buckmaster PS, Amaral DG (2001) Intracellular recording and labeling of mossy cells and proximal CA3 pyramidal cells in macaque monkeys. J Comp Neurol 430**:** 264-281.

Bui AD, Nguyen TM, Limouse C, Kim HK, Szabo GG, Felong S, Maroso M, Soltesz I (2018) Dentate gyrus mossy cells control spontaneous convulsive seizures and spatial memory. Science 359**:** 787-790.

Buzsaki G (1986) Hippocampal sharp waves: Their origin and significance. Brain Res 398**:** 242-252.

Buzsaki G (2015) Hippocampal sharp wave-ripple: A cognitive biomarker for episodic memory and planning. Hippocampus 25**:** 1073-1188.

Chancey JH, Poulsen DJ, Wadiche JI, Overstreet-Wadiche L (2014) Hilar mossy cells provide the first glutamatergic synapses to adult-born dentate granule cells. J Neurosci 34**:** 2349-2354.

Chapman CA, Xu Y, Haykin S, Racine RJ (1998) Beta-frequency (15-35 Hz) electroencephalogram activities elicited by toluene and electrical stimulation in the behaving rat. Neuroscience 86: 1307-1319.

Chiu CQ, Castillo PE (2008) Input-specific plasticity at excitatory synapses mediated by endocannabinoids in the dentate gyrus. Neuropharmacology 54: 68-78.

Choi YS, Lin SL, Lee B, Kurup P, Cho HY, Naegele JR, Lombroso PJ, Obrietan K (2007) Status epilepticus-induced somatostatinergic hilar interneuron degeneration is regulated by striatal enriched protein tyrosine phosphatase. J Neurosci 27: 2999-3009.

Danielson NB, Turi GF, Ladow M, Chavlis S, Petrantonakis PC, Poirazi P, Losonczy A (2017) In vivo imaging of dentate gyrus mossy cells in behaving mice. Neuron 93: 552-559 e554.

Deng M, Zhang Q, Wu Z, Ma T, He A, Zhang T, Ke X, Yu Q, Han Y, Lu Y (2020) Mossy cell synaptic dysfunction causes memory imprecision via mir-128 inhibition of STIM2 in Alzheimer's disease mouse model. Aging Cell e13144.

Diamantaki M, Frey M, Berens P, Preston-Ferrer P, Burgalossi A (2016) Sparse activity of identified dentate granule cells during spatial exploration. Elife 5.

Duffy AM, Schaner MJ, Chin J, Scharfman HE (2013) Expression of c-fos in hilar mossy cells of the dentate gyrus in vivo. Hippocampus 23: 649-655.

Esposito MS, Piatti VC, Laplagne DA, Morgenstern NA, Ferrari CC, Pitossi FJ, Schinder AF (2005) Neuronal differentiation in the adult hippocampus recapitulates embryonic development. J Neurosci 25: 10074-10086.

Frankowski JC, Kim YJ, Hunt RF (2019) Selective vulnerability of hippocampal interneurons to graded traumatic brain injury. Neurobiol Dis 129: 208-216.

Freund TF, Buzsaki G (1996) Interneurons of the hippocampus. Hippocampus 6: 347-470.

Freund TF, Gulyas AI (1997) Inhibitory control of GABAergic interneurons in the hippocampus. Can J Physiol Pharmacol 75: 479-487.

Frotscher M, Drakew A, Heimrich B (2000) Role of afferent innervation and neuronal activity in dendritic development and spine maturation of fascia dentata granule cells. Cereb Cortex 10: 946-951.

Fujise N, Liu Y, Hori N, Kosaka T (1998) Distribution of calretinin immunoreactivity in the mouse dentate gyrus: II. Mossy cells, with special reference to their dorsoventral difference in calretinin immunoreactivity. Neuroscience 82: 181-200.

Gangarossa G, Longueville S, De Bundel D, Perroy J, Herve D, Girault JA, Valjent E (2012) Characterization of dopamine D1 and D2 receptor-expressing neurons in the mouse hippocampus. Hippocampus 22: 2199-2207.

Ge S, Yang CH, Hsu KS, Ming GL, Song H (2007) A critical period for enhanced synaptic plasticity in newly generated neurons of the adult brain. Neuron 54: 559-566.

GoodSmith D, Chen X, Wang C, Kim SH, Song H, Burgalossi A, Christian KM, Knierim JJ (2017) Spatial representations of granule cells and mossy cells of the dentate gyrus. Neuron 93: 677-690.

GoodSmith D, Lee H, Neunuebel JP, Song H, Knierim JJ (2019) Dentate gyrus mossy cells share a role in pattern separation with dentate granule cells and proximal CA3 pyramidal cells. J Neurosci 39: 9570-9584.

Haas HL, Rose GM (1987) Noradrenaline blocks potassium conductance in rat dentate granule cells in vitro. Neurosci Lett 78**:** 171-174.

Hainmueller T, Bartos M (2020) Dentate gyrus circuits for encoding, retrieval and discrimination of episodic memories. Nat Rev Neurosci 21**:** 153-168.

Hajos N, Freund TF (2002) Pharmacological separation of cannabinoid sensitive receptors on hippocampal excitatory and inhibitory fibers. Neuropharmacology 43**:** 503-510.

Harte-Hargrove LC, Varga-Wesson A, Duffy AM, Milner TA, Scharfman HE (2015) Opioid receptor-dependent sex differences in synaptic plasticity in the hippocampal mossy fiber pathway of the adult rat. J Neurosci 35**:** 1723-1738.

Hashimotodani Y, Nasrallah K, Jensen KR, Chavez AE, Carrera D, Castillo PE (2017) LTP at hilar mossy cell-dentate granule cell synapses modulates dentate gyrus output by increasing excitation/inhibition balance. Neuron 95**:** 928-943.

Henze DA, Urban NN, Barrionuevo G (2000) The multifarious hippocampal mossy fiber pathway: A review. Neuroscience 98**:** 407-427.

Henze DA, Buzsáki G (2007) Hilar mossy cells: Functional identification and activity in vivo. Prog Brain Res 163**:** 199-216.

Hetherington PA, Austin KB, Shapiro ML (1994) Ipsilateral associational pathway in the dentate gyrus: An excitatory feedback system that supports N-methyl-D-aspartate-dependent long-term potentiation. Hippocampus 4**:** 422-438.

Hosp JA, Struber M, Yanagawa Y, Obata K, Vida I, Jonas P, Bartos M (2014) Morpho-physiological criteria divide dentate gyrus interneurons into classes. Hippocampus 24: 189-203.

Houser CR (2007) Interneurons of the dentate gyrus: An overview of cell types, terminal fields and neurochemical identity. Prog Brain Res 163: 217-232.

Hsu D (2007) The dentate gyrus as a filter or gate: A look back and a look ahead. Prog Brain Res 163: 601-613.

Hsu TT, Lee CT, Tai MH, Lien CC (2015) Differential recruitment of dentate gyrus interneuron types by commissural versus perforant pathways. Cereb Cortex.

Hu H, Jonas P (2014) A supercritical density of na(+) channels ensures fast signaling in GABAergic interneuron axons. Nat Neurosci 17: 686-693.

Jackson MB, Scharfman HE (1996) Positive feedback from hilar mossy cells to granule cells in the dentate gyrus revealed by voltage-sensitive dye and microelectrode recording. J Neurophysiol 76: 601-616.

Jinde S, Zsiros V, Jiang Z, Nakao K, Pickel J, Kohno K, Belforte JE, Nakazawa K (2012) Hilar mossy cell degeneration causes transient dentate granule cell hyperexcitability and impaired pattern separation. Neuron 76: 1189-1200.

Jinno S, Ishizuka S, Kosaka T (2003) Ionic currents underlying rhythmic bursting of ventral mossy cells in the developing mouse dentate gyrus. Eur J Neurosci 17: 1338-1354.

Johansen FF, Zimmer J, Diemer NH (1987) Early loss of somatostatin neurons in dentate hilus after cerebral ischemia in the rat precedes CA-1 pyramidal cell loss. Acta Neuropathol 73: 110-114.

Jung D, Kim S, Sariev A, Sharif F, Kim D, Royer S (2019) Dentate granule and mossy cells exhibit distinct spatiotemporal responses to local change in a one-dimensional landscape of visual-tactile cues. Sci Rep 9**:** 9545.

Jung MW, McNaughton BL (1993) Spatial selectivity of unit activity in the hippocampal granular layer. Hippocampus 3**:** 165-182.

Kay LM (2014) Circuit oscillations in odor perception and memory. Prog Brain Res 208**:** 223-251.

Kesner RP (2018) An analysis of dentate gyrus function (an update). Behav Brain Res 354**:** 84-91.

Kheirbek MA, Drew LJ, Burghardt NS, Costantini DO, Tannenholz L, Ahmari SE, Zeng H, Fenton AA, Hen R (2013) Differential control of learning and anxiety along the dorsoventral axis of the dentate gyrus. Neuron 77**:** 955-968.

Kleschevnikov AM, Routtenberg A (2003) Long-term potentiation recruits a trisynaptic excitatory associative network within the mouse dentate gyrus. Eur J Neurosci 17**:** 2690-2702.

Knierim JJ, Neunuebel JP (2016) Tracking the flow of hippocampal computation: Pattern separation, pattern completion, and attractor dynamics. Neurobiol Learn Mem 129**:** 38-49.

Krook-Magnuson E, Armstrong C, Bui A, Lew S, Oijala M, Soltesz I (2015) In vivo evaluation of the dentate gate theory in epilepsy. J Physiol 593**:** 2379-2388.

Lacaille JC, Schwartzkroin PA (1988) Intracellular responses of rat hippocampal granule cells in vitro to discrete applications of norepinephrine. Neurosci Lett 89**:** 176-181.

Larimer P, Strowbridge BW (2008) Nonrandom local circuits in the dentate gyrus. J Neurosci 28**:** 12212-12223.

Leranth C, Szeidemann Z, Hsu M, Buzsaki G (1996) AMPA receptors in the rat and primate hippocampus: A possible absence of GluR2/3 subunits in most interneurons. Neuroscience 70**:** 631-652.

Leutgeb JK, Leutgeb S, Moser MB, Moser EI (2007) Pattern separation in the dentate gyrus and CA3 of the hippocampus. Science 315**:** 961-966.

Lillis KP, Kramer MA, Mertz J, Staley KJ, White JA (2012) Pyramidal cells accumulate chloride at seizure onset. Neurobiol Dis 47**:** 358-366.

Lisman JE, Talamini LM, Raffone A (2005) Recall of memory sequences by interaction of the dentate and CA3: A revised model of the phase precession. Neural Netw 18**:** 1191-1201.

Maguire JL, Stell BM, Rafizadeh M, Mody I (2005) Ovarian cycle-linked changes in GABA(a) receptors mediating tonic inhibition alter seizure susceptibility and anxiety. Nat Neurosci 8**:** 797-804.

Matsuyama T, Tsuchiyama M, Nakamura H, Matsumoto M, Sugita M (1993) Hilar somatostatin neurons are more vulnerable to an ischemic insult than CA1 pyramidal neurons. J Cereb Blood Flow Metab 13**:** 229-234.

Moser MB, Moser EI (1998) Functional differentiation in the hippocampus. Hippocampus 8**:** 608-619.

Myers CE, Scharfman HE (2009) A role for hilar cells in pattern separation in the dentate gyrus: A computational approach. Hippocampus 19**:** 321-337.

Myers CE, Scharfman HE (2011) Pattern separation in the dentate gyrus: A role for the CA3 backprojection. Hippocampus 21**:** 1190-1215.

Nakazawa K (2017) Dentate mossy cell and pattern separation. Neuron 93**:** 465-467.

Neunuebel JP, Knierim JJ (2012) Spatial firing correlates of physiologically distinct cell types of the rat dentate gyrus. J Neurosci 32**:** 3848-3858.

Newman EL, Hasselmo ME (2014) CA3 sees the big picture while dentate gyrus splits hairs. Neuron 81**:** 226-228.

Norenberg A, Hu H, Vida I, Bartos M, Jonas P (2010) Distinct nonuniform cable properties optimize rapid and efficient activation of fast-spiking GABAergic interneurons. Proc Natl Acad Sci U S A 107**:** 894-899.

Overstreet LS, Hentges ST, Bumaschny VF, de Souza FS, Smart JL, Santangelo AM, Low MJ, Westbrook GL, Rubinstein M (2004) A transgenic marker for newly born granule cells in dentate gyrus. J Neurosci 24**:** 3251-3259.

Penttonen M, Kamondi A, Sik A, Acsady L, Buzsaki G (1997) Feed-forward and feed-back activation of the dentate gyrus in vivo during dentate spikes and sharp wave bursts. Hippocampus 7**:** 437-450.

Pierce JP, McCloskey DP, Scharfman HE (2011) Morphometry of hilar ectopic granule cells in the rat. J Comp Neurol 519**:** 1196-1218.

Pilz GA, Carta S, Stauble A, Ayaz A, Jessberger S, Helmchen F (2016) Functional imaging of dentate granule cells in the adult mouse hippocampus. J Neurosci 36: 7407-7414.

Puighermanal E, Biever A, Espallergues J, Gangarossa G, De Bundel D, Valjent E (2015) Drd2-cre:Ribotag mouse line unravels the possible diversity of dopamine d2 receptor-expressing cells of the dorsal mouse hippocampus. Hippocampus 25: 858-875.

Radic T, Jungenitz T, Singer M, Beining M, Cuntz H, Vlachos A, Deller T, Schwarzacher SW (2017) Time-lapse imaging reveals highly dynamic structural maturation of postnatally born dentate granule cells in organotypic entorhino-hippocampal slice cultures. Sci Rep 7: 43724.

Rahimi O, Claiborne BJ (2007) Morphological development and maturation of granule neuron dendrites in the rat dentate gyrus. Prog Brain Res 163: 167-181.

Ratzliff A, Santhakumar V, Howard A, Soltesz I (2002) Mossy cells in epilepsy: Rigor mortis or vigor mortis? Trends Neurosci 25: 140-144.

Ribak CE, Seress L, Amaral DG (1985) The development, ultrastructure and synaptic connections of the mossy cells of the dentate gyrus. J Neurocytol 14: 835-857.

Salin PA, Scanziani M, Malenka RC, Nicoll RA (1996) Distinct short-term plasticity at two excitatory synapses in the hippocampus. Proc Natl Acad Sci U S A 93: 13304-13309.

Santhakumar V, Bender R, Frotscher M, Ross ST, Hollrigel GS, Toth Z, Soltesz I (2000) Granule cell hyperexcitability in the early post-traumatic rat dentate gyrus: The 'irritable mossy cell' hypothesis. J Physiol 524 117-134.

Scharfman HE, Schwartzkroin PA (1988) Electrophysiology of morphologically identified mossy cells of the dentate hilus recorded in guinea pig hippocampal slices. J Neurosci 8: 3812-3821.

Scharfman HE, Kunkel DD, Schwartzkroin PA (1990) Synaptic connections of dentate granule cells and hilar neurons: Results of paired intracellular recordings and intracellular horseradish peroxidase injections. Neuroscience 37: 693-707.

Scharfman HE (1991) Dentate hilar cells with dendrites in the molecular layer have lower thresholds for synaptic activation by perforant path than granule cells. J Neurosci 11: 1660-1673.

Scharfman HE (1993) Characteristics of spontaneous and evoked epsps recorded from dentate spiny hilar cells in rat hippocampal slices. J Neurophysiol 70: 742-757.

Scharfman HE (1994a) Evidence from simultaneous intracellular recordings in rat hippocampal slices that area CA3 pyramidal cells innervate dentate hilar mossy cells. J Neurophysiol 72: 2167-2180.

Scharfman HE (1994b) Epsps of dentate gyrus granule cells during epileptiform bursts of dentate hilar "mossy" cells and area CA3 pyramidal cells in disinhibited rat hippocampal slices. J Neurosci 14: 6041-6057.

Scharfman HE (1995a) Electrophysiological diversity of pyramidal-shaped neurons at the granule cell layer/hilus border of the rat dentate gyrus recorded in vitro. Hippocampus 5: 287-305.

Scharfman HE (1995b) Electrophysiological evidence that dentate hilar mossy cells are excitatory and innervate both granule cells and interneurons. J Neurophysiol 74: 179-194.

Scharfman HE (1999) The role of nonprincipal cells in dentate gyrus excitability and its relevance to animal models of epilepsy and temporal lobe epilepsy. Adv Neurol 79**:** 805-820.

Scharfman HE, Goodman JH, Sollas AL (2000) Granule-like neurons at the hilar/CA3 border after status epilepticus and their synchrony with area CA3 pyramidal cells: Functional implications of seizure-induced neurogenesis. J Neurosci 20**:** 6144-6158.

Scharfman HE, Sollas AL, Smith KL, Jackson MB, Goodman JH (2002) Structural and functional asymmetry in the normal and epileptic rat dentate gyrus. J Comp Neurol 454**:** 424-439.

Scharfman HE, Mercurio TC, Goodman JH, Wilson MA, MacLusky NJ (2003) Hippocampal excitability increases during the estrous cycle in the rat: A potential role for brain-derived neurotrophic factor. J Neurosci 23**:** 11641-11652.

Scharfman HE, Gray WP (2006) Plasticity of neuropeptide Y in the dentate gyrus after seizures, and its relevance to seizure-induced neurogenesis. EXS 193-211.

Scharfman HE (2007) The CA3 "backprojection" to the dentate gyrus. Prog Brain Res 163**:** 627-637.

Scharfman HE, Witter MP (2007) Preface. In: The dentate gyrus: A comprehensive guide to structure, function, and clinical implications (ed Scharfman HE), ppix-xvii. Elsevier: New York.

Scharfman HE, Myers CE (2012) Hilar mossy cells of the dentate gyrus: A historical perspective. Front Neural Circuits 6**:** 106.

Scharfman HE (2016) The enigmatic mossy cell of the dentate gyrus. Nat Rev Neurosci 17**:** 562-575.

Schmidt-Hieber C, Jonas P, Bischofberger J (2004) Enhanced synaptic plasticity in newly generated granule cells of the adult hippocampus. Nature 429: 184-187.

Senzai Y, Buzsaki G (2017) Physiological properties and behavioral correlates of hippocampal granule cells and mossy cells. Neuron 93: 691-704.

Skucas VA, Duffy AM, Harte-Hargrove LC, Magagna-Poveda A, Radman T, Chakraborty G, Schroeder CE, MacLusky NJ, Scharfman HE (2013) Testosterone depletion in adult male rats increases mossy fiber transmission, LTP, and sprouting in area CA3 of hippocampus. J Neurosci 33: 2338-2355.

Sloviter RS (1989) Calcium-binding protein (calbindin-d28k) and parvalbumin immunocytochemistry: Localization in the rat hippocampus with specific reference to the selective vulnerability of hippocampal neurons to seizure activity. J Comp Neurol 280: 183-196.

Sloviter RS (1991) Permanently altered hippocampal structure, excitability, and inhibition after experimental status epilepticus in the rat: The "dormant basket cell" hypothesis and its possible relevance to temporal lobe epilepsy. Hippocampus 1: 41-66.

Sloviter RS (1994) The functional organization of the hippocampal dentate gyrus and its relevance to the pathogenesis of temporal lobe epilepsy. Ann Neurol 35: 640-654.

Soltesz I, Bourassa J, Deschenes M (1993) The behavior of mossy cells of the rat dentate gyrus during theta oscillations in vivo. Neuroscience 57: 555-564.

Soriano E, Frotscher M (1994) Mossy cells of the rat fascia dentata are glutamate-immunoreactive. Hippocampus 4: 65-69.

Sperk G, Hamilton T, Colmers WF (2007) Neuropeptide Y in the dentate gyrus. Prog Brain Res 163: 285-297.

Staley KJ, Otis TS, Mody I (1992) Membrane properties of dentate gyrus granule cells: Comparison of sharp microelectrode and whole-cell recordings. J Neurophysiol 67: 1346-1358.

Stanton PK, Mody I, Heinemann U (1989) A role for N-methyl-D-aspartate receptors in norepinephrine-induced long-lasting potentiation in the dentate gyrus. Exp Brain Res 77: 517-530.

Swaminathan A, Wichert I, Schmitz D, Maier N (2018) Involvement of mossy cells in sharp wave-ripple activity in vitro. Cell Rep 23: 2541-2549.

Thomson AM, Deuchars J (1997) Synaptic interactions in neocortical local circuits: Dual intracellular recordings in vitro. Cereb Cortex 7: 510-522.

Wang H, Peca J, Matsuzaki M, Matsuzaki K, Noguchi J, Qiu L, Wang D, Zhang F, Boyden E, Deisseroth K, Kasai H, Hall WC, Feng G, Augustine GJ (2007) High-speed mapping of synaptic connectivity using photostimulation in channelrhodopsin-2 transgenic mice. Proc Natl Acad Sci U S A 104: 8143-8148.

Wenzel HJ, Buckmaster PS, Anderson NL, Wenzel ME, Schwartzkroin PA (1997) Ultrastructural localization of neurotransmitter immunoreactivity in mossy cell axons and their synaptic targets in the rat dentate gyrus. Hippocampus 7: 559-570.

Williams PA, Larimer P, Gao Y, Strowbridge BW (2007) Semilunar granule cells: Glutamatergic neurons in the rat dentate gyrus with axon collaterals in the inner molecular layer. J Neurosci 27: 13756-13761.

Williamson A, Patrylo PR (2007) Physiological studies of human dentate granule cells. Prog Brain Res 163**:** 183-198.

Wright BJ, Jackson MB (2014) Long-term potentiation in hilar circuitry modulates gating by the dentate gyrus. J Neurosci 34**:** 9743-9753.

Yassa MA, Stark CE (2011) Pattern separation in the hippocampus. Trends Neurosci 34**:** 515-525.

Zhang ZJ, Koifman J, Shin DS, Ye H, Florez CM, Zhang L, Valiante TA, Carlen PL (2012) Transition to seizure: Ictal discharge is preceded by exhausted presynaptic GABA release in the hippocampal CA3 region. J Neurosci 32**:** 2499-2512.

Figure 1

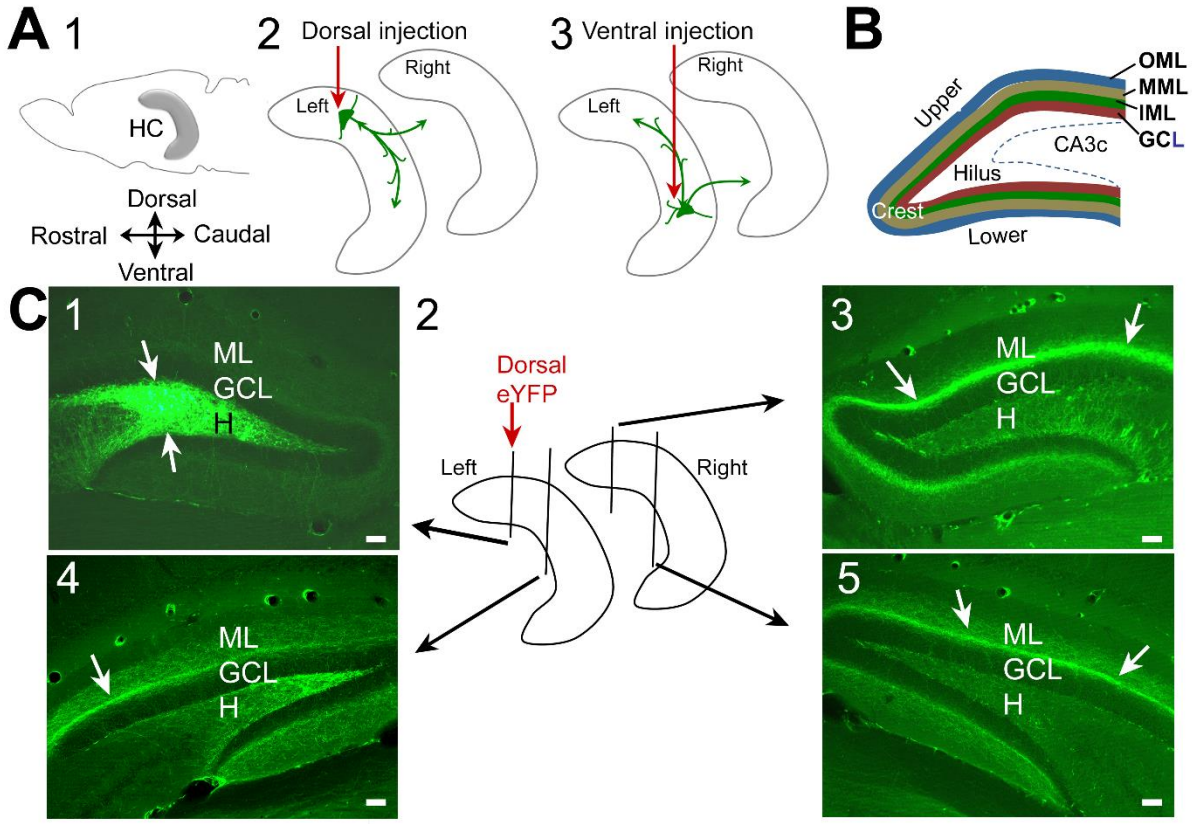
A
1
HC
Dorsal
Rostral
Caudal
Ventral
2
Dorsal injection
Left
Right
3
Ventral injection
Left
Right
B
Upper
OML
MML
IML
GCL
CA3c
Hilus
Crest
Lower
C
1
ML
GCL
H
2
Dorsal
eYFP
Left
Right
3
ML
GCL
H
4
ML
GCL
H
5
ML
GCL
H

Figure 2

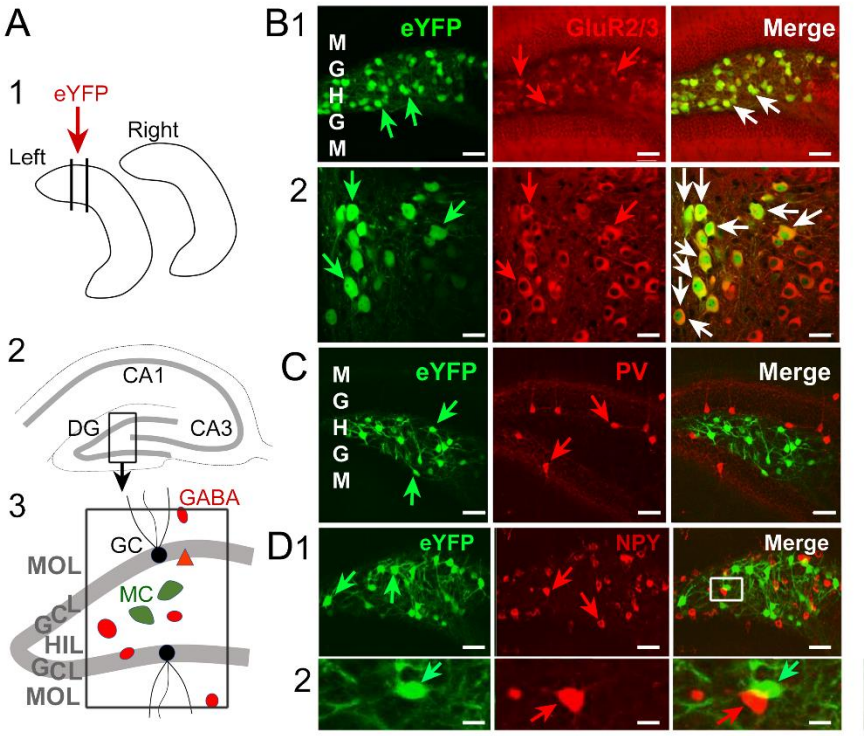
A
1
eYFP
Left
Right
2
CA1
DG
CA3
3
GABA
GC
MOL
MC
GCL
HIL
GCL
MOL
B1
M
G
H
G
M
eYFP
GluR2/3
Merge
2
C
eYFP
PV
Merge
D1
eYFP
NPY
Merge
2

Figure 3

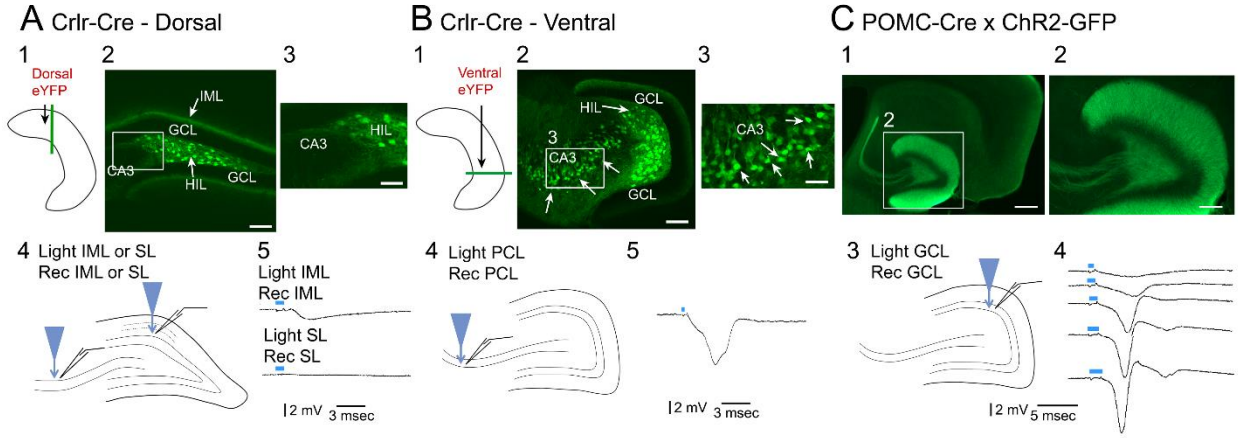
A Crlr-Cre - Dorsal
1
2
3
Dorsal
eYFP
IML
GCL
CA3
HIL
GCL
CA3
HIL
B Crlr-Cre - Ventral
1
2
3
Ventral
eYFP
HIL
GCL
3
CA3
GCL
CA3
C POMC-Cre x ChR2-GFP
1
2
2
4 Light IML or SL
Rec IML or SL
5
Light IML
Rec IML
Light SL
Rec SL
2 mV
3 msec
4 Light PCL
Rec PCL
5
2 mV
3 msec
3 Light GCL
Rec GCL
4
2 mV
5 msec

Figure 4

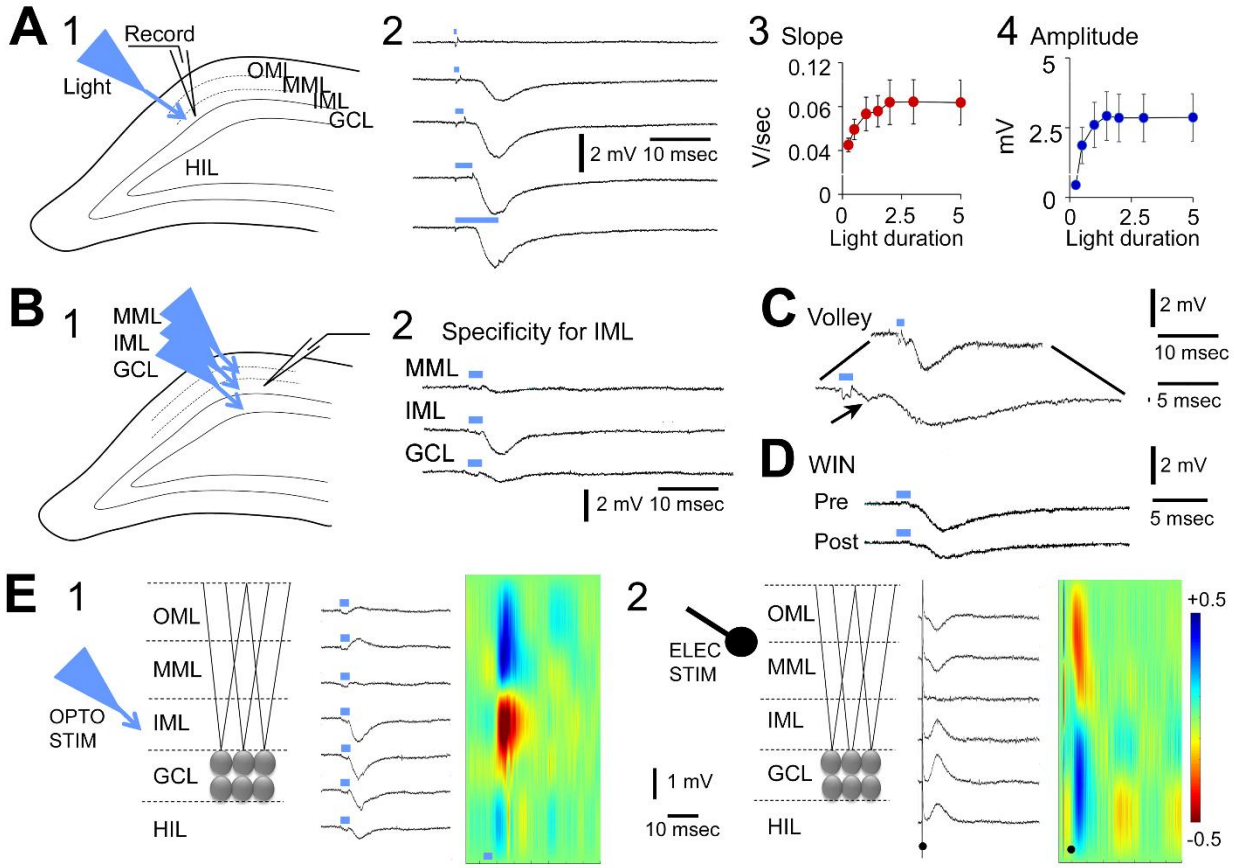
A
1
Record
Light
OML
MML
IML
GCL
HIL
2
2 mV 10 msec
3 Slope
V/sec
0.12
0.06
0.04
0
0
2.5
5
Light duration
4 Amplitude
mV
5
2.5
0
0
2.5
5
Light duration
B
1
MML
IML
GCL
2 Specificity for IML
MML
IML
GCL
2 mV 10 msec
C Volley
2 mV
10 msec
5 msec
D WIN
Pre
Post
2 mV
5 msec
E
1
OML
MML
IML
GCL
HIL
OPTO
STIM
2
ELEC
STIM
1 mV
10 msec
OML
MML
IML
GCL
HIL
+0.5
-0.5

Figure 5

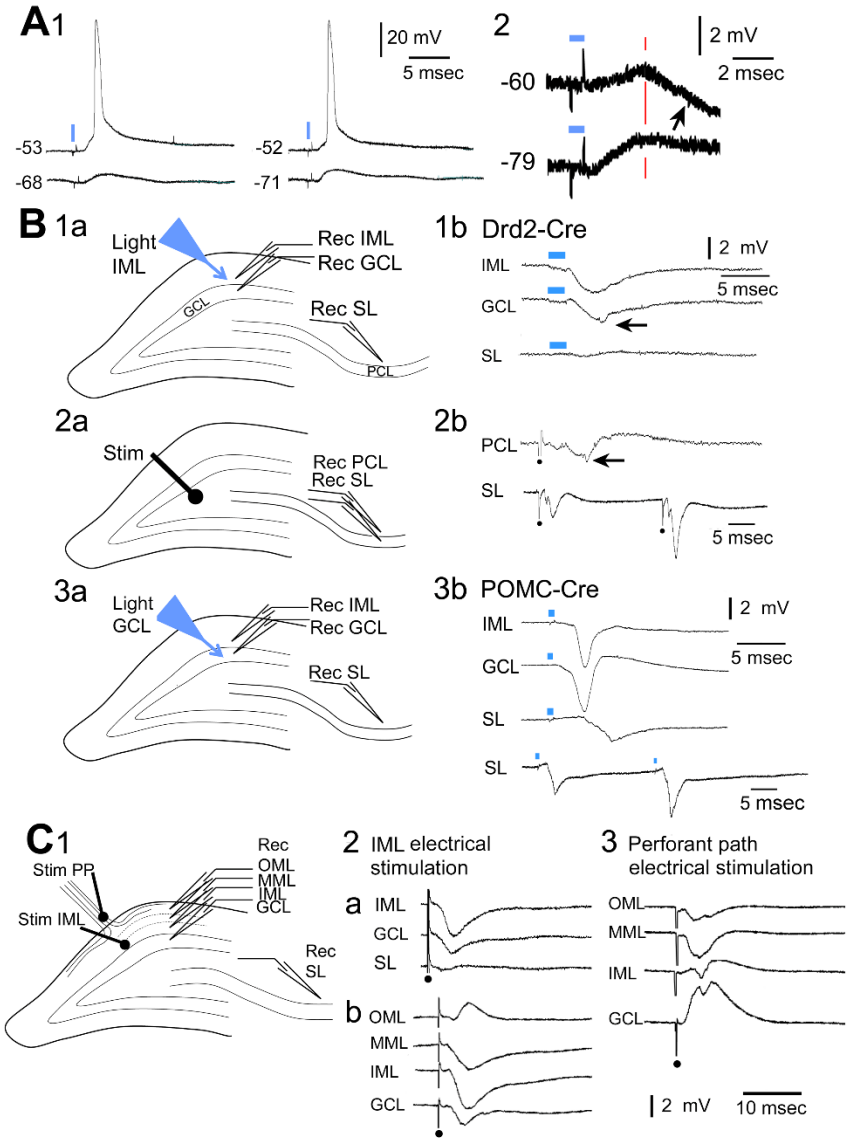
A1
20 mV
5 msec
-53
-68
-52
-71
2
2 mV
2 msec
-60
-79
B 1a
Light
IML
Rec IML
Rec GCL
GCL
Rec SL
PCL
1b Drd2-Cre
2 mV
5 msec
IML
GCL
SL
2a
Stim
Rec PCL
Rec SL
2b
PCL
SL
5 msec
3a
Light
GCL
Rec IML
Rec GCL
Rec SL
3b POMC-Cre
2 mV
5 msec
IML
GCL
SL
SL
5 msec
C1
Stim PP
Stim IML
Rec
OML
MML
IML
GCL
Rec
SL
2 IML electrical stimulation
a IML
GCL
SL
b OML
MML
IML
GCL
3 Perforant path electrical stimulation
OML
MML
IML
GCL
2 mV
10 msec

Figure 6

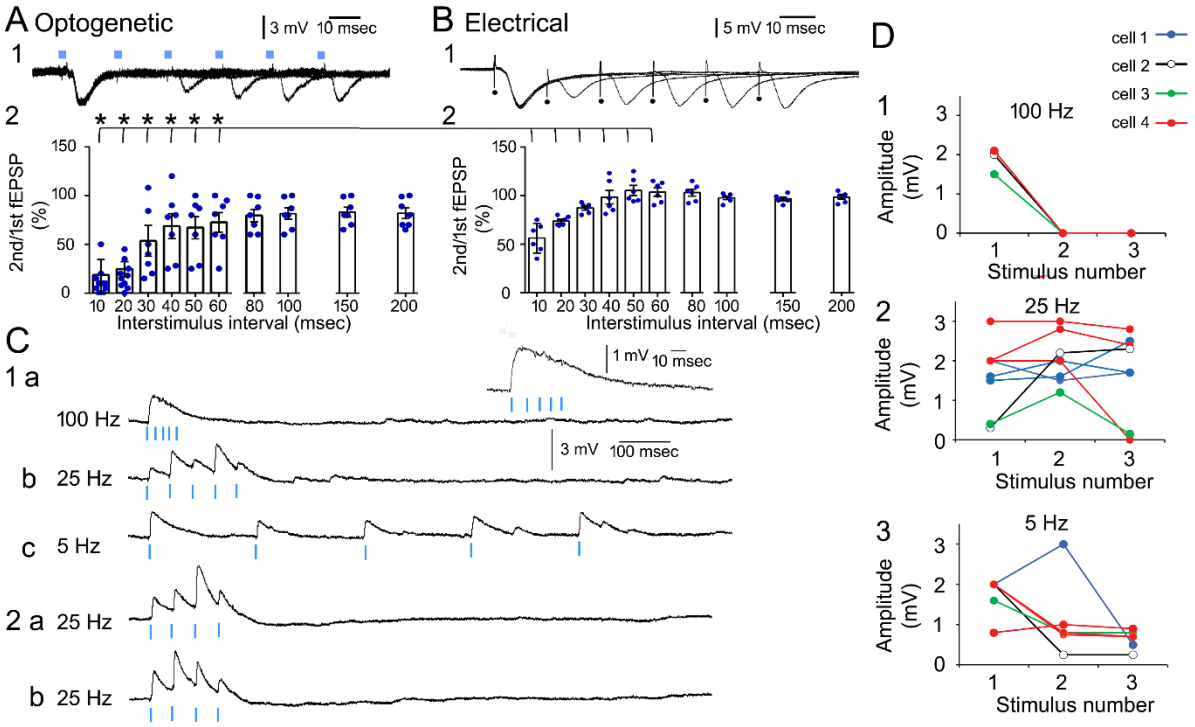
A Optogenetic
3 mV 10 msec
1
2
2nd/1st fEPSP (%)
Interstimulus interval (msec)
B Electrical
5 mV 10 msec
1
2
2nd/1st fEPSP (%)
Interstimulus interval (msec)
C
1 a
100 Hz
1 mV 10 msec
3 mV 100 msec
b 25 Hz
c 5 Hz
2 a 25 Hz
b 25 Hz
D
cell 1
cell 2
cell 3
cell 4
1
100 Hz
Amplitude (mV)
Stimulus number
2
25 Hz
Amplitude (mV)
Stimulus number
3
5 Hz
Amplitude (mV)
Stimulus number

Figure 7

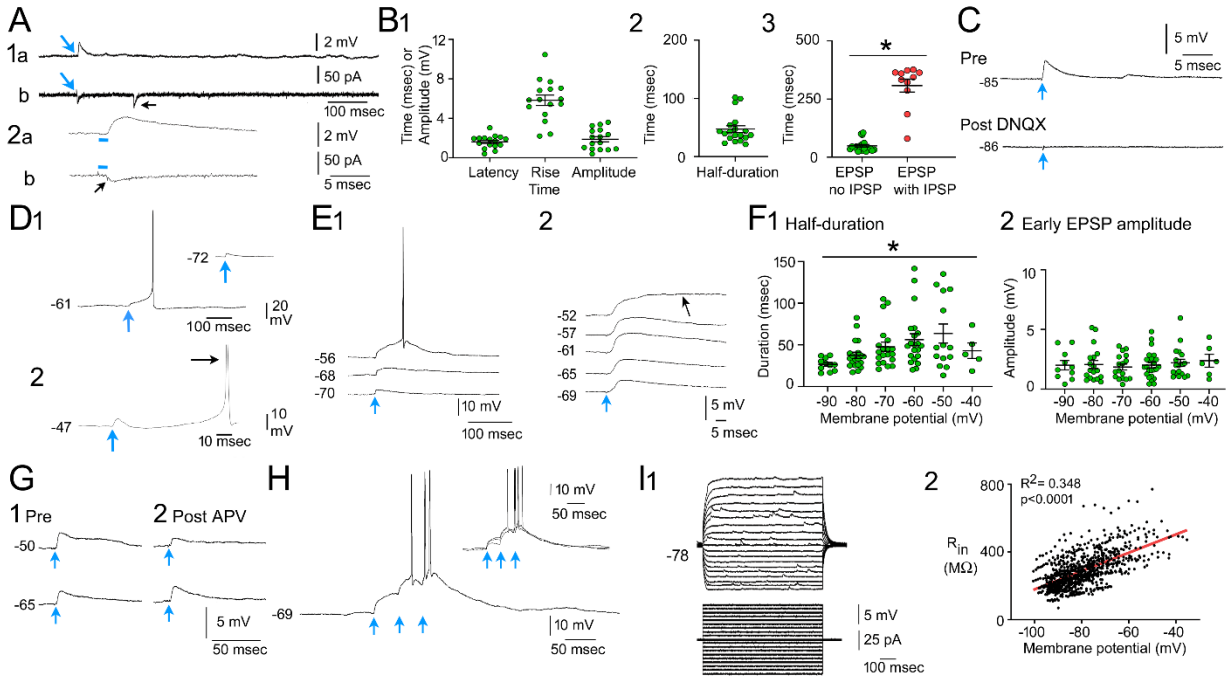
A
1a
b
2a
b
2 mV
50 pA
100 msec
2 mV
50 pA
5 msec
B1
Time (msec) or Amplitude (mV)
Latency
Rise Time
Amplitude
2
Time (msec)
Half-duration
3
Time (msec)
EPSP no IPSP
EPSP with IPSP
C
Pre
Post DNQX
5 mV
5 msec
D1
-72
-61
100 msec
20 mV
2
-47
10 msec
10 mV
E1
-56
-68
-70
10 mV
100 msec
2
-52
-57
-61
-65
-69
5 mV
5 msec
F1 Half-duration
Duration (msec)
Membrane potential (mV)
2 Early EPSP amplitude
Amplitude (mV)
Membrane potential (mV)
G
1 Pre
2 Post APV
-50
-65
5 mV
50 msec
H
-69
10 mV
50 msec
10 mV
50 msec
I1
-78
5 mV
25 pA
100 msec
2
R2= 0.348
p<0.0001
Rin (MΩ)
Membrane potential (mV)

Figure 8

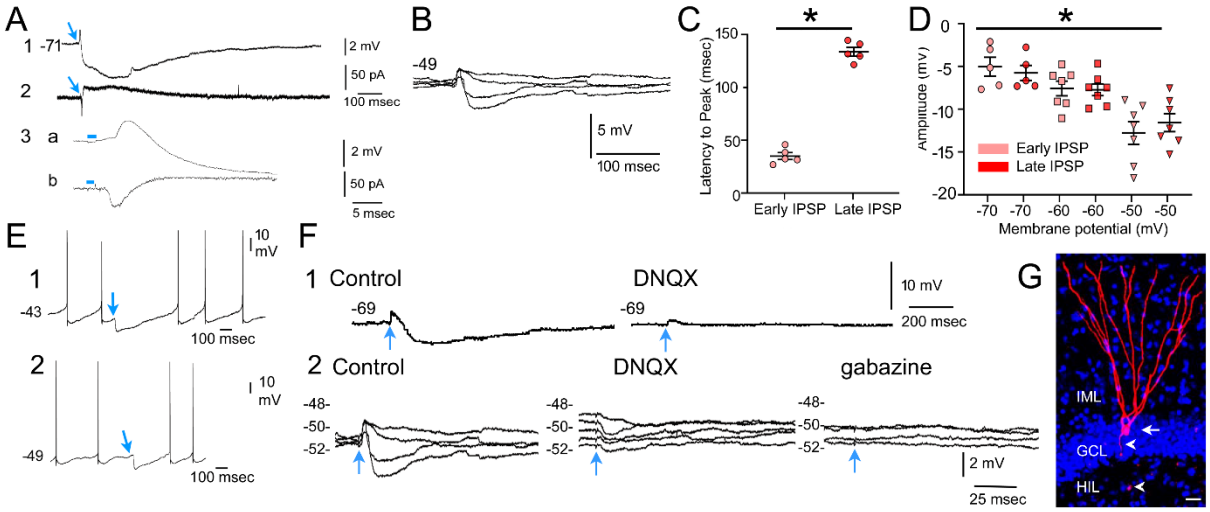
A
1 -71
2
3 a
b
2 mV
50 pA
100 msec
2 mV
50 pA
5 msec
B
-49
5 mV
100 msec
C
*
Latency to Peak (msec)
150
100
50
0
Early IPSP
Late IPSP
D
*
Amplitude (mV)
0
-5
-10
-15
-20
Early IPSP
Late IPSP
-70 -70 -60 -60 -50 -50
Membrane potential (mV)
E
1
-43
10 mV
100 msec
2
-49
10 mV
100 msec
F
1 Control
DNQX
-69
-69
10 mV
200 msec
2 Control
DNQX
gabazine
-48-
-50-
-52-
2 mV
25 msec
G
IML
GCL
HIL

Figure 9

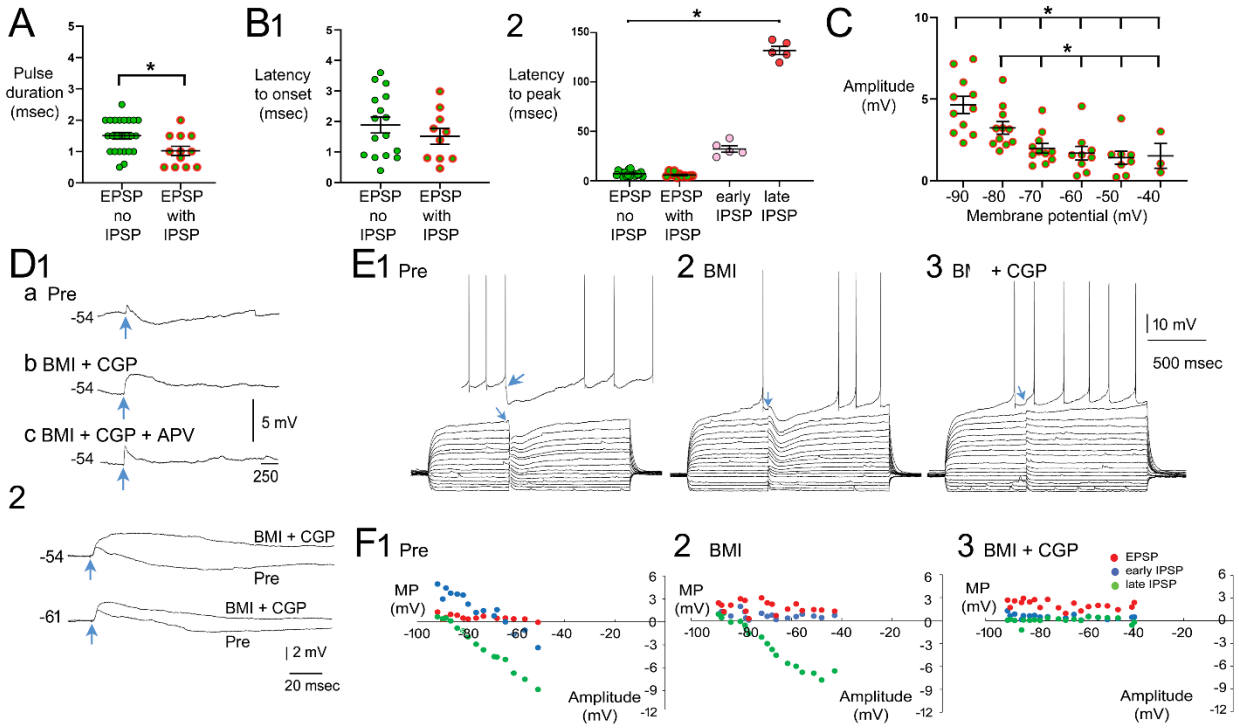
A
Pulse duration (msec)
EPSP no IPSP
EPSP with IPSP
B1
Latency to onset (msec)
2
Latency to peak (msec)
early IPSP
late IPSP
C
Amplitude (mV)
Membrane potential (mV)
D1
a Pre
b BMI + CGP
c BMI + CGP + APV
5 mV
250
2
BMI + CGP
Pre
2 mV
20 msec
E1 Pre
2 BMI
3 BMI + CGP
10 mV
500 msec
F1 Pre
2 BMI
3 BMI + CGP
EPSP
early IPSP
late IPSP
MP (mV)
Amplitude (mV)

Figure 10

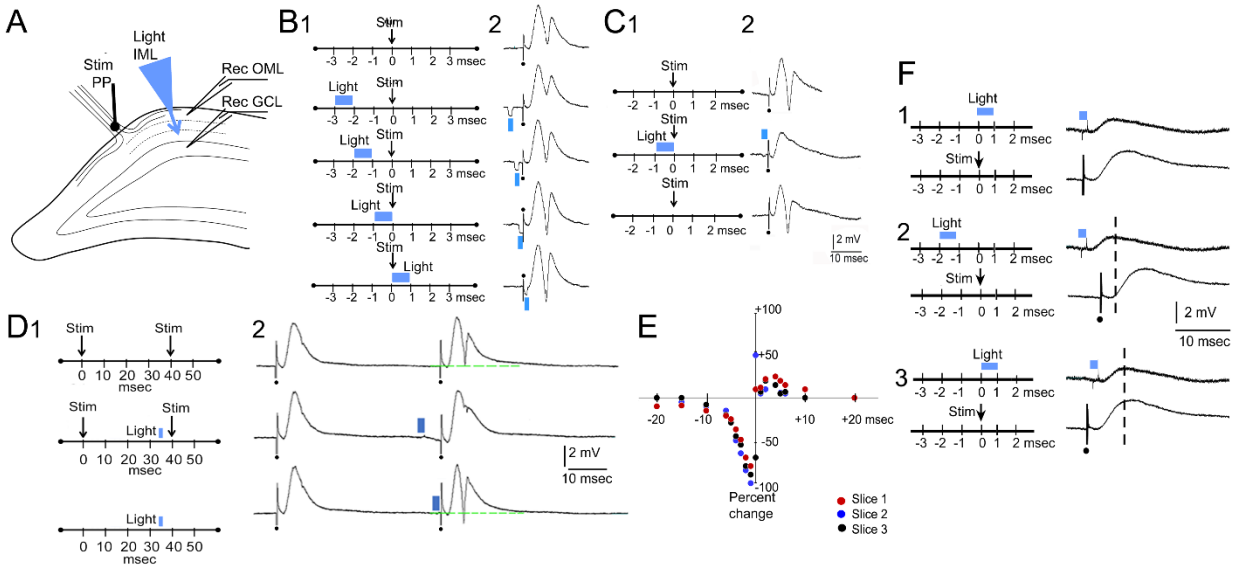
A
Light
IML
Stim
PP
Rec OML
Rec GCL
B1
Stim
Light
-3 -2 -1 0 1 2 3 msec
2
C1
2
Stim
Light
-2 -1 0 1 2 msec
2 mV
10 msec
F
1
2
3
Light
Stim
-3 -2 -1 0 1 2 msec
2 mV
10 msec
D1
Stim
Light
0 10 20 30 40 50
msec
2
2 mV
10 msec
E
+100
+50
-50
-100
-20
-10
+10
+20 msec
Percent
change
Slice 1
Slice 2
Slice 3

Figure 11

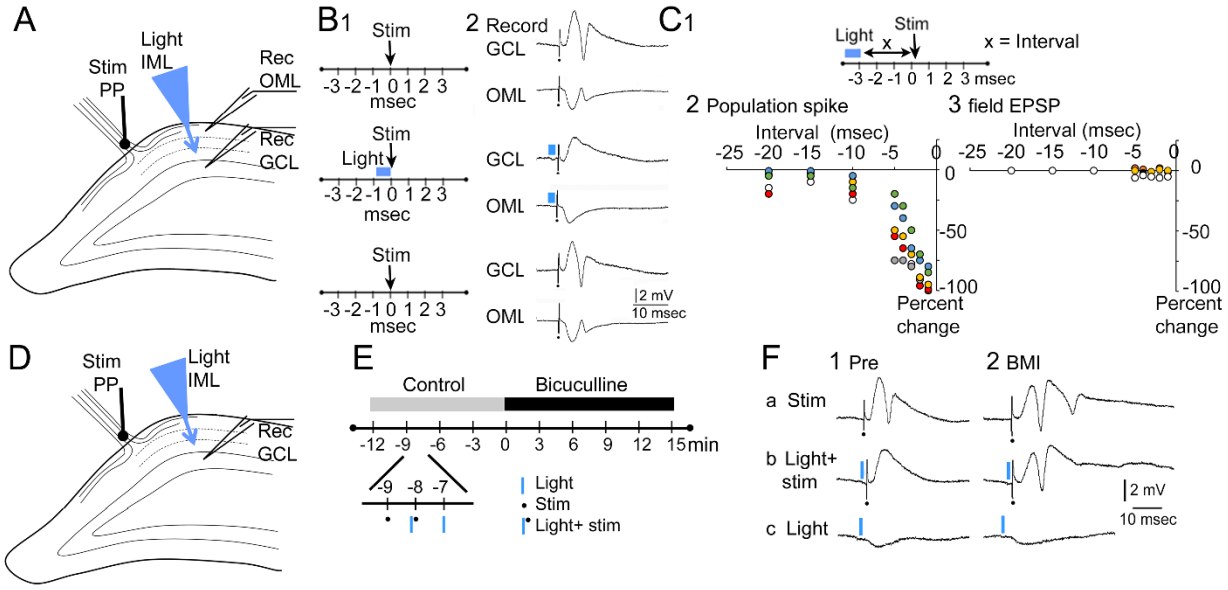
A
Light
IML
Stim
PP
Rec
OML
Rec
GCL
B1
Stim
-3 -2 -1 0 1 2 3
msec
Stim
Light
-3 -2 -1 0 1 2 3
msec
Stim
-3 -2 -1 0 1 2 3
msec
2 Record
GCL
OML
GCL
OML
GCL
OML
2 mV
10 msec
C1
Light
x
Stim
x = Interval
-3 -2 -1 0 1 2 3 msec
2 Population spike
3 field EPSP
Interval (msec)
-25 -20 -15 -10 -5 0
0
-50
-100
Percent change
Interval (msec)
-25 -20 -15 -10 -5 0
0
-50
-100
Percent change
D
Stim
PP
Light
IML
Rec
GCL
E
Control
Bicuculline
-12 -9 -6 -3 0 3 6 9 12 15min
-9 -8 -7
Light
Stim
Light+ stim
F
1 Pre
2 BMI
a Stim
b Light+ stim
c Light
2 mV
10 msec

Figure 12

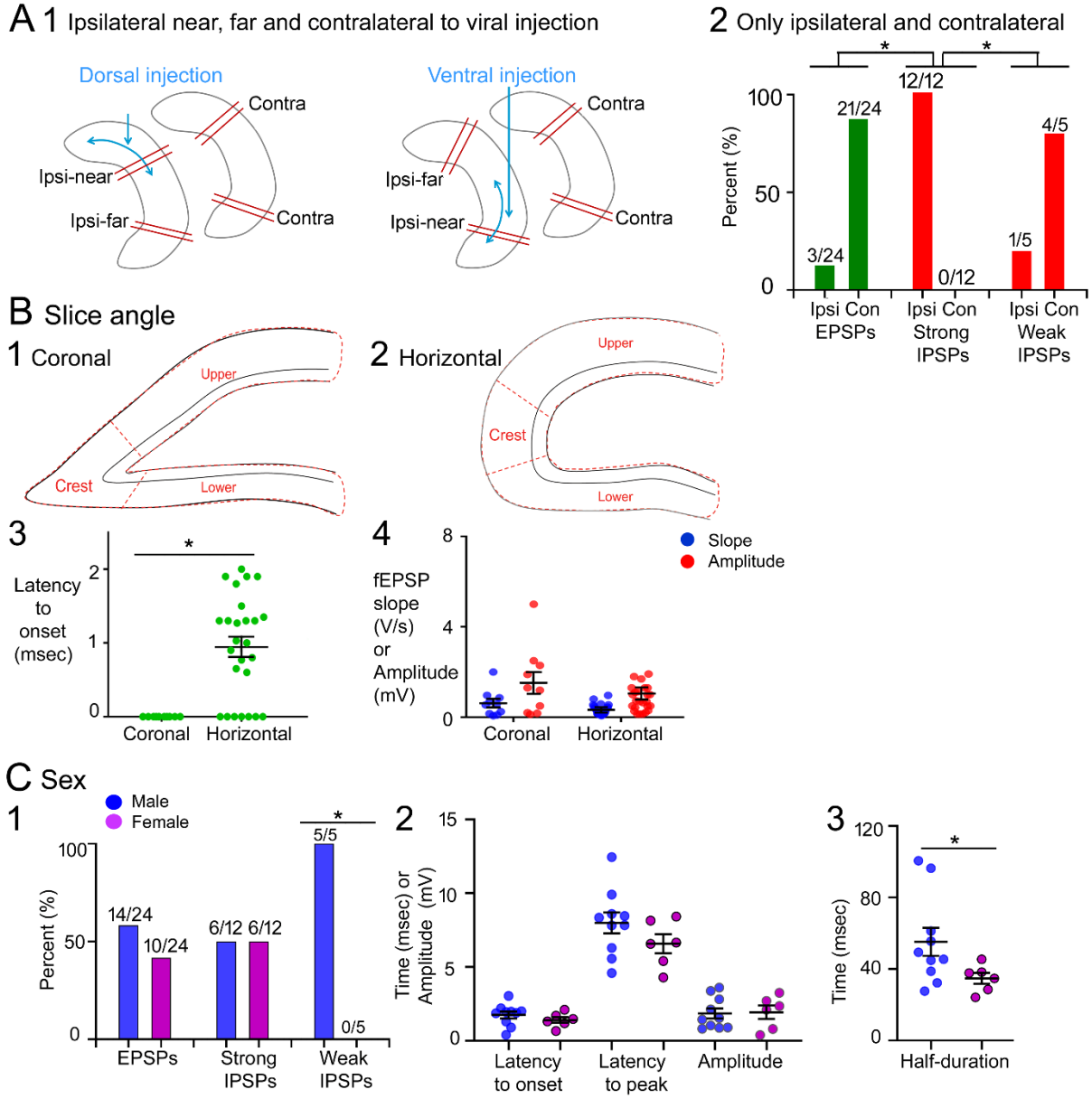
A 1 Ipsilateral near, far and contralateral to viral injection
Dorsal injection
Contra
Ipsi-near
Ipsi-far
Contra
Ventral injection
Contra
Ipsi-far
Ipsi-near
Contra
2 Only ipsilateral and contralateral
Percent (%)
100
50
0
3/24
21/24
12/12
0/12
1/5
4/5
Ipsi Con EPSPs
Ipsi Con Strong IPSPs
Ipsi Con Weak IPSPs
B Slice angle
1 Coronal
Upper
Crest
Lower
2 Horizontal
Upper
Crest
Lower
3
Latency to onset (msec)
Coronal
Horizontal
4
fEPSP slope (V/s) or Amplitude (mV)
Slope
Amplitude
Coronal
Horizontal
C Sex
1
Male
Female
Percent (%)
14/24
10/24
6/12
6/12
5/5
0/5
EPSPs
Strong IPSPs
Weak IPSPs
2
Time (msec) or Amplitude (mV)
Latency to onset
Latency to peak
Amplitude
3
Time (msec)
Half-duration

Figure 13

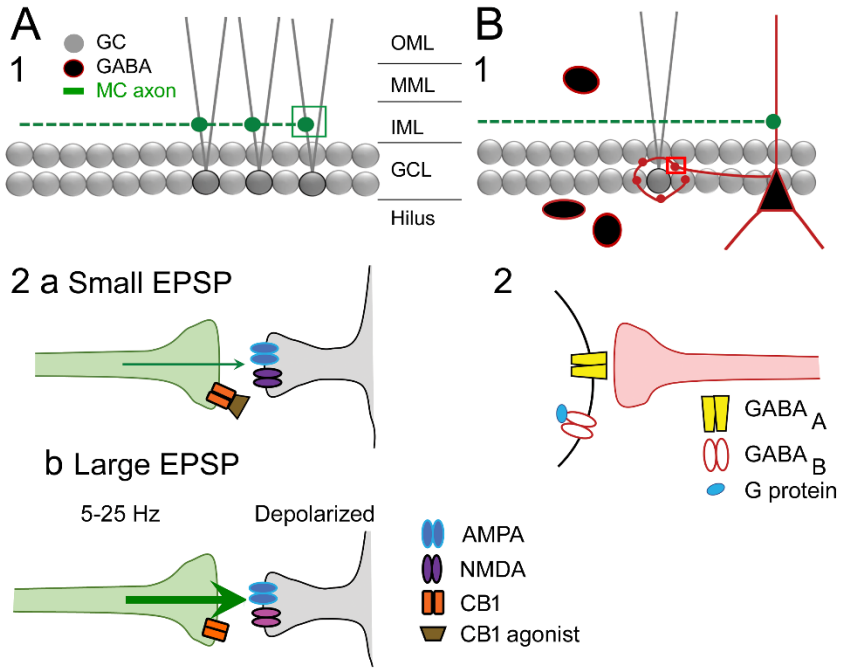
A
1
GC
GABA
MC axon
OML
MML
IML
GCL
Hilus
B
1
2 a Small EPSP
b Large EPSP
5-25 Hz
Depolarized
2
GABA A
GABA B
G protein
AMPA
NMDA
CB1
CB1 agonist